

**THE EFFECTS OF CONTACT GUIDANCE AND  
ELECTRICAL FIELD STIMULATION ON THE  
MATURATION OF CARDIAC PROGENITORS AND  
CARDIOMYOCYTES**

**By**

**Hoi Ting Heidi Au**

A thesis submitted in conformity with the requirements  
for the degree of Master of Applied Science  
Graduate Department of Chemical Engineering and Applied Chemistry  
University of Toronto

© Copyright Hoi Ting Heidi Au 2008



Library and  
Archives Canada

Bibliothèque et  
Archives Canada

Published Heritage  
Branch

Direction du  
Patrimoine de l'édition

395 Wellington Street  
Ottawa ON K1A 0N4  
Canada

395, rue Wellington  
Ottawa ON K1A 0N4  
Canada

*Your file* *Votre référence*  
*ISBN: 978-0-494-44906-6*  
*Our file* *Notre référence*  
*ISBN: 978-0-494-44906-6*

**NOTICE:**

The author has granted a non-exclusive license allowing Library and Archives Canada to reproduce, publish, archive, preserve, conserve, communicate to the public by telecommunication or on the Internet, loan, distribute and sell theses worldwide, for commercial or non-commercial purposes, in microform, paper, electronic and/or any other formats.

The author retains copyright ownership and moral rights in this thesis. Neither the thesis nor substantial extracts from it may be printed or otherwise reproduced without the author's permission.

**AVIS:**

L'auteur a accordé une licence non exclusive permettant à la Bibliothèque et Archives Canada de reproduire, publier, archiver, sauvegarder, conserver, transmettre au public par télécommunication ou par l'Internet, prêter, distribuer et vendre des thèses partout dans le monde, à des fins commerciales ou autres, sur support microforme, papier, électronique et/ou autres formats.

L'auteur conserve la propriété du droit d'auteur et des droits moraux qui protègent cette thèse. Ni la thèse ni des extraits substantiels de celle-ci ne doivent être imprimés ou autrement reproduits sans son autorisation.

---

In compliance with the Canadian Privacy Act some supporting forms may have been removed from this thesis.

Conformément à la loi canadienne sur la protection de la vie privée, quelques formulaires secondaires ont été enlevés de cette thèse.

While these forms may be included in the document page count, their removal does not represent any loss of content from the thesis.

Bien que ces formulaires aient inclus dans la pagination, il n'y aura aucun contenu manquant.

  
**Canada**

**THE EFFECTS OF CONTACT GUIDANCE AND ELECTRICAL FIELD  
STIMULATION ON THE MATURATION OF CARDIAC PROGENITORS AND  
CARDIOMYOCYTES**

**Hoi Ting Heidi Au**

**Master of Applied Science, 2008**

**Graduate Department of Chemical Engineering and Applied Chemistry**

**University of Toronto**

**ABSTRACT**

Cardiac tissue engineering requires an appropriate cell source. We investigated the feasibility of various immature cardiac cells, namely neonatal heart cells and embryonic stem cell derived cardiomyocytes and progenitors, in their ability to create the desired adult cardiomyocyte (CM) phenotype. We found that the application of contact guidance and electrical field stimulation improved the alignment and elongation of neonatal cells within a monolayer cultured polyvinyl carbonate or tissue culture polystyrene, as well as the contractile function of the culture. These cells were found to express mature cardiac cell markers such as Troponin I and  $\alpha$ -sacromeric actinin, in addition to forming gap junctions with neighbouring cells. A similar approach, applied to human embryonic stem cells derived-cardiomyocytes (hESC-CM), shows some promise in maturing these cells into the adult cardiomyocyte phenotype. Finally, we also explored various methods for isolating  $isl1^+$  cardiac progenitors from the neonatal rat heart.

## Acknowledgements

I would like to sincerely thank my supervisor, Dr. Milica Radisic, for giving me the opportunity to be exposed to the cutting-edge research in this field. Her continual guidance, support and encouragement, in both academic and personal matters, was invaluable. I also greatly appreciate the assistance and support from all members of the Laboratory of Functional Tissue Engineering. Thank you also to my family and friends for the all their encouragement over the last 2 years, especially during tough periods, and to my parents for allowing me the freedom to pursue my personal goals.

In addition, I would like to thank Rohin Iyer for help with SEM, Dr Christopher Yip, and respectively Dr. Partick Yang and Gary Mo for assistance with AFM and confocal microscopy. This work was supported by the grants from National Science and Engineering Research Council (NSERC DG), Canada Foundation for Innovation (Leaders Opportunity Fund), Ontario Research and Development Challenge Fund (ARTEC), NIH grant R01HL076485 and University of Toronto Open Fellowships.

## Table of Contents

<b>ABSTRACT</b> .....	ii
<b>Acknowledgements</b> .....	iii
<b>LIST OF FIGURES</b> .....	vii
<b>LIST OF TABLES</b> .....	ix
<b>LIST OF SYMBOLS AND ABBREVIATIONS</b> .....	x
<b>1. Background</b> .....	1
<b>1.1 Motivation</b> .....	1
<b>1.2 Hypothesis</b> .....	3
<b>1.3 Overall Objective and Specific Aims</b> .....	3
<b>1.3 References</b> .....	4
<b>2. Interactive effects of contact guidance and of surface topography and pulsatile electrical field stimulation on orientation and elongation of fibroblasts and cardiomyocytes</b> .....	5
<b>2.1 Introduction</b> .....	5
<b>2.2 Methods</b> .....	6
2.2.1 <i>Microabraded surfaces</i> .....	6
2.2.2 <i>Cells</i> .....	7
2.2.3 <i>Cell culture</i> .....	7
2.2.4 <i>Pharmacologic studies</i> .....	9
2.2.5 <i>Assessments</i> .....	9
2.2.6 <i>Statistical analysis</i> .....	11
<b>2.3 Results</b> .....	11
2.3.1 <i>Abraded surfaces as a model system for study of topographical cues</i> .....	11
2.3.2 <i>Interactive effects of contact guidance and electrical field stimulation on fibroblasts and cardiomyocytes</i> .....	12
2.3.3 <i>Presence of cardiac markers and contractile properties</i> .....	14
2.3.4 <i>Pharmacological studies</i> .....	15
<b>2.4 Discussion</b> .....	17
2.4.1 <i>Selection of topographical cues, electrical field stimulation conditions and pharmacological agents</i> .....	18
2.4.2 <i>Effects of surface topography and electrical field stimulation on orientation and elongation of fibroblasts and cardiomyocytes</i> .....	19
2.4.3 <i>Significance of the findings</i> .....	21
2.4.4 <i>Implications of the findings for cardiac tissue engineering</i> .....	23
<b>2.5 Conclusions</b> .....	24
<b>2.6 Figures and Tables</b> .....	25

<b>3. Microgrooved surfaces with integrated electrodes for simultaneous application of topographical and electrical cues in cell culture</b> .....	38
<b>3.1 Introduction</b> .....	38
<b>3.2 Methods</b> .....	40
3.2.1 <i>Hot embossing mold fabrication</i> .....	40
3.2.2 <i>Hot embossing for preparation of microstructured polystyrene surfaces</i> .....	40
3.3.3 <i>Electrode fabrication</i> .....	40
3.3.4 <i>O2 Plasma Treatment</i> .....	41
3.3.5 <i>Scanning electron microscopy</i> .....	41
3.3.6 <i>Cell Source</i> .....	41
3.3.7 <i>Cell Culture</i> .....	41
3.3.8 <i>Cell Staining and Assessment</i> .....	42
3.3.9 <i>Image Analysis</i> .....	43
3.3.10 <i>Excitation threshold and maximum capture rate</i> .....	43
3.3.11 <i>Statistical Analysis</i> .....	43
<b>3.3 Results and Discussion</b> .....	44
3.3.1 <i>Hot embossing of polystyrene for fabrication of microgrooved surfaces with built-in electrodes</i> .....	44
3.3.2 <i>Cardiomyocyte phenotype and function on microgrooved polystyrene surfaces</i> .....	45
3.3.3 <i>Electrical stimulation during culture of cardiomyocytes</i> .....	48
3.3.4 <i>Advantages over previous cell culture set-ups</i> .....	50
<b>3.4 Conclusions</b> .....	52
<b>3.5 Figures and Tables</b> .....	53
<b>3.6 References</b> .....	57
<b>4. The differentiation of human embryonic stem cells derived cardiomyocytes</b> .....	60
<b>4.1 Introduction</b> .....	60
<b>4.2 Methods</b> .....	63
4.2.1 <i>Cells</i> .....	63
4.2.2 <i>Cell culture</i> .....	63
4.2.3 <i>Cell staining and assessment</i> .....	64
4.2.4 <i>Image Analysis</i> .....	64
4.2.5 <i>Excitation Threshold and Maximum Capture Rate</i> .....	64
4.2.6 <i>Statistical Analysis</i> .....	65
<b>4.3 Results</b> .....	65
4.3.1 <i>Morphology of cell cultures seeded on various surfaces</i> .....	65
4.3.2 <i>Functional properties</i> .....	66
<b>4.4 Discussion</b> .....	66
4.3.2 <i>Presence of cardiac marker and contractile apparatus</i> .....	68
4.3.3 <i>Cellular alignment and elongation for non-stimulated constructs</i> .....	68
4.3.4 <i>Contractile Properties for non-stimulated constructs</i> .....	69
4.3.5 <i>Selection of an abraded surface</i> .....	70
4.3.6 <i>Application of electrical field stimulation</i> .....	71
<b>4.4 Conclusions</b> .....	72
<b>4.5 Figures and Tables</b> .....	73

4.6 References.....	74
<b>5. The identification and isolation of <i>isl1</i><sup>+</sup> cardiac progenitors in the neonatal rat heart</b> .....	76
<b>5.1 Introduction</b> .....	76
<b>5.2 Methods</b> .....	80
5.2.1 <i>Cells</i> .....	80
5.2.2 <i>Cell Culture</i> .....	80
5.2.3 <i>Identification of the <i>isl1</i><sup>+</sup> progenitors</i> .....	81
<b>5.3 Results</b> .....	82
5.3.1 <i>Autofluorescence and immunostaining for <i>isl1</i></i> .....	82
5.3.2 <i>Flow cytometry</i> .....	83
5.3.3 <i>Cell morphology during the cultivation period</i> .....	83
5.3.4 <i>Immunostaining for <i>DDR2</i></i> .....	84
<b>5.4 Discussion</b> .....	84
5.4.1 <i>Issues with identification</i> .....	84
5.4.2 <i>Improving the culture medium</i> .....	86
5.4.3 <i>Prospects of isolating and enriching for the <i>isl1</i><sup>+</sup> population</i> .....	87
<b>5.5 Conclusions</b> .....	88
<b>5.6 Figures</b> .....	89
<b>5.7 References</b> .....	92
<b>6. Summary</b> .....	94
<b>6.1 Future Work</b> .....	97
<b>6.2 Recommendations</b> .....	98
<b>7. Appendices</b> .....	A-1
<b>S2. Supplementary Figures for Chapter 2</b> .....	A-1
<b>S5. Appendices for Chapter 5</b> .....	A-5
<b>S5.1 Methods to isolate and expand <i>isl1</i><sup>+</sup> progenitors</b> .....	A-5
<b>S5.2 Discussion: Problems with the separation techniques</b> .....	A-7
<b>S5.3 Supplemental Figures</b> .....	A-9

## LIST OF FIGURES

Figure		Page
2.1	Abraded surfaces	25
2.2	Elongation and orientation of fibroblasts and cardiomyocytes cultivated on abraded and non-abraded surfaces	26
2.3	Interactive effects of topographical cues and electrical stimulation on fibroblasts and cardiomyocytes	27
2.4	Immunostaining for cardiac Troponin I of cardiomyocytes cultivated in the presence of electrical field stimulation on abraded surfaces	28
2.5	Actin cytoskeleton in cardiomyocytes cultivated in the presence of electrical field stimulation on abraded surfaces	29
2.6	Effects of pharmacological agents on elongation and orientation of cardiomyocytes cultivated on non-abraded and abraded surfaces	30
2.7	Immunostaining for cardiac Troponin I of cardiomyocytes treated with pharmacologic agents	31
2.8	Actin cytoskeleton in cardiomyocytes treated with pharmacologic agents	32
3.1	Microgrooved surfaces prepared by hot embossing of polystyrene	54
3.2	Cardiomyocytes cultivated on microgrooved polystyrene surfaces without electrical field stimulation	55
3.3	Sarcomeric $\alpha$ -actinin staining of cardiomyocytes cultivated on the microgrooved polystyrene surfaces	55
3.4	Cardiomyocytes cultivated on microgrooved surfaces (1 $\mu\text{m}$ ) in the presence of electric field stimulation	56
3.5	Sarcomeric $\alpha$ -actinin staining of cardiomyocytes cultivated on the microgrooved polystyrene surfaces in the presence of electric field stimulation	56
4.1	Immunostaining for sarcomeric $\alpha$ -actinin of hESC-CMs cultivated manually abraded coverslips	74
4.2	Immunostaining for sarcomeric $\alpha$ -actinin of hESC-CMs cultivated microstructured surfaces made by hot embossing	74

5.1	Autofluorescence and non-specific staining in primary cells	90
5.2	Flow cytometry analysis on PP1 cells cultured in various media at day 4	91
5.4	Effects of BIO on cell morphology	92
5.5	Immunostaining of cell surface receptor DDR2 in NIH3T3 fibroblasts	92

## LIST OF TABLES

<b>Table</b>		<b>Page</b>
2.1	Contractile properties of cardiomyocytes as a function of surface abrasins and electrical field stimulation	33
2.2	Effect of pharmacologic agents on contractile properties of cardiomyocytes cultivated in the presence of electrical field stimulation on non-abraded and abarded surfaces placed parallel to the field lines	33
3.1	Functional properties of cardiomyocytes cultivated on microgrooved surfaces without electric field stimulation	57
3.2	Electrical excitability of cardiomyocytes cultivated on microgrooved surfaces of 1 $\mu\text{m}$ period in the presence of electric filed stimulation	57
4.1	Approximate ET and MCR values of non-stimulated hESC-CMs after 5 days of cultivation	75

## LIST OF SYMBOLS AND ABBREVIATIONS

AFM	atomic force microscopy
AMCA	7-amino-4-methyl-3-coumarinylacetic acid
bFGF	basic fibroblast growth factor
BIO	6-bromoindirubin-3'-oxime
BMP4	bone morphogenetic protein 4
CFDA	carboxyfluorescein diacetate, succinimidyl ester
c-kit	CD311 cytokine receptor
CM	cardiomyocyte
CO <sub>2</sub>	carbon dioxide
Cx43	connexin 43
CXCR4	chemokine (c-x-c motif) receptor 4
DC	direct current
DKK1	dickkopf homolog 1
DMEM	Dulbecca's Modified Eagle Medium
EB	embryoid body
ECM	extracellular matrix
EDTA	ethylenediamine tetra-acetic acid
EGF	epidermal growth facotr
ESC	embryonic stem cell
ET	excitation threshold
FBS	fetal bovine serum
FITC	fluorescein isothiocyanate
flk1	vascular endothelial growth factor receptor 2
GSK3	glycogen synthase kinase-3
HBSS	Hank's balanced salt solution
HEPES	N-2-hydroxyethylpiperazine-N-2-ethanesulfonic acid
hESC	human embryonic stem cell
hESC-CM	human embryonic stem cell-derived cardiomyocyte
iPS	induced pluripotent stem (cell)
Isl1	islet-1
KDR	kinase insert domain receptor
MCR	maximum capture rate
MDR1	multidrug-resistant gene product 1
MI	myocardial infarction
MLC-2	myosin light chain-2
MTG	monothioglycerol
NCS	newborn calf serum
Nkx2.5	NK2 transcription factor related, locus 5
PBS	phosphate buffered saline
PFA	paraformaldehyde
PI	propidium iodide
PI3K	phosphatidyl-inosital 3 kinase
PLA	poly(lactide)
sca-1	stem cell antigen 1

SEM	scanning electron microscopy
SMC	smooth muscle cell
SSEA-1	stage specific embryonic antigen 1
TCPS	tissue culture polystyrene
TnI	troponin I
TRITC	tetramethyl rhodamine iso-thiocyanate
VEGF	vascular endothelial growth factor

## 1. Background

### 1.1 Motivation

Myocardial infarction (MI) affects approximately 1 million people every year in North America [1]. The heart, unlike other organs such as the liver, does not self-regenerate once damaged; as a result, a significant number of cardiomyocytes (the contractile cells of the heart) which die in the area of infarct leads to the emergence of a “dead zone”. Substantial death results in the loss of heart function as well as pathological remodelling of the organ, including the thinning of the myocardium and cardiac dilation, which in itself can lead to further deterioration of contractile function. Other cardiovascular conditions, such as genetic disorders, may also cause a loss, albeit less abrupt, of cardiomyocytes (CMs). It is important to note that the heart will fail to function properly should the number of functional CMs fall below a certain threshold. The inability of the myocardium to regenerate or repair itself means that substantial heart injury will lead to severe problems for other organs of the body, and ultimately death of the person.

Currently, heart transplants represent one of the only means to sustain life and restore heart function at the later stages of heart failure. However, due to shortage of heart donors and biocompatibility issues (such as immune rejection), a more feasible alternative is required to treat MI patients and patients with degenerative cardiac diseases. Cardiac tissue engineering may represent a possible solution to this problem. Tissue-engineered contractile patches, which have contractile properties and cellular composition similar to native heart tissue, may replace the damaged tissue portion in the organ and restore or improve functionality. In this approach, cells are cultivated in a scaffold (preferably biodegradable) to generate tissue constructs that can mimic the native tissue of the myocardium. This construct can then be implanted into the infarct zone for restore function.

One of the major obstacles in creating this tissue-engineered construct is harnessing the appropriate cell source. The ideal cell source should be autologous (harvested from the patient) in the interest of lowering the risk of immune rejection. The selected candidate should be able to differentiate into a mature phenotype similar to that of the cells in the

native heart, especially that of ventricular cardiomyocytes, which consist of most of the volume (70-80%) in the native myocardium [2]. They should also ideally possess some capacity of expansion and proliferation, such that the cells can be maintained and passaged. Cell sources which have been considered for cardiac repair include skeletal muscle cells [3], embryonic stem cells (ESCs) [4], mesenchymal stem cells [5], all of which have demonstrated some promise for this application. However, problems which hamper their feasibility include low survival rate, lack of proper integration or engraftment between the graft and host cells, and more seriously, in the case of ESCs, tumour formation due to the presence of some undifferentiated cells. In the search for an autologous source, Laugwitz et al. reported in 2005 a group of *isl1*<sup>+</sup> progenitors in the neonatal mouse and human hearts which have the capacity to self-renew and to differentiate into functional cardiomyocytes [6]. However, the isolation and expansion of this population, to the extent required by tissue engineering applications, remains an issue. In addition to *isl1*, others have also reported the presence of “cardiac stem cells” or cardiac progenitors identified by other markers including *c-kit*, *1* [7], *sca-1* [7, 8], *SSEA-1* [8], *KDR/flk1* [9, 10], *CXCR4* [9, 10], *Nkx2.5* [10]. Other potential cell sources include ESC derived cardiomyocytes (ESC-CMs) [11] and induced pluripotent stem (iPS) cells [12], both of which have demonstrated the ability to differentiate into contractile cells and as well as other cell types that support or promote the survival of CMs.

Once an appropriate cell source has been identified, it would be necessary to find the means to achieve the proper phenotype in culture for the purpose of tissue engineering. *In vivo*, CMs are exposed to multiple biochemical and physical cues, including topographical and electrical cues, from their surrounding environment. These microenvironmental cues direct cell maturation, differentiation and phenotype to create a mosaic of cells, in the proper proportions, in order to fulfill their intended roles within the heart. Thus, this study strives to investigate the methodologies by which various immature cardiac cell sources can be matured into the desired CM phenotype, under the application of external stimuli such as contact guidance and electrical field stimulation. The tissue constructs were subjected to the external cues under two different systems, which will be explained below. The cell types considered in this study were neonatal rat CMs and hESC-CMs. This study also explored ways in which *isl1*<sup>+</sup> progenitors in the rat

heart could be isolated and examined their potential as a self-renewing source for myocardium repair.

## **1.2 Hypothesis**

We hypothesized that a combination of electrical stimulation and contact guidance would enhance the maturation and differentiation of cardiac progenitors and cardiomyocytes, based on the belief that external stimuli are important not only to cellular development, but also to the orientation of cells within their extracellular matrix (ECM) with respect to their surrounding cells. Contact guidance and electrical field stimulation may also enhance contractile properties of the cells.

## **1.3 Overall Objective and Specific Aims**

This project falls into the bigger scheme of research activities which surround the search for methods to produce better tissue engineering constructs for the purpose of myocardium repair, as an alternative to organ transplant. The overall objective of this study was to achieve the *in vivo*-like cardiomyocyte phenotype from immature cardiac cells, with the application of contact guidance and electrical field stimulation. The study involved the following specific aims:

- i. To develop a cell culture system that combines electrical and contact guidance cues via the following:
  - a. polyvinyl carbonate substrates with manually made microabrasions, placed within in electrical stimulation chamber
  - b. microfabricated (via hot embossing) tissue culture polystyrene substrates, with built-in gold electrodes
- ii. To determine the effect of electrical stimulation and contact guidance on neonatal rat heart cells (fibroblasts and CMs)

- iii. To determine the interactive effect of electrical stimulation and contact guidance in the maturation of hESC-CMs.
- iv. To identify and isolate  $isl1^+$  progenitors population from the neonatal rat heart, to characterize the population and to differentiate the cells via the application of electrical stimulation and contact guidance.

Each of the specific aims will be addressed individually in each of the following chapters.

### 1.3 References

1. American Heart Association, 2004.
2. Schaub, M.C., et al., Various hypertrophic stimuli induce distinct phenotypes in cardiomyocytes. *J Mol Med*, 1997. 75(11-12): p. 901-20.
3. Dorfman, J., et al., Myocardial tissue engineering with autologous myoblast implantation. *J Thorac Cardiovasc Surg*, 1998. 116(5): p. 744-51.
4. Klug, M.G., et al., Genetically selected cardiomyocytes from differentiating embryonic stem cells form stable intracardiac grafts. *J Clin Invest*, 1996. 98(1): p. 216-24.
5. Toma, C., et al., Human mesenchymal stem cells differentiate to a cardiomyocyte phenotype in the adult murine heart. *Circulation*, 2002. 105(1): p. 93-8.
6. Laugwitz, K.L., et al., Postnatal  $isl1^+$  cardioblasts enter fully differentiated cardiomyocyte lineages. *Nature*, 2005. 433(7026): p. 647-53.
7. Bearzi, C., et al., Human cardiac stem cells. *Proc Natl Acad Sci U S A*, 2007. 104(35): p. 14068-73.
8. Ott, H.C., et al., The adult human heart as a source for stem cells: repair strategies with embryonic-like progenitor cells. *Nat Clin Pract Cardiovasc Med*, 2007. 4 Suppl 1: p. S27-39.
9. Yang, L., et al., Human cardiovascular progenitor cells develop from a  $KDR^+$  embryonic-stem-cell-derived population. *Nature*, 2008. 453(7194): p. 524-8.
10. Nelson, T.J., et al.,  $CXCR4^+/FLK-1^+$  biomarkers select a cardiopoietic lineage from embryonic stem cells. *Stem Cells*, 2008. 26(6): p. 1464-73.
11. Kubo, A., et al., Development of definitive endoderm from embryonic stem cells in culture. *Development*, 2004. 131(7): p. 1651-62.
12. Schenke-Layland, K., et al., Reprogrammed mouse fibroblasts differentiate into cells of the cardiovascular and hematopoietic lineages. *Stem Cells*, 2008. 26(6): p. 1537-46.

## **2. Interactive effects of contact guidance and of surface topography and pulsatile electrical field stimulation on orientation and elongation of fibroblasts and cardiomyocytes<sup>1</sup>**

### **2.1 Introduction**

Tissue engineering of functional cardiac patches critically depends on our ability to achieve appropriate structural organization of cardiomyocytes and fibroblasts, two major cell populations found in the native myocardium. Orientation and elongation of these cells is governed by a number of cues, including electrical and topographical cues. Understanding the individual and interactive effects of these cues will ultimately enable design of improved tissue culture systems.

In previous studies, it has been shown that embryonic fibroblasts cultivated in DC electric fields, oriented perpendicular to the electric field lines and migrated towards the cathodal end of the field [1]. Chronic supra-threshold electrical field stimulation of cardiomyocytes in 2D was shown to preserve contractility [2], maintain calcium transients [3], promote hypertrophy [4], increase protein synthesis [5,6] and maintain action potential duration and maximum capture rate [7]. The beneficial effects of field stimulation were depended on the occurrence of contraction following field-stimulated excitation, as evidenced by the lack of observed effects in the presence of excitation-contraction decouplers: verapamil or 2,3-butanedione monoxime [8]. In 3D studies we demonstrated [9], that electrical field stimulation can be used to engineer functional cardiac tissue expressing hallmarks of cardiac differentiation. Stimulated constructs had thick elongated and aligned myofibers expressing cardiac markers, in contrast to non-stimulated constructs that contained round cells [9]. Importantly, the collagen scaffold used in these studies had isotropic pore structure, thus no preferential topographical cues were provided for guidance of cellular orientation and elongation.

Microstructured grooves were used previously in 2D to direct orientation and elongation of fibroblasts [10- 13]. The process was dependent upon the orientation of actin cytoskeleton [12] that also oriented along the direction of the grooves. Nuclear

---

<sup>1</sup> This chapter contains identical text as a paper published in *Biomaterials* 28(2007) under the same title, with the following authors: Hoi Ting H. Au, Irene Cheng, Mohammad F. Chowdhury, Milica Radisic

deformation and elongation was linked to the changes in gene expression on microstructured surfaces [14]. Elongated cardiomyocyte phenotype and alignment was achieved by cultivating cardiomyocytes on microtextured silicone membranes [15 -17] that were in some cases microfluidically patterned with extracellular matrix molecules [18]. Topographical cues or microcontact printing of extracellular matrix components were previously used to improve tissue engineering of cardiac patches. Zong and colleagues [19] used electrospinning to fabricate oriented biodegradable non-woven poly(lactide) (PLA) scaffolds that guided cardiomyocyte orientation. The orientation and cardiomyocyte phenotype could also be improved by microcontact printing of extracellular matrix components (e.g. laminin) on thin polyurethane and PLA films [20,21].

Yet, the interaction of topographical cues and pulsatile electrical field stimulation on the phenotypic changes in fibroblasts and cardiomyocytes has not been studied. The main objective of this study was to determine the interactive effects of contact guidance and electrical field stimulation on elongation and orientation of fibroblasts and cardiomyocytes, the major cell populations of myocardium. The cells were cultivated on 2D-abraded surfaces and field-stimulated using regime of relevance for heart tissue in vivo as well as for cardiac tissue engineering (square supra-threshold pulses, 1 ms duration, 1 Hz). We hypothesized that the same molecular pathways may be involved in cellular response to both cues and performed pharmacologic studies to assess the relevance of actin cytoskeleton and phosphatidylinositol 3 kinase (PI3K) pathway. Our findings indicate that contact guidance more strongly determined cellular orientation in both cell types than electrical field stimulation, while elongation on non-abraded surfaces could effectively be modulated by electrical field stimulation.

## **2.2 Methods**

### ***2.2.1 Microabraded surfaces***

Microrstructured surfaces were prepared using the method previously described for cultivation of cardiomyocytes by Bursac et al. [22]. Polyvinyl carbonate cover slips (22×22 mm<sup>2</sup>) were abraded using lapping paper with various abrasion grain sizes from McMaster-Carr (aluminum oxide 30, 40, 60, 80 μm) and Ultratech, USA (silicone

carbide 1, 3, 5, 9, 12  $\mu\text{m}$ ). One half of the cover slip was abraded in one direction and the other half of the cover slip was abraded in the perpendicular direction in order to observe the cells' response to two different topographical cues on the same cover slip. The control surfaces were left non-abraded. Particulate debris was removed by sonicating (Misonix Ultrasound cleaner, model 1510R-MT) the surfaces in soap and water followed by rinsing in distilled water. The surfaces were sterilized in 95% ethanol for 24 h, followed by drying and UV irradiation for 30 min. For cardiomyocyte culture, the surfaces were coated with 25  $\mu\text{g}/\text{mL}$  of bovine fibronectin in PBS for 2 h [22] to enhance cell attachment.

### 2.2.2. Cells

NIH3T3 fibroblasts were cultivated in T-75 flasks in Dulbecco's Modified Eagle Medium (DMEM) containing 4.5 g/L glucose, supplemented with 10% v/v fetal bovine serum (FBS), 1% v/v of N-2-hydroxyethylpiperazine-N-2ethanesulfonic acid (HEPES) (Gibco), and penicillin–streptomycin (Gibco, 100 units/mL and 100  $\mu\text{g}/\text{mL}$ , respectively). Cells were subcultured and passaged as they reached 80% confluency, typically every 3–4 days.

Cardiomyocytes were obtained from the hearts of 2-day neonatal Sprague–Dawley rats as in our previous studies [23-25] and according to the protocol approved by the University of Toronto Committee on Animal Care. Briefly, the hearts were quartered and incubated overnight at 4 °C in a 0.06% (w/v) solution of trypsin (Sigma) in freshly prepared Hank's balanced salt solution (HBSS) (Gibco). Subsequently, the hearts were subjected to a series of five digestions (8 min, 37 °C, 70 rpm) in collagenase type II (Worthington, 220 units/mL) in HBSS. The cell suspension was then pre-plated for 60 min to enrich for cardiomyocytes. Cell count and viability were determined via trypan blue exclusion using a hemocytometer. Culture medium was the same as for NIH 3T3 fibroblasts.

### 2.2.3 Cell culture

For experiments without electrical field stimulation, we followed the procedure developed by Bursac et al. [26]. Briefly, the abraded cover slips were cut into circular

discs of 15 mm diameter and placed in a 24-well tissue culture plate (1 cover slip/well). The fibroblasts (100,000 cells per disc) and cardiomyocytes (50,000 cells per disc) were seeded in 1 mL of culture media. The cells were cultured in a 37 °C, 5% CO<sub>2</sub> incubator for 1 week. The culture medium was replaced by 100% every other day.

The electrical stimulation chamber setup was based on the one we developed previously [9]. The cells were placed in between two carbon electrodes (Ladd Research Industries) that were held 1 cm apart via a polycarbonate holder positioned in a 100×15 mm<sup>2</sup> glass Petri dish. The electrodes were connected via Platinum wires to the programmable stimulator (Grass s88x, Astromed, Longueuil, QC).

For electrical stimulation experiments, the abraded cover slips (described in Section 2.1) were cut into 8×22 mm<sup>2</sup> rectangles and then, folded along the two shorter edges to form a construct resembling a table with a surface area of 8×10 mm<sup>2</sup>. The purpose of folding the cover slips was to ensure that the cells cultured on the cover slips were placed at the identical height in the center between the carbon electrodes used for electrical stimulation. Each chamber contained four cover slips; two cover slips with one half of the abrasions parallel and the other half perpendicular to the electrodes and two non-abraded cover slips to serve as controls (Figure S1). The fibroblasts and cardiomyocytes (20,000 cells and 500,000 cells per cover slip, respectively) were seeded using 60 μL of culture medium for 60 min, followed by addition of 30 mL of culture medium. The cells were cultivated for 24 h without electrical field stimulation in order to allow the cells to attach, followed by electrical field stimulation for additional 72 h using square monophasic pulses, 1 ms duration and 1 Hz. In preliminary studies, excitation threshold for cardiomyocytes after 24 h in culture was determined to be 2.3 V/cm. Electrical field stimulation conditions were selected to correspond to the excitation threshold (2.3 V/cm), and 200% of excitation threshold (4.6 V/cm) to ensure that all cells, and not just the most excitable cells, are contracting in response to field stimulation. The control group was not stimulated (0.0 V/cm). The desired stimulation regime was confirmed using an oscilloscope. The medium pH was maintained during culture; no observable gas formation occurred. There were three independent experiments with a total of N=6 samples per group.

#### 2.2.4 Pharmacologic studies

To explore the mechanism of the cells' response to topographical cues and electrical field stimulation we treated cardiomyocytes during cultivation with Cytochalasin D (2  $\mu\text{m}$ , Sigma) an inhibitor of actin polymerization, or LY294002 (50  $\mu\text{m}$ , Sigma) a blocker of PI3K pathway. The drugs were applied to cardiomyocytes 24 h after seeding and they were maintained in the culture medium for the duration of the experiment (additional 72 h). Electrical field stimulation using monophasic square pulses 1 ms duration, 1 Hz and 4.6 V/cm was initiated 24 h after seeding (upon the addition of pharmacological agents). Non-stimulated samples (0.0 V/cm) served as controls. The abraded surfaces were placed in the chamber with abrasions parallel to the field lines. Two independent experiments were conducted with a total of N=3 independent samples per group.

#### 2.2.5 Assessments

##### *2.2.5.1 Scanning electron microscopy (SEM)*

Cell-free abraded cover slips were sonicated in soap and water (Misonix Ultrasound cleaner, model 1510R-MT) to remove dust and debris. The samples were sputter coated with gold and imaged via SEM (Hitachi S-570) with a backscatter detector.

##### *2.2.5.2 Atomic force microscopy (AFM)*

Tapping mode AFM (TMAFM) images of surfaces abraded using lapping paper with 1, 2, 9, 12, 40 and 90  $\mu\text{m}$  grain size were acquired in ambient air on a Veeco Multimode SPM (Santa Barbara, CA) equipped with a "J" scanner (150 $\times$ 150  $\mu\text{m}^2$  maximum lateral scan area), using 125  $\mu\text{m}$  long PPP-NCH Nanosensors (NanoWorld AG, Neuchatel, Switzerland). The images were captured at a frequency of 280 kHz and adjusted for individual cantilever. All AFM images were collected with a resolution of 512 $\times$ 512 pixel<sup>2</sup>, at scan rates of 1 Hz. All images were flattened and plane fitted using the Nanoscope IIIa version 4.42r9 (Veeco, Santa Barbara, CA). For each grain size, two independent surfaces were imaged. At each surface 2–3 independent regions of 20, 40 or 60  $\mu\text{m}$  wide and 512 lines high were captured. Abrasion width and depth were

determined with the Nanoscope IIIa version 4.42r9 software on cross-sectional profiles of the captured AFM images (Figure S1B). Total of N=20–30 data points were collected for each grain size. The number of abrasions was manually counted in each AFM image, and divided by the width of the image in microns (20, 40, or 60  $\mu\text{m}$  width) to determine the abrasion density.

#### *2.2.5.3 Cell staining and microscopy*

Tapping mode AFM (TMAFM) images of surfaces abraded using lapping paper with 1, 2, 9, 12, 40 and 90  $\mu\text{m}$  grain size were acquired in ambient air on a Veeco Multimode SPM (Santa Barbara, CA) equipped with a “J” scanner ( $150 \times 150 \mu\text{m}^2$  maximum lateral scan area), using 125  $\mu\text{m}$  long PPP-NCH Nanosensors (NanoWorld AG, Neuchatel, Switzerland). The images were captured at a frequency of 280 kHz and adjusted for individual cantilever. All AFM images were collected with a resolution of  $512 \times 512$  pixel<sup>2</sup>, at scan rates of 1 Hz. All images were flattened and plane fitted using the Nanoscope IIIa version 4.42r9 (Veeco, Santa Barbara, CA). For each grain size, two independent surfaces were imaged. At each surface 2–3 independent regions of 20, 40 or 60  $\mu\text{m}$  wide and 512 lines high were captured. Abrasion width and depth were determined with the Nanoscope IIIa version 4.42r9 software on cross-sectional profiles of the captured AFM images (Figure S1B). Total of N=20–30 data points were collected for each grain size. The number of abrasions was manually counted in each AFM image, and divided by the width of the image in microns (20, 40, or 60  $\mu\text{m}$  width) to determine the abrasion density.

#### *2.2.5.4 Image analysis*

ImageJ software was used to determine cell alignment and elongation. Cell alignment was determined from live/dead stained images by measuring the angle between the abrasion and the long axis of the cell. Region of interest in the images was enlarged until the cell outlines (bright green) were clearly visible. For each fluorescent image, a corresponding bright field image was taken in order to determine abrasion direction relative to the long axis of the cell. Elongation was determined by measuring the long and short axes of the cell and calculating the aspect ratio (long to short axis ratio). Cells of which the perimeters could not be precisely determined were excluded from the analysis

(10%). For cells that were cultured on non-abraded surfaces, the angle between the cell's long axis and either the axis that was perpendicular (for fibroblasts) or parallel (for cardiomyocytes) to the electric field was measured. These direction were selected based on the previous studies that have demonstrated that fibroblasts aligned perpendicular [1], while cardiomyocytes aligned parallel to the electric field lines [9].

#### *2.2.5.5 Excitation threshold and maximum capture rate for cardiomyocytes*

We determined the contractile function of the cardiomyocytes by measuring the excitation threshold (ET) and maximum capture rate (MCR) before and after the electrical stimulation period as described in our previous studies [24]. ET was defined as a minimum voltage required to induce synchronous contractions of at least 75% of the cells in the field of view using monophasic pulses 2 ms duration and 1 Hz. MCR was defined as a maximum beating frequency at 200% of ET. The measurement was performed at room temperature in culture medium using a tissue culture microscope (Olympus CKX41).

#### *2.2.6 Statistical analysis*

Tests for normality and equality of variance were performed on all data sets. For data that were normally distributed and with equal variance we performed one-way ANOVA in conjunction with Student–Newman–Keuls test for pairwise comparisons. Otherwise, Kruskal–Wallis one-way ANOVA on ranks was utilized followed by pairwise comparisons using Dunn's test (Sigma Sat 3.0). The significance level for all tests was  $P < 0.05$ .

### **2.3 Results**

#### *2.3.1 Abraded surfaces as a model system for study of topographical cues*

Abraded surfaces with topographic cues of the micron size were prepared on polyvinyl cover slips by the previously described method [22], using a lapping paper with grain size in the range of 1–80  $\mu\text{m}$ . Scanning electron microscopy demonstrated that with the increased grain size, the width and the depth of the abrasions obtained on the surface

increased (Figure 2.1A and B) while abrasion density decreased (Figure 2.1C). AFM analysis indicated that the abrasions were V-shaped, although they were significantly less uniform than abrasions prepared previously by micromachining [27, 28] and microfabrication [17] techniques.

Although all abraded surfaces qualitatively improved the elongation of NIH 3T3 fibroblasts (Figure 2.2A–C and, Figure S2), the effect was statistically significant (compared to non-abraded) for the surfaces abraded with grain size 30–60  $\mu\text{m}$  (average width from 9.7 to 13  $\mu\text{m}$ , and depth from 640 to 700 nm). Box plots were utilized to represent cellular orientation, since on abraded surfaces cells cluster around a low orientation angle, i.e. the angle distribution is not Gaussian. In box plots, the line in the middle of the box defines the median value; the ends of the boxes define the 25th and 75th percentiles, and error bars defining the 10th and 90th percentiles. Fibroblasts cultivated on non-abraded surfaces had a random distribution (Figure 2.2A and C). The surfaces abraded with grain size from 9 to 80  $\mu\text{m}$  significantly improved cell orientation along the direction of the grooves compared to the non-abraded controls.

Cardiomyocyte cultivation on abraded surfaces resulted in high viability in all groups (live/dead staining, Figure 2.2D) and a statistically significant effect on elongation (aspect ratio, Figure 2.2E). Cardiomyocytes cultivated on the surfaces abraded with lapping paper of grain size 40 and 80  $\mu\text{m}$  were significantly more elongated (Figure 2.2E) and aligned (Figure 2.2F) than those cultivated on non-abraded surfaces. Since surfaces abraded with lapping paper of 80  $\mu\text{m}$  grain size (average abrasion width of 13  $\mu\text{m}$  and depth of 700 nm) exhibited the strongest effect on cardiomyocyte elongation and orientation as well as statistically significant effect on orientation of fibroblasts, they were used for electrical field stimulation experiments. The non-abraded polyvinyl cover slips served as controls.

### 2.3.2 Interactive effects of contact guidance and electrical field stimulation on fibroblasts and cardiomyocytes

Electrical field stimulation did not have any adverse effects on viability of fibroblasts (Figure S3) and cardiomyocytes (Figure S4) as indicated by majority of green

(live) cells in the live/dead staining. At low voltage (0.0 and 2.3 V/cm) fibroblasts were significantly more elongated on abraded compared to non-abraded surfaces (Figure 2.3A, stars). Yet, at 4.6 V/cm there was no statistically significant difference in the elongation of fibroblasts cultivated on abraded vs. non-abraded surfaces, due to the fact that elongation on non-abraded surfaces increased significantly in the stimulated groups (Figure 2.3A, white bars). Fibroblasts cultivated on abraded surfaces were also significantly more aligned (smaller angle, Figure 2.3B) compared to those cultivated on non-abraded surfaces at all field strengths (0.0, 2.3 and 4.6 V/cm). Yet, electrical field stimulation significantly enhanced the alignment of fibroblasts on abrasions that were placed perpendicular to the field lines (Figure 2.3B, light-gray bars). This result is consistent with previously reported findings that fibroblasts preferentially orient perpendicular to the field lines in DC fields [1]. For fibroblasts cultivated on non-abraded surfaces, there was a qualitative shift in orientation angle towards the direction perpendicular to the field lines at the highest field strength investigated (4.6 V/cm) (Figure 2.3B, white bars).

Overall we observed two effects of the field stimulation on fibroblasts: (i) fibroblast elongation on non-abraded surfaces was significantly enhanced by electrical field stimulation and (ii) electrical field stimulation promoted orientation of fibroblasts in the direction perpendicular to the field lines when the abrasions were also placed perpendicular to the field lines.

We observed similar effects of the field stimulation on the elongation of cardiomyocytes as a function of topographical cues (Figure 2.3C). At 0.0 and 2.3 V/cm, cardiomyocytes were significantly more elongated on abraded surfaces compared to the non-abraded surfaces (Figure 2.3C, stars), while there was no significant difference at 4.6 V/cm. Specifically, cardiomyocyte elongation on non-abraded surfaces increased significantly at the highest field strength and became comparable to that of abraded surfaces (Figure 2.3C, white bars). Topographical cues had significantly stronger effect on cardiomyocyte orientation. At all field strengths investigated, the abraded surfaces had significantly smaller average orientation angle compared to the non-abraded surfaces (Figure 2.3D). There was a slight, but not significant, decrease of the orientation angle on

non-abraded surfaces (Figure 2.3D, white bars) stimulated at 4.6 V/cm, indicating that the cells may be starting to orient parallel to the field lines.

Overall we observed that (i) cardiomyocyte elongation on non-abraded surfaces was significantly enhanced by electrical field stimulation and (ii) topographical cues were a significantly stronger determinant of cardiomyocyte orientation than the electrical field stimulation.

### 2.3.3 Presence of cardiac markers and contractile properties

The cell phenotype was validated by immunostaining for phenotypic markers vimentin for fibroblasts (data not shown), and Troponin I for cardiomyocytes (Figure 2.4). Presence of connexin-43, a gap junctional protein required for electrical communication between the cells was also documented (Figure S6). Morphometry following immunostaining for cardiac Troponin I, indicated that 97–99% of cells on the surfaces were cardiomyocytes. Cross-striations in individual cardiomyocytes were generally oriented perpendicular to the abrasion direction (Figure 2.4) with a remarkably well-developed contractile apparatus for cells cultivated at 4.6 V/cm on surfaces with abrasions perpendicular to the field lines (Figure 2.4B). On non-abraded surfaces, there was no preferential directionality in cross-striation orientation, due to the random cellular orientation. Cross-striations were present only in the short domains (Figure 4B, non-abraded).

Low magnification images of phalloidin-TRITC stained cardiomyocytes (Figure 2.5A) indicated that actin filaments generally followed the direction of surface abrasions. For cells cultivated on non-abraded surfaces, actin cytoskeleton was disorganized. Higher magnification images (Figure 2.5B) revealed remarkable differences in orientation of actin filaments as a function of surface abrasion and electrical field stimulation. On abraded surfaces, actin filaments were clearly aligned in the direction of surface abrasions (either perpendicular or parallel to the field lines) with elements of cross-striations observable in some groups (e.g. Figure 2.5B 2.3 V/cm, perpendicular). For cardiomyocytes cultivated on non-abraded surfaces at 0.0 and 2.3 V/cm (Figure 2.5B) actin cytoskeleton was clearly disorganized, with overlapping filaments extending in multiple directions. Yet, at 4.6 V/cm on non-abraded surfaces (Figure 2.5B), there was an

appreciable improvement in the organization of the actin filaments, so that they were clearly parallel and following the long axis of the cell.

Consistent with our previous data [9], we found that ET significantly decreased with time in culture for all experimental groups. At the end of cultivation, cells on abraded surfaces had slightly lower ET when cultured with field stimulation in comparison to their non-stimulated controls; on non-abraded surfaces ET was slightly increased with stimulation. Field stimulation and topographical cues had interactive effects on the MCR. Overall higher MCR was achieved with cardiomyocytes cultivated on the non-abraded surfaces compared to those cultivated on the abraded surfaces. In general, MCR decreased significantly at 72 h of culture compared to the 24 h of culture for all groups, with the exception of non-abraded and perpendicular abrasions at 2.3 V/cm. At the end of cultivation, cardiomyocytes cultivated on abraded surfaces placed parallel to the field lines, exhibited a slight but significant increase in MCR with the increase of stimulation field strength from 2.3 to 4.6 V/cm.

#### 2.3.4 Pharmacological studies

Pharmacological studies focused on cardiomyocytes, a cell type that is responsible for contractile function. Inhibition of actin polymerization had dramatic effects on the ability of cardiomyocytes to respond to either topographical cues or field stimulation. Regardless of the experimental conditions, the cell morphology was round, the cells appeared mono-nucleated (Figure S5) when treated with Cytochalasin D and maintained aspect ratio of 2 (Figure 2.6A and C). They were also unable to orient, either in response to the electrical field stimulation or topography (Figure 2.6B and D). Yet, live/dead staining indicated no significant difference in cell viability between samples treated with Cytochalasin D and drug-free controls (Figure S5).

Elongated cells were observed in the groups treated with LY294002. However, cell viability was significantly lower in the LY294002-treated samples compared to the drug-free controls or samples treated with Cytochalasin D (Figure S5), consistent with the well-known effects of the PI3K pathway in prevention of apoptosis in cardiomyocytes [29]. Expression of constitutively active phosphatidylinositol 3-kinase inhibits activation of caspase 3 and apoptosis of cardiac muscle cells [29]. When field stimulation was

applied, the drug-free cardiomyocytes and those treated with LY294002 exhibited a statistically significant increase in the aspect ratio (Figure 2.6A and B). Specifically, in non-stimulated LY294002 group, cell elongation on abraded surfaces was slightly but significantly lower than that of drug-free controls (Figure 2.6C). Application of field stimulation completely reversed this effect resulting in a comparable elongation in LY294002-treated cells and the controls on abraded surfaces (Figure 2.6C) as well as a significantly higher elongation in LY294002-treated cells compared to the drug-free controls on non-abraded surfaces (Figure 2.6A). Blocking of PI3K pathway only partially inhibited the orientation response of cardiomyocytes (Figure 2.6B and D). For non-stimulated samples on abraded surfaces (Figure 2.6D), the average orientation angle of LY294002-treated cells was significantly larger than that of controls, but also significantly smaller compared to the Cytochalasin D-treated cells. The application of electrical field stimulation (4.6 V/cm) reversed this effect and resulted in the orientation levels in LY294002 groups comparable to those of drug-free controls (Figure 2.6D).

Overall our results indicate that blocking of actin polymerization significantly inhibited the ability of cardiomyocytes to elongate and orient in response to topographical cues or electrical field stimulation. Blocking of the PI3K pathway resulted in a partial reduction in cellular elongation and alignment on abraded surfaces. However, this reduction was reversed by the application of electrical field stimulation. Qualitatively, overall cell morphology and contractile apparatus were most developed in the drug-free controls cultivated on abraded surfaces in the presence of electrical field stimulation (4.6 V/cm). The Cytochalasin D-treated cells did exhibit the presence of Troponin I (Figure 2.7), but a developed contractile apparatus in individual cardiomyocytes could not be identified in majority of the cells. Blocking of PI3K pathway resulted in the overall qualitative decrease in cell size compared to drug-free controls consistent with the involvement of PI3K pathway in the hypertrophic response [30] and the contractile apparatus still present in a number of cells (Figure 2.7).

Staining with Phalloidin-TRITC revealed dramatic differences in actin cytoskeleton (Figure 2.8) as a function of drug treatment. The application of Cytochalasin D completely abolished actin polymerization as demonstrated by the complete lack of microfilaments in this group regardless of the surface abrasions or electrical field

stimulation (Figure 2.8). Cells treated with LY294002, exhibited staining for actin microfilaments with the improved cytoskeletal organization upon the application of electrical field stimulation (Figure 2.8). The major difference between the drug-free and LY294002 cells is that LY294002 cells assumed a more flat morphology in all groups.

At the end of cultivation the drugs were removed and we evaluated the ability of all our test groups to contract in response to electrical field stimulation. Drug-free constructs had lower ET at 72 h of culture compared to the 24 h of culture (Table 2.2), consistent with the results presented in Table 2.1. The application of either Cytochalasin D or LY294002 significantly affected the contractile response and prevented synchronous contractions of the cells. In these two groups, we only observed contractions of single randomly scattered cells (Table 2.2).

## **2.4 Discussion**

In vivo multiple guidance cues determine cell orientation and phenotype. These include topographical, adhesive, electrical, mechanical and chemical cues. The interactive effects of topographical and adhesive cues [31-33] have been studied extensively. Lesser attention was devoted to the interaction between adhesive and electrical cues [34], indicating that adhesive cues guided neurite outgrowth more strongly than electrical cues. Yet, the interaction between electrical cues and topography especially at conditions relevant for tissue engineering remained largely unstudied.

In adult myocardium, the cardiomyocytes are elongated, oriented in parallel, forming a three-dimensional syncytium that enables propagation of electrical signals. Cardiac fibroblasts are scattered amongst the myofibers, secreting components of the extracellular matrix (ECM) and transmitting mechanical force by the receptor-mediated connections to the ECM [35, 36]. One of the challenges of cardiac tissue engineering is reproducing the “in-vivo-like” orientation and elongation of the cells in an engineered cardiac patch.

The main objective of this study was to determine interactive effects of topographical cues and electrical field stimulation on cellular elongation and orientation at conditions relevant for cardiac tissue engineering. We focused on neonatal rat cardiomyocytes, a contractile cell documented to be responsive to both contact guidance

[16] and electrical field stimulation [2, 7]. We also studied the response of fibroblasts a non-contractile cell type with documented ability to align in response to contact guidance [37] and DC fields [1].

#### 2.4.1. Selection of topographical cues, electrical field stimulation conditions and pharmacological agents

To introduce topographical cues (Figure 1), we used a previously established method of abrading polyvinyl cover slips using lapping paper [22, 38]. Bursac et al. demonstrated that these surfaces resulted in a similar degree of cardiomyocyte orientation and elongation as the surfaces prepared using microcontact printing of laminin lanes [22] and that they could be utilized as model for electrophysiological studies [22, 38].

Fibroblasts and cardiomyocytes were cultivated on the surfaces with the average abrasion width ranging from 3 to 13  $\mu\text{m}$  and depth from 140 to 700 nm. From these experiments a group of surfaces that elicited the most significant orientation and elongation of both cell types, in comparison to non-abraded surfaces, was selected to be further studied with electrical field stimulation. The non-abraded surfaces (corresponding to the smallest cellular orientation and elongation), were used as a control. Although in vivo, ECM proteins assemble into structures on the order of 10–100 nm, the, guidance cues of the structures on the order of  $\mu\text{m}$  are well documented [12, 39, 40]. In the native rat heart, elongated cardiomyocytes are tightly positioned between capillaries (7  $\mu\text{m}$  in diameter) that are spaced 20  $\mu\text{m}$  apart [41], thus structures on the order of 1–10  $\mu\text{m}$  have physiological relevance.

For electrical field stimulation we used monophasic square pulses of 1 ms duration at the rate of 1 Hz and field strength of 2.3 or 4.6 V/cm. Stimulus pulse width corresponds to that found in the hearts of 1-week-old rats [42]. The frequency of 1 Hz is physiological for humans and at the low end of physiological regime for rats. The duration of culture and selection of field intensity was consistent with previous cardiac tissue engineering studies (5 V/cm, [9]) and cardiomyocyte monolayer studies (2.6 V/cm, [2, 7]). The selected field strengths are within the order of magnitude of the fields that occur in vivo [43]. Most importantly, the selected field strengths were at (2.3 V/cm) or above the excitation threshold (4.6 V/cm) for our cultures (Table 2.1) to ensure

synchronous cardiomyocyte contractions. In addition, the DC fields of comparable strength were previously demonstrated to affect the alignment and orientation of fibroblasts [1].

The electrical field stimulation was initiated 24 h after cell seeding. The lag period was intended to provide the cells with enough time to recover from trypsinization/isolation procedure and enable attachment. This lag period is also consistent with our results [9] and those of others [2] indicating that initiation of field stimulation too early in culture (less than 24 h) had detrimental effects on cellularity and failed to induce cardiomyocyte hypertrophy and improved contractile function.

It is important to note that we utilized a high cell seeding density in order to achieve confluent monolayers, as these conditions are of relevance for tissue engineering. In order to be functional, engineered cardiac constructs require a formation of syncytium at a cell density close to physiological ( $10^8$  cells/cm<sup>3</sup>). However, observing the effects of topographical cues [44] as well as electrical cues [34] is more conveniently performed at a low cell density.

For pharmacological studies we utilized Cytochalasin D and LY294002. Cytochalasin D is a fungal alkaloid that depolymerizes actin filaments by binding to the +end of F-actin thus blocking the addition of more units. It was used previously in the range of 1–40  $\mu$ m [45] to disrupt actin cytoskeleton in cardiomyocytes [46, 47]. Our use of 2  $\mu$ m is consistent with those studies. LY294002 is a standard inhibitor of PI3K that was used in a large number of studies at a concentration range 10–50  $\mu$ m [29, 30, 48]. It was documented to completely abolish PI3K activity with concentration required for 50% inhibition (IC<sub>50</sub>) of 1.40  $\mu$ m [49]. Our choice of 50  $\mu$ m is consistent with those studies.

#### 2.4.2. Effects of surface topography and electrical field stimulation on orientation and elongation of fibroblasts and cardiomyocytes

We observed that both fibroblasts and cardiomyocyte elongated and aligned with their axis parallel to the surface abrasions (Figure 2.2). The degree of alignment and elongation was significantly higher for deeper abrasions, consistent with previously reported studies that utilized grooves of precisely defined dimensions [11, 44, 50] as well as the rough surfaces [51]. We expect that utilizing surfaces with more uniform abrasion

features, such as those that can be prepared by microfabrication [16], would decrease the spread (i.e. error bars) in the measurement of aspect ratio and the elongation angle, yet the mean values would be comparable.

The surface abrasions were placed either perpendicular or parallel to the field lines. This way the two cues (topography and field) act on the cell either in a parallel or in an orthogonal direction. Overall, our results indicated that on non-abraded surfaces, pulsatile electrical field stimulation significantly enhanced elongation of fibroblasts and cardiomyocytes to reach the levels comparable to that achieved by surface abrasion (Figure 2.3A and C). The fact that field stimulation failed to promote elongation at higher levels than that obtained by topographical cues, prompted us to hypothesize that the same signaling pathways may be involved in the cellular response (i.e. elongation) to topographical cues and electrical field stimulation. In addition, pulsatile electrical field stimulation significantly enhanced orientation of both of fibroblasts and cardiomyocytes when they were cultivated on abrasions placed perpendicular to the field lines (Figure 2.3B and D). Yet, within every voltage group, the non-abraded surfaces had approximately two times higher average orientation angle than the abraded surfaces (Figure 2.3B and D), indicating that that topographical cues are overall stronger regulator of cellular orientation than field stimulation.

The cardiomyocytes were capable of contracting in response to electrical field stimulation (Table 2.1), consistent with the presence of a contractile protein cardiac Troponin I and a well-developed contractile apparatus (Figure 2.5A). In general, cardiomyocytes exhibited a decrease in ET, most likely due to the improved cellular coupling [26] consistent with our previous studies [9].

In general, MCR either decreased (Table 2.1) or remained comparable at 72 h in culture compared to 24 h in culture. Previous studies reported a significant increase in the MCR in monolayers of non-stimulated cardiomyocytes (cultivated on non-abraded surfaces) with time in culture, whereas paced cardiomyocyte monolayers exhibited a slight but not significant decrease in MCR [7]. Our previous studies with cardiac tissue constructs demonstrated a significant increase in MCR with time in culture. The increase in MCR was higher for constructs cultivated with the electrical field stimulation, thus the monolayer results (Table 2.1) are not consistent with those observed previously for the

3D constructs. The stiffness of the underlying substrate may be a likely cause for this discrepancy. When cultured on collagen sponges, the cardiomyocytes cause macroscopic contractions of the collagen scaffold at each beat. For cells cultured on rigid polystyrene surfaces such movement of the underlying substrate is not possible, thus affecting synchronized contractions of the cells at higher frequencies.

The application of electrical field stimulation to cultured cells induces hyperpolarization at the anode end of the cell and depolarization at the cathode end of the cell [52]. The higher the field, the more likely a cell is to reach the depolarization threshold, generate action potentials and contract in response to the stimulus. It is the contraction part of this excitation–contraction coupling and active tension development that enables the assembly and maintenance of the contractile apparatus in a 2D and 3D culture of cardiomyocytes [2, 4, 9, 53, 54]. If contractions are prevented, degradation and decrease in synthesis of sarcomeric proteins occurs, a process that can be reversed by regular contractile activity [53]. Thus, regular supra-threshold electrical stimuli can be utilized to induce a hypertrophic response in cardiomyocytes [4] and enhance cellular elongation, via mechanically activated signalling pathways [8].

#### 2.4.3. Significance of the findings

According to one hypothesis, grooved surfaces enable cellular orientation by confining cell adhesion molecules (e.g. focal adhesions) to an orientation parallel to the groove direction [12, 13]. As the ridge size of the grooved surfaces decreases (to e.g. 2  $\mu\text{m}$ ) focal adhesions which are also 2  $\mu\text{m}$  in width can assume only one possible orientation on the surface: the one that is parallel to the grooves. In addition, ECM proteins orient parallel to the groove direction on microstructured surfaces, affecting the orientation of integrins. Since adhesion molecules are coupled to the actin cytoskeleton, this causes the orientation of the actin filaments parallel to the groove direction [12] and [13], as we also observed in Figure 5. Numerous previous studies demonstrated that polymerization of F-actin is critical in cell motility and response of fibroblasts to surface topography [12, 55, 56]. Thus not surprisingly, we found that the disruption of actin cytoskeleton by Cytochalasin D had a detrimental effect on the ability of cardiomyocytes

to elongate and orient in response to topographical as well as electrical cues (Figure 2.6, Figure 2.7 and Figure 2.8).

In our experimental design, the cells were exposed to the topographical cues first, by allowing them to attach to the grooved surfaces for 24 h prior to the initiation of the pulsatile electrical field stimulation. We found that the electrical field stimulation could not reorient the cells that assumed an orientation defined by the topographical cues (Figure 3B and D). Pulsatile field stimulation enhanced the cellular elongation (Figure 2.3A and B), enabled the formation of more organized sarcomeres (Figure 2.4B) and improved local organization of actin cytoskeleton (Figure 2.5B).

Importantly, the cover slips used for cell growth were rigid and non-degradable, thus cells had no ability to remodel the substrate during cultivation. Substrate remodeling may be required for cells to change their orientation in response to field stimulation. It is possible that the utilization of the higher field strength would reorient the cells on the abraded surfaces. However, higher field strength may not be a feasible approach as continuous stimulation would lead to a decrease in cell viability (Radisic, unpublished observations). It is also possible that had a different abrasion feature been chosen (e.g. nano-structured surfaces) pulsatile electrical field stimulation would be more effective at directing cellular orientation.

To control changes in cell orientation and elongation, extracellular stimuli must initiate intracellular signaling that modifies organization of the cytoskeleton. PI3Ks take part in extracellular signal transduction by phosphorylating the hydroxyl group at positions 3 of membrane lipid phosphoinositides. The PI3 phosphates then transduce signals downstream by acting as docking sites for a number of signal-transducing proteins (e.g. protein kinase B, etc.). The PI3K pathway was documented to regulate a number of physiological functions, including cell growth, survival and actin cytoskeleton rearrangement [57]. It was documented to be involved in a physiological hypertrophy of cardiomyocytes [58, 59] as well as in the response of endothelial cells [60], keratinocytes and epithelial cells to stimulation with DC fields [61]. In activated platelets, PI3K associates with cytoskeleton when significant actin polymerization occurs [62]. Thus it was a logical pathway to investigate in the response of cardiomyocytes to topographical cues and pulsatile electrical field stimulation.

Inhibition of PI3K pathway significantly decreased cardiomyocyte orientation and elongation on abraded surfaces, implying a role of this pathway in response to topographical cues (Figure 2.6C and D). Yet pulsatile field stimulation was able to reverse this effect (Figure 2.6C and D), indicating that a parallel pathway may be involved in transduction of the electrical stimulation signals. Zhao et al. [60] documented that in addition to PI3K pathway, Rho kinase pathway was involved in the response of endothelial cells to DC field stimulation. LY294002-treated monolayers could not contract synchronously in response to electrical field stimulation, although both actin cytoskeleton (Figure 2.8) and sarcomeres (Figure 2.7) were identified, an observation consistent with our previous findings on cardiac tissue constructs [9].

#### 2.4.4. Implications of the findings for cardiac tissue engineering

Our findings indicate that orientation of fibroblasts and cardiomyocytes is primarily determined by surface topography. Thus, in order to engineer tissue with a desired cellular orientation scaffolds with anisotropic structure, such as those created by electrospinning and post-processing to achieve unidirectional fibre orientation [19, 63, 64] are required. Once desired cellular orientation is achieved, electrical field stimulation can be initiated 1–3 days after cell seeding on scaffolds to further modulate cellular elongation, contractile properties and organization of cytoskeletal and contractile proteins. The stimulus amplitude should be adjusted so that it surpasses the ET for synchronous contractions of the patch.

Two more approaches enable direct translation of our findings to improved methods of tissue engineering. In one approach biodegradable polymer films can be directly cast over the microstructured surfaces to obtain thin scaffolds capable of guiding cellular orientation, followed by the application of electrical field stimulation 1–3 days after cell seeding. In another approach, microstructured surfaces can be combined with cell sheet technology developed by Shimizu and colleagues [65] and used to stack oriented layers of cardiomyocytes. As orientation of myofibres changes along thickness of the ventricular wall, this approach could in principle yield a patch of myofibres aligned in parallel, with orientation angles changing as a function of patch thickness to mimic that found in the native heart. Application of electrical field stimulation would then enhance

the overall contractile properties of the patch, but it is not expected to significantly change the fibre orientation.

## **2.5 Conclusions**

Taken together, our data suggest that surface topography more strongly determines orientation of fibroblasts and cardiomyocytes than pulsatile electrical field stimulation. Yet, pulsatile electrical field stimulation had appreciable effects on cellular elongation. On non-abraded surfaces electrical field stimulation significantly promoted elongation of cardiomyocytes and fibroblasts to the levels comparable to that obtained by topographical cues. On abraded surfaces the electrical field stimulation enhanced orientation and elongation along the abrasion direction, but it could not reverse the effect of the cues provided by surface topography. The orientation and elongation response of cardiomyocytes to the abraded surfaces and electrical field stimulation was completely abolished by inhibition of actin polymerization and only partially by inhibition of PI3K pathway. These findings have significant implications for the design of scaffolds for cardiac tissue engineering. A feasible strategy would be to design scaffolds of desired microarchitecture (i.e. by electrospinning) to drive cellular elongation and orientation in the desired direction, followed by the application of electrical field stimulation for enhancement of these properties.

## 2.6 Figures and Tables

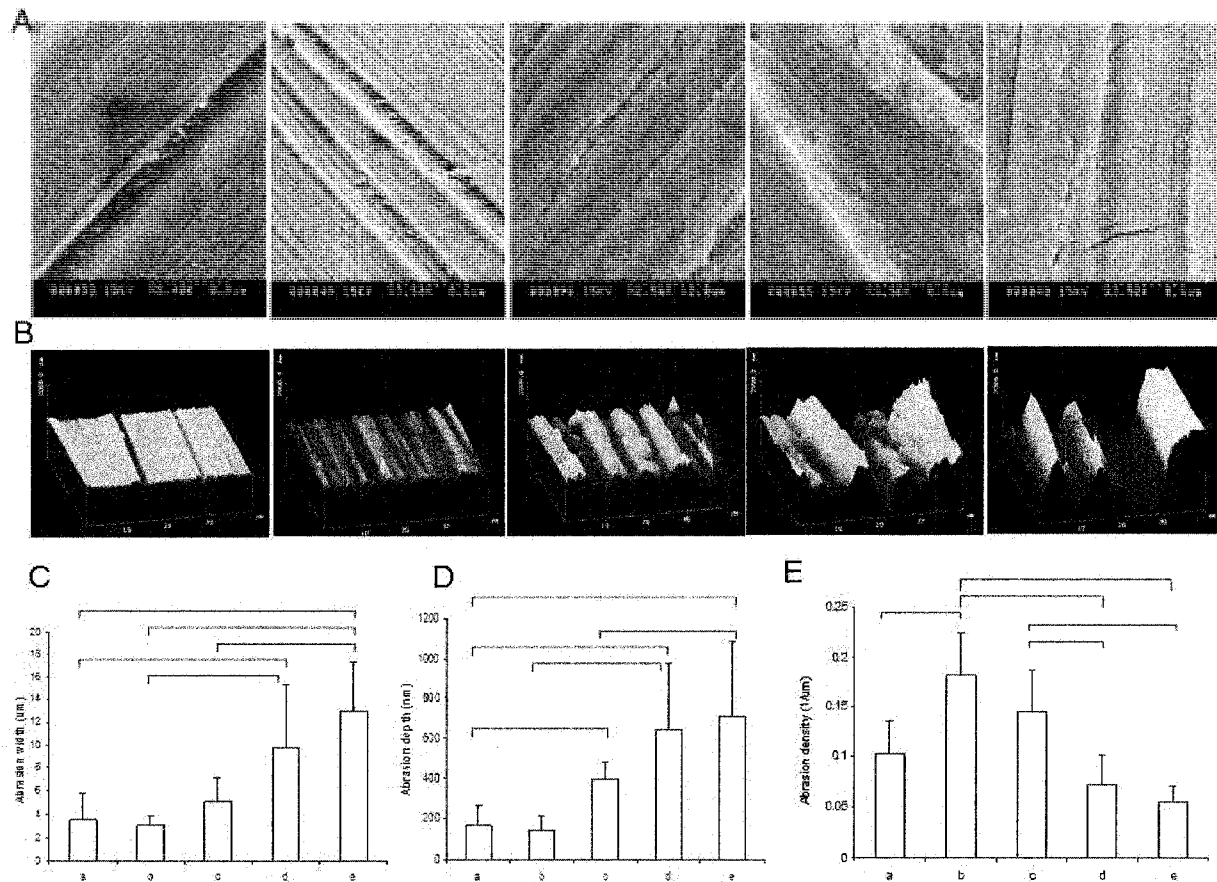


**Figure 2.1. Abraded surfaces.** A) SEMs of abraded surfaces. B) Abrasion width and depth as estimated by image analysis from SEMs. C) Abrasion density as estimated from by image analysis SEMs. The letters a,b,c,d and e represent abrasions made by lapping paper of grain size 1 μm, 9 μm, 12 μm, 40 μm and 80 μm respectively. ( $p < 0.05$ , Dunn's test).

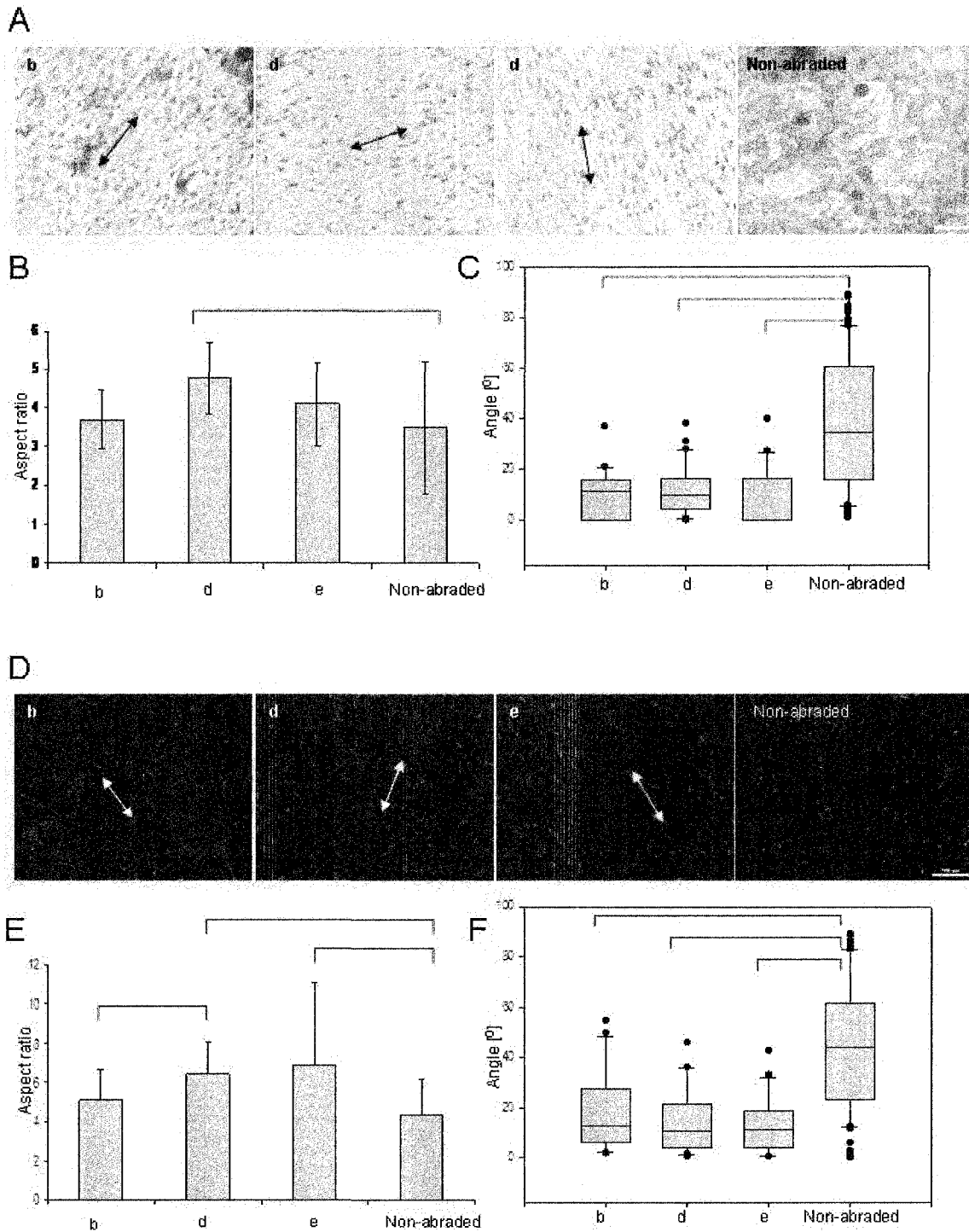


**Figure 2.2. Elongation and orientation of fibroblasts (A-C) and cardiomyocytes (D-E) cultivated on abraded and non-abraded surfaces.** Abraded surfaces were created by lapping paper with grain sizes of 9  $\mu\text{m}$ , 40  $\mu\text{m}$  and 80  $\mu\text{m}$  respectively (b,d,e). Aspect ratio is defined as the ratio between the long and the short axis of the cell. Orientation angle is defined as the angle between the long axis of the cell and the direction of abrasion. Arrows indicate direction of abrasion. For cells cultured on non-abraded surfaces orientation angle is measured with respect to the horizontal axis of the image. A) Giemsa staining of fibroblasts. (Scale bar: 100  $\mu\text{m}$  for b,d,e and 50  $\mu\text{m}$  for non-abraded). B) Elongation of fibroblasts as

measured by the aspect ratio. C) Alignment of fibroblasts as measured by the orientation angle (box plots). D) Live/dead (green/red) staining of cardiomyocytes. (Scale bar: 100  $\mu\text{m}$ ) E) Elongation of cardiomyocytes as measured by the aspect ratio. F) Alignment of cardiomyocytes as measured by the orientation angle (box plots).

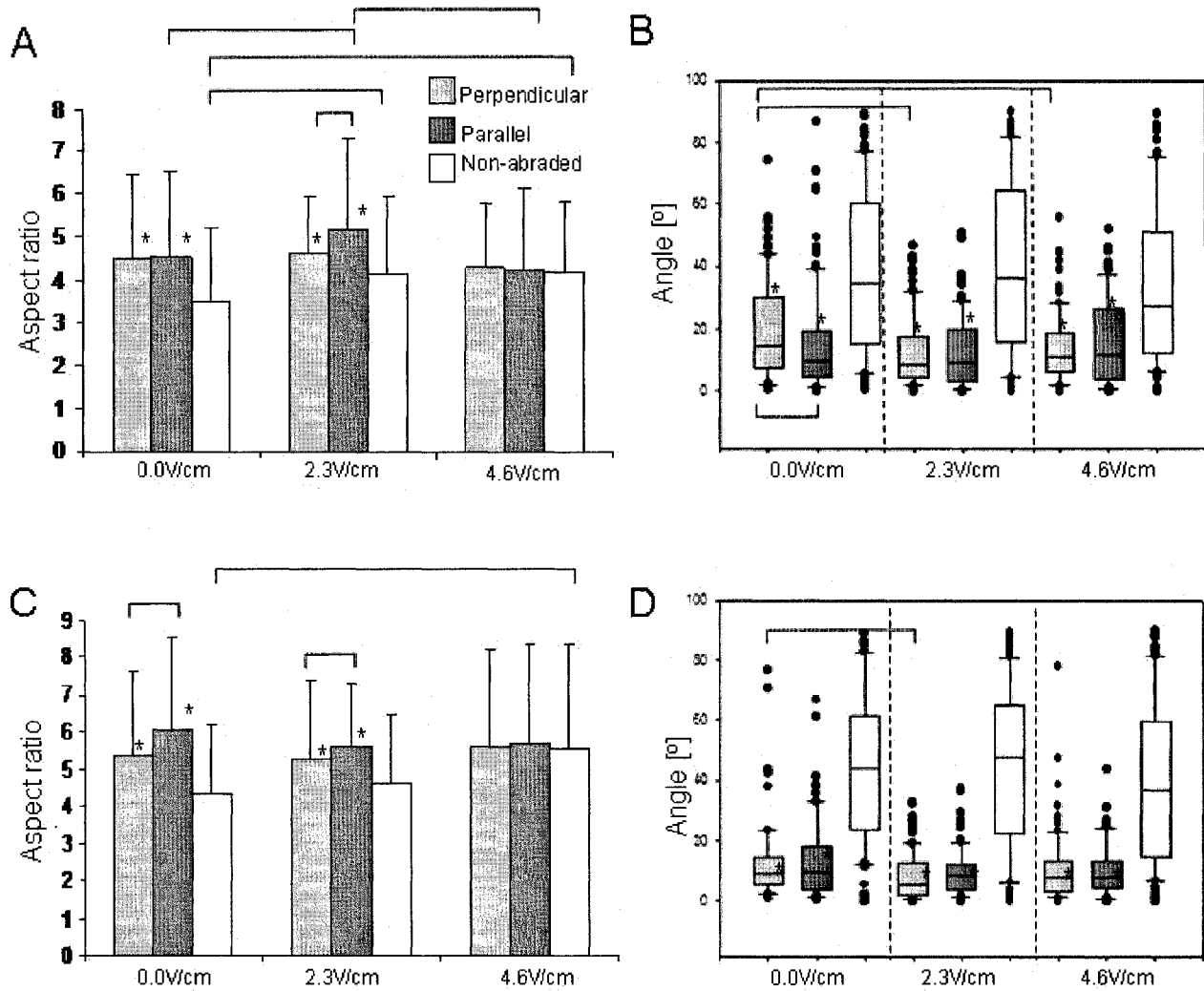


**Figure 2.3. Interactive effects of topographical cues and electrical field stimulation on fibroblasts (A,B) and cardiomyocytes (C,D).** Electrical field stimulation using square pulses 1ms duration, 1Hz and 2.3V/cm or 4.6 V/cm was initiated 24 hr after cell seeding and maintained for additional 72 hr. Abraded surfaces were placed between the electrodes so that the abrasions were either perpendicular or parallel to the field lines. A) Elongation of fibroblasts as measured by the aspect ratio. B) Alignment of fibroblasts as measured by the orientation angle (box plots). C) Elongation of cardiomyocytes as measured by the aspect ratio. D) Alignment of cardiomyocytes as measured by the orientation angle (box plots). Total N = 2-3 independent samples (cover slips) per group; 30-90 cells were analysed per group. ( $p < 0.05$  was considered significant). \*significantly different than non-abraded surface at identical stimulation voltage.

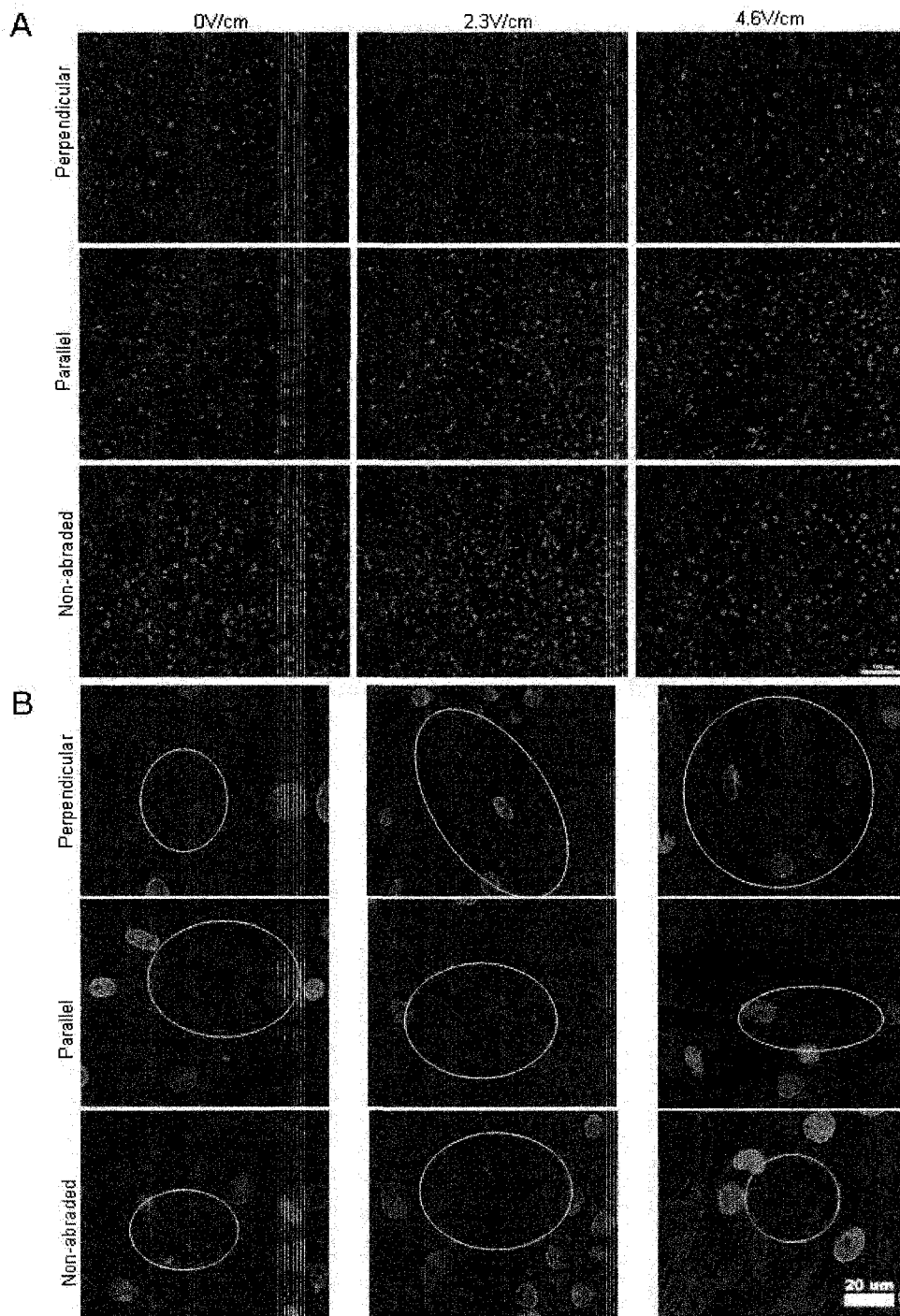


**Figure 2.4. Immunostaining for cardiac Troponin I of cardiomyocytes cultivated in the presence of electrical field stimulation on abraded surfaces.** Abraded surfaces were placed either perpendicular or parallel to the field line. Field stimulation (square pulses, 1ms duration, 1Hz and voltage as indicated) was applied 24 hr after seeding and maintained for additional 72 hr. A) Orientation and morphology of cells expressing cardiac troponin I. Scale bar= 100μm. B) Higher magnification images indicate the presence of contractile apparatus (cross-striations). Scale bar= 20 μm.

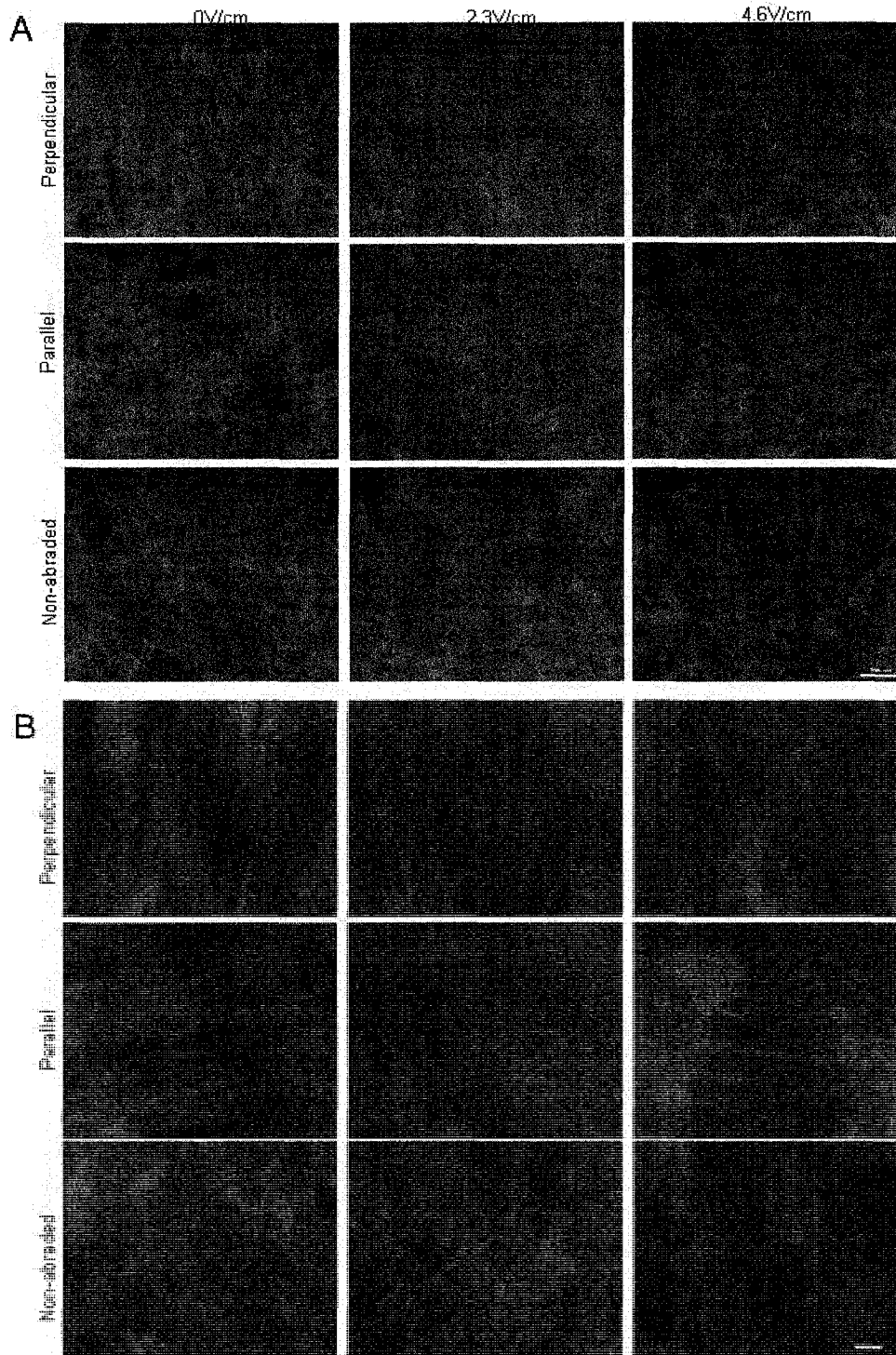


**Figure 2.5. Actin cytoskeleton in cardiomyocytes cultivated in the presence of electrical field stimulation on abraded surfaces.** Abraded surfaces were placed either perpendicular or parallel to the field lines. Field stimulation, (square pulses, 1ms duration, 1Hz and voltage as indicated) was applied 24 hr after seeding and maintained for additional 72 hr. A) Orientation and morphology of cells stained with phalloidin-TRITC. Scale bar =100 $\mu$ m. B) Higher magnification images indicate orientation of actin microfilaments. Scale bar =10  $\mu$ m.

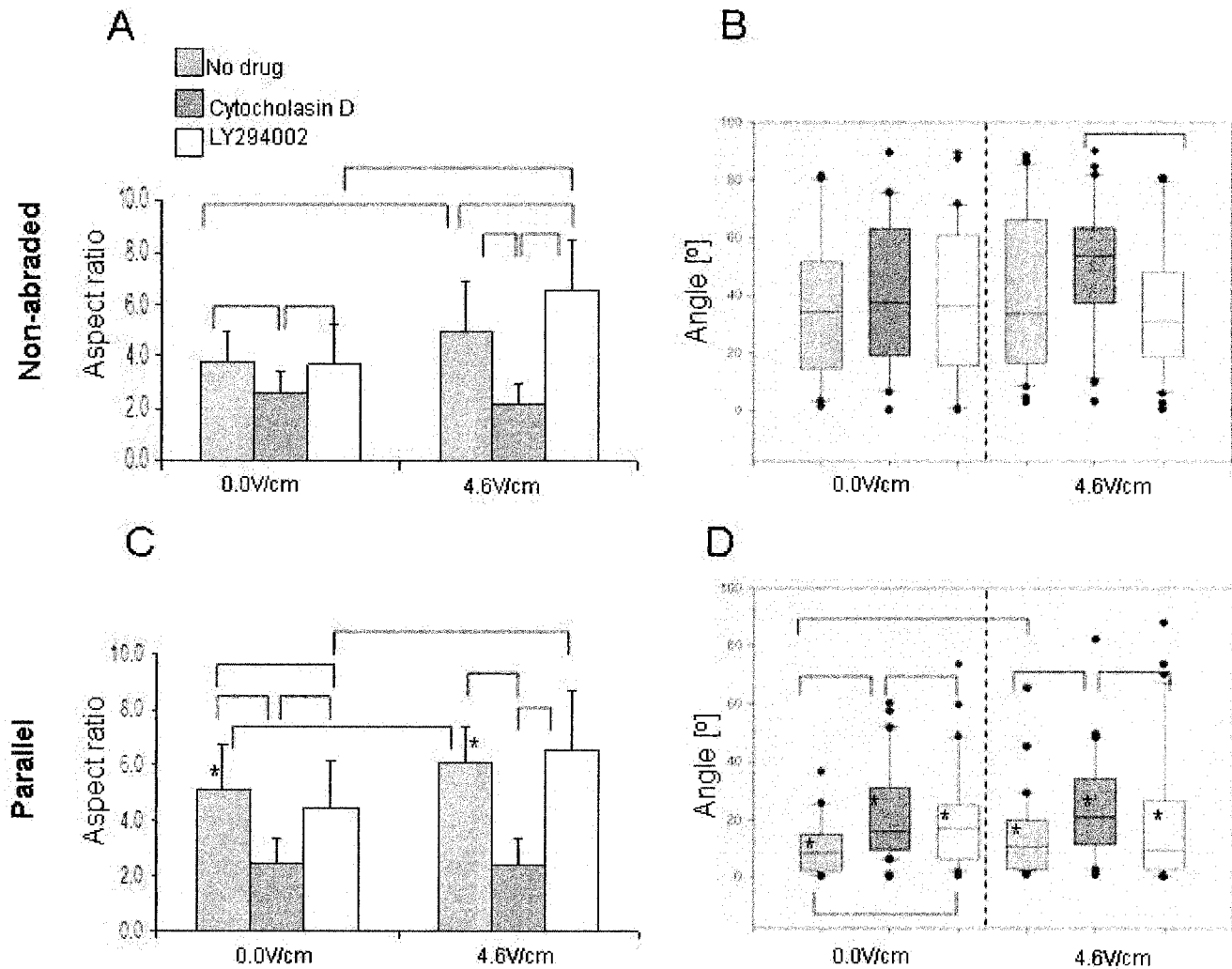


**Figure 2.6. Effects of pharmacological agents on elongation (A, C) and orientation (B,D) of cardiomyocytes cultivated on non-abraded (A,B) and abraded (C,D) surfaces.** Electrical field stimulation using square pulses 1ms duration, 1Hz and 2.3V/cm or 4.6 V/cm was initiated 24 hr after cell seeding and maintained for additional 72 hr. Abraded surfaces were placed between the electrodes so that the abrasions were parallel to the field lines. A) Elongation of cardiomyocytes on non-abraded surfaces B) Alignment of cardiomyocytes on non-abraded surfaces C) Elongation of cardiomyocytes on abrasions placed parallel to the field lines D) Alignment of cardiomyocytes on abrasions placed parallel to the field lines N = 2 -3 independent samples per treatment; 30 cells were analyzed per treatment. ( $p < 0.05$  was considered significant). \*significantly different than non-abraded surface at identical stimulation voltage.

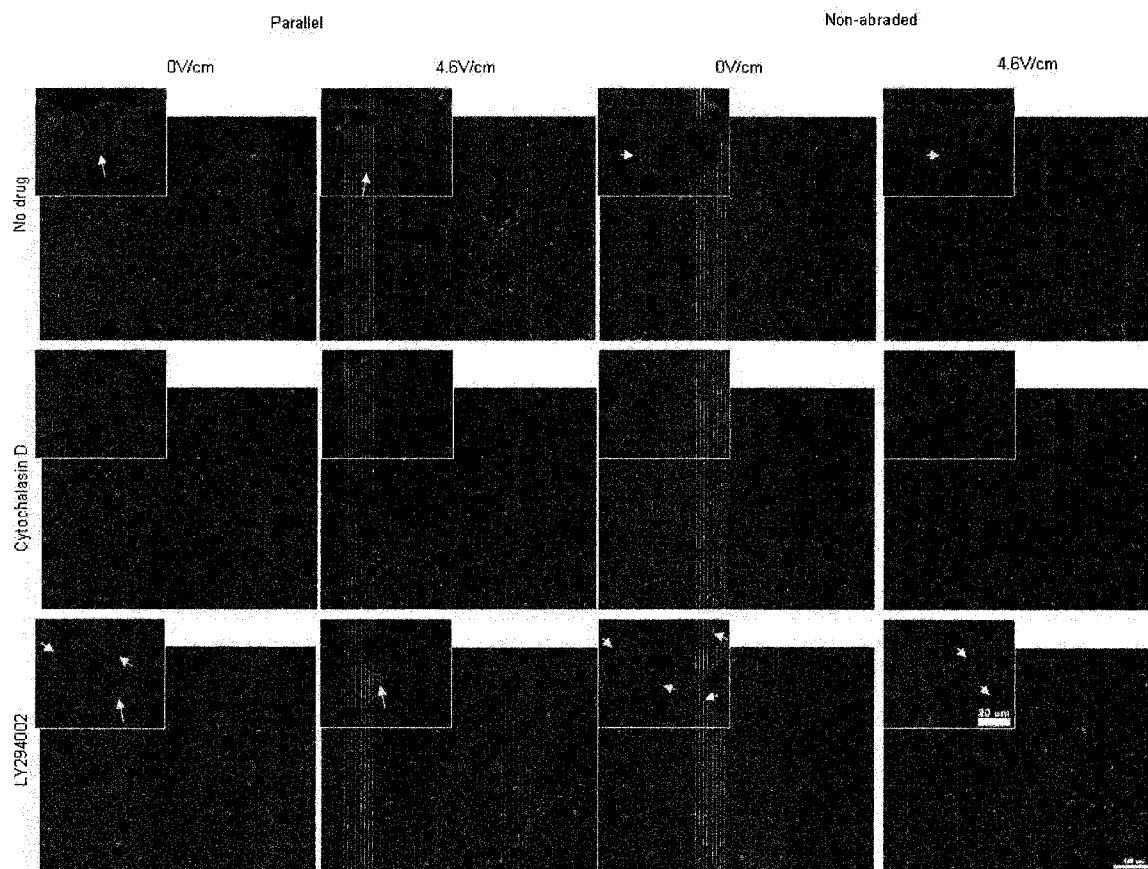


**Figure 2.7. Immunostaining for cardiac Troponin I of cardiomyocytes treated with pharmacologic agents.** Field stimulation (square pulses, 1ms duration, 1Hz and voltage as indicated), was applied 24 hr after seeding and maintained for additional 72 hr. Abraded surfaces were placed parallel to the field lines. Main panels indicate the orientation and morphology of cells expressing cardiac troponin I. Scale bar 100mm. Insets: Higher magnification images indicate the presence of contractile apparatus (cross-striations) in No- drug and LY294002 group (arrows). Scale bar =20  $\mu$ m.

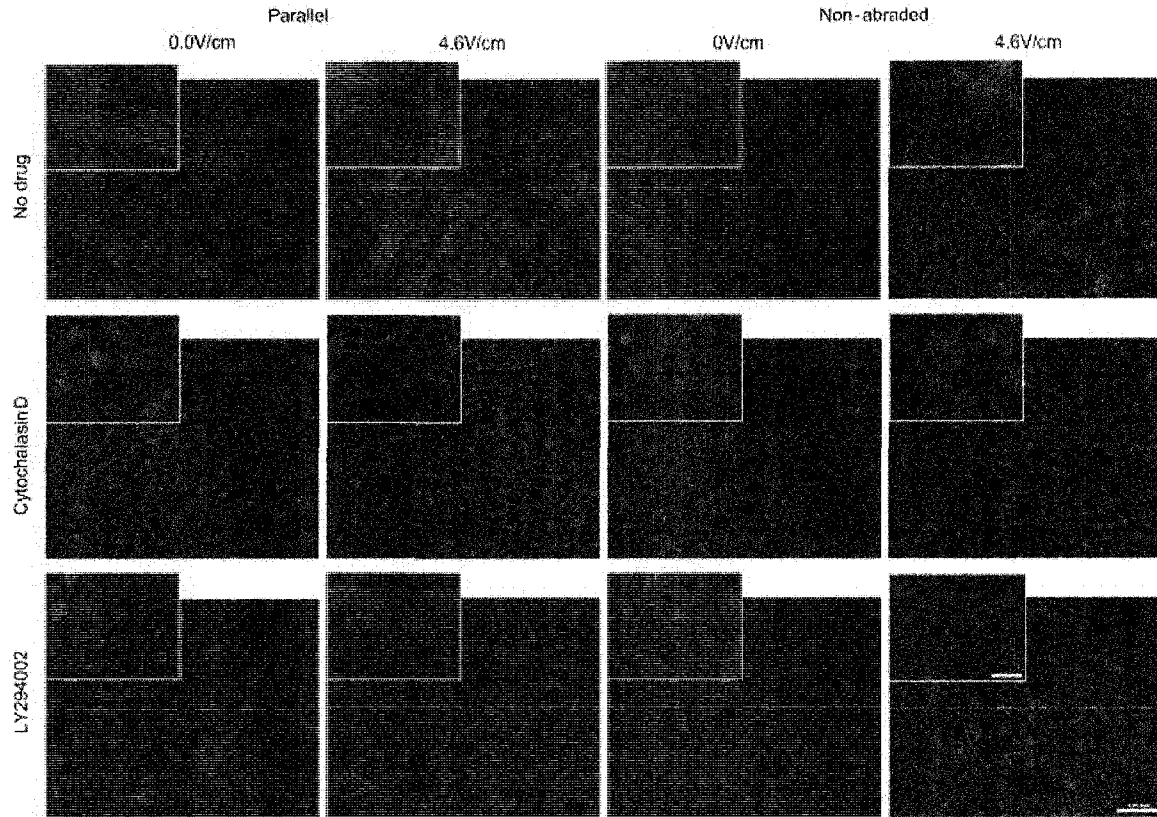


**Figure 2.8. Actin cytoskeleton in cardiomyocytes treated with pharmacologic agents.** Field stimulation (square pulses, 1ms duration, 1Hz and voltage as indicated, was applied 24 hr after seeding) and maintained for additional 72 hr. Abraded surfaces were placed parallel to the field line. Main panels indicate the orientation and morphology of cells expressing stained with phalloidin-TRITC. Scale bar =100µm. Insets: Higher magnification images indicate orientation of actin microfilaments. Scale bar =20 µm.

**Table 2.1 Contractile properties of cardiomyocytes as a function of surface abrasions and electrical field stimulation.** Cardiomyocytes were seeded on polyvinyl cover slips (abraded and non-abraded) and cultivated for 24 h without field stimulation to allow for the cell attachment. After 24 h in culture field stimulation was initiated using square pulses 1 ms duration, 1 Hz with two different field strengths: 2.3 and 4.6 V/cm. Abraded surfaces were placed between the carbon electrodes so that the abrasions were either perpendicular or parallel to the field lines. The cells were cultivated for addition 72 h followed by evaluation of contractile properties (ET and MCR).

Contractile properties at 24 hr in culture:

	Perpendicular	Parallel	Non-abraded
ET (V/cm)	2.8 ± 0.7 (18/18)	2.6 ± 0.5 (18/20)	2.6 ± 0.4 (15/17)
MCR (Hz)	3.7 ± 1.0 (17/18)	4.2 ± 1.1 (18/20)	4.6 ± 1.5 (15/17)

Contractile properties at 96 hr in culture:

Type of stimulation	0.0V/cm			2.3V/cm			4.6V/cm		
Type of abrasion	Perpendicular	Parallel	Non-abraded	Perpendicular	Parallel	Non-abraded	Perpendicular	Parallel	Non-abraded
ET (V/cm)	2.2 ± 0.5 <sup>&amp;</sup> (3/4)	2.0 ± 0.4 <sup>&amp;</sup> (7/7)	1.7 ± 0.4 (6/6)	1.9 ± 0.4 <sup>&amp;</sup> (5/6)	1.9 ± 0.6 <sup>&amp;</sup> (5/6)	2.0 ± 0.5 <sup>&amp;</sup> (4/5)	1.9 ± 0.9 <sup>&amp;</sup> (5/6)	1.8 ± 1.4 <sup>&amp;</sup> (7/9)	2.6 ± 1.5 (8/8)
MCR (Hz)	2.7 ± 0.3 <sup>&amp;</sup> (3/4)	2.8 ± 0.3 <sup>&amp;</sup> (5/7)	3.5 ± 1.5 (3/6)	3.6 ± 1.6 (5/6)	2.7 ± 1.1 <sup>&amp;§</sup> (5/6)	5.3 ± 3.4 (4/5)	2.6 ± 0.4 <sup>&amp;*§</sup> (5/6)	3.1 ± 0.8 <sup>&amp;*§</sup> (7/9)	3.9 ± 1.3 (8/8)

<sup>&</sup> significantly different than the same group at 24hr

<sup>\*</sup> significantly different than non-abraded at the same time point and stimulation regime

<sup>§</sup> significantly different than parallel at 4.6V/cm

**Table 2.2 Effect of pharmacologic agents on contractile properties of cardiomyocytes cultivated in the presence of electrical field stimulation (0.0 or 4.6 V/cm) on non-abraded and abraded surfaces placed parallel to the field lines.** Cardiomyocytes were seeded on polyvinyl cover slips (abraded and non-abraded) and cultivated for 24 h without field stimulation to allow for the cell attachment. After 24 h, pharmacologic agents (Cytochalasin D, 2 μM and LY294002, 50 μM) were added to the cover slips and field stimulation was initiated using square pulses 1 ms duration, 1 Hz and 4.6 V/cm. The abraded cover-slips were placed such that the abrasions were parallel to the field lines. Field stimulation in the presence of pharmacologic agents was maintained for additional 72 h. The ET and MCR were measured at 24 h prior to addition of pharmacologic agents and the averages were: 2.6±0.1 V/cm and 4.1±0.2 Hz for abraded surfaces; 2.6±0.1 V/cm and 3.8±0.2 Hz for non-abraded surfaces. N/A indicates that the sample could not be induced to contract by field stimulation at all, or only isolated cells (less than 75% of area) were responding. The numbers in brackets indicate the number of samples that were successfully paced/number of samples tested.

	Type of stimulation	0V/cm		4.6V/cm	
	Type of surface	Non-abraded	Parallel	Non-abraded	Parallel
ET (V/cm)	No drug	1.7 ± 0.2 <sup>&amp;</sup> (3/3)	1.8 ± 0.3 <sup>&amp;</sup> (3/3)	2.1 ± 0.6 (3/3)	1.8 ± 0.3 <sup>&amp;</sup> (3/3)
	Cytochalasin D	N/A (0/3)	N/A (0/3)	N/A (0/3)	N/A (0/3)
	LY294002	N/A (0/3)	N/A (0/3)	N/A (0/3)	N/A (0/3)
MCR (Hz)	No drug	3.0 ± 0.1 <sup>&amp;</sup> (3/3)	3.0 ± 0.2 <sup>&amp;</sup> (3/3)	3.1 ± 0.4 <sup>&amp;</sup> (3/3)	3.0 ± 0.1 <sup>&amp;</sup> (3/3)
	Cytochalasin D	N/A (0/3)	N/A (0/3)	N/A (0/3)	N/A (0/3)
	LY294002	N/A (0/3)	N/A (0/3)	N/A (0/3)	N/A (0/3)

<sup>&</sup> significantly different than the same group at 24hr

**Supplementary Figures can be found in the Appendix S2**

## 2.7 References

1. C.A. Erickson and R. Nuccitelli, Embryonic fibroblast motility and orientation can be influenced by physiological electric fields, *J Cell Biol* 98 (1984), pp. 296–307.
2. H.J. Berger, S.K. Prasad, A.J. Davidoff, D. Pimental, O. Ellingsen and J.D. Marsh et al., Continual electric field stimulation preserves contractile function of adult ventricular myocytes in primary culture, *Am J Physiol* 266 (1994), pp. H341–H349.
3. E. Holt, P.K. Lunde, O.M. Sejersted and G. Christensen, Electrical stimulation of adult rat cardiomyocytes in culture improves contractile properties and is associated with altered calcium handling, *Basic Res Cardiol* 92 (1997), pp. 289–298.
4. T.B. Johnson, R.L. Kent, B.A. Bubolz and P.J. McDermott, Electrical stimulation of contractile activity accelerates growth of cultured neonatal cardiocytes,
5. C.T. Ivester, W.J. Tuxworth, G.t. Cooper and P.J. McDermott, Contraction accelerates myosin heavy chain synthesis rates in adult cardiocytes by an increase in the rate of translational initiation, *J Biol Chem* 270 (1995), pp. 21950–21957.
6. S. Kato, C.T. Ivester, G.t. Cooper, M.R. Zile and P.J. McDermott, Growth effects of electrically stimulated contraction on adult feline cardiocytes in primary culture, *Am J Physiol* 268 (1995), pp. H2495–H2504.
7. A. Sathaye, N. Bursac, S. Sheehy and L. Tung, Electrical pacing counteracts intrinsic shortening of action potential duration of neonatal rat ventricular cells in culture, *J Mol Cell Cardiol* 41 (2006), pp. 633–641.
8. J.B. Strait and A.M. Samarel, Isoenzyme-specific protein kinase C and c-Jun N-terminal kinase activation by electrically stimulated contraction of neonatal rat ventricular myocytes, *J Mol Cell Cardiol* 32 (2000), pp. 1553–1566.
9. M. Radisic, H. Park, H. Shing, T. Consi, F.J. Schoen and R. Langer et al., Functional assembly of engineered myocardium by electrical stimulation of cardiac myocytes cultured on scaffolds, *Proc Natl Acad Sci USA* 101 (2004), pp. 18129–18134.
10. R.B. Vernon, M.D. Gooden, S.L. Lara and T.N. Wight, Microgrooved fibrillar collagen membranes as scaffolds for cell support and alignment, *Biomaterials* 26 (2005), pp. 3131–3140.
11. R.G. Flemming, C.J. Murphy, G.A. Abrams, S.L. Goodman and P.F. Nealey, Effects of synthetic micro- and nano-structured surfaces on cell behavior, *Biomaterials* 20 (1999), pp. 573–588.
12. E.T. den Braber, J.E. de Ruijter, L.A. Ginsel, A.F. von Recum and J.A. Jansen, Orientation of ECM protein deposition, fibroblast cytoskeleton, and attachment complex components on silicone microgrooved surfaces, *J Biomed Mater Res* 40 (1998), pp. 291–300.
13. E.T. den Braber, J.E. de Ruijter, L.A. Ginsel, A.F. von Recum and J.A. Jansen, Quantitative analysis of fibroblast morphology on microgrooved surfaces with various groove and ridge dimensions, *Biomaterials* 17 (1996), pp. 2037–2044.
14. M.J. Dalby, M.O. Riehle, S.J. Yarwood, C.D. Wilkinson and A.S. Curtis, Nucleus alignment and cell signaling in fibroblasts: response to a micro-grooved topography, *Exp Cell Res* 284 (2003), pp. 274–282.
15. J. Deutsch, D. Motlagh, B. Russell and T.A. Desai, Fabrication of microtextured membranes for cardiac myocyte attachment and orientation, *J Biomed Mater Res* 53 (2000), pp. 267–275.
16. D. Motlagh, T.J. Hartman, T.A. Desai and B. Russell, Microfabricated grooves recapitulate neonatal myocyte connexin43 and N-cadherin expression and localization, *J Biomed Mater Res A* 67 (2003), pp. 148–157.
17. D. Motlagh, S.E. Senyo, T.A. Desai and B. Russell, Microtextured substrata alter gene expression, protein localization and the shape of cardiac myocytes, *Biomaterials* 24 (2003), pp. 2463–2476.

18. S.M. Gopalan, C. Flaim, S.N. Bhatia, M. Hoshijima, R. Knoell and K.R. Chien et al., Anisotropic stretch-induced hypertrophy in neonatal ventricular myocytes micropatterned on deformable elastomers, *Biotechnol Bioeng* 81 (2003), pp. 578–587.
19. X. Zong, H. Bien, C.Y. Chung, L. Yin, D. Fang and B.S. Hsiao et al., Electrospun fine-textured scaffolds for heart tissue constructs, *Biomaterials* 26 (2005), pp. 5330–5338.
20. T.C. McDevitt, K.A. Woodhouse, S.D. Hauschka, C.E. Murry and P.S. Stayton, Spatially organized layers of cardiomyocytes on biodegradable polyurethane films for myocardial repair, *J Biomed Mater Res A* 66 (2003), pp. 586–595.
21. T.C. McDevitt, J.C. Angello, M.L. Whitney, H. Reinecke, S.D. Hauschka and C.E. Murry et al., In vitro generation of differentiated cardiac myofibers on micropatterned laminin surfaces, *J Biomed Mater Res* 60 (2002), pp. 472–479.
22. N. Bursac, K.K. Parker, S. Iravanian and L. Tung, Cardiomyocyte cultures with controlled macroscopic anisotropy: a model for functional electrophysiological studies of cardiac muscle, *Circ Res* 91 (2002), pp. e45–e54.
23. M. Radisic, M. Euloth, L. Yang, R. Langer, L.E. Freed and G. Vunjak-Novakovic, High-density seeding of myocyte cells for cardiac tissue engineering, *Biotechnol Bioeng* 82 (2003), pp. 403–414.
24. M. Radisic, L. Yang, J. Boublik, R.J. Cohen, R. Langer and L.E. Freed et al., Medium perfusion enables engineering of compact and contractile cardiac tissue, *Am J Physiol Heart Circ Physiol* 286 (2004), pp. H507–H516.
25. M. Radisic, J. Malda, E. Epping, W. Geng, R. Langer and G. Vunjak-Novakovic, Oxygen gradients correlate with cell density and cell viability in engineered cardiac tissue, *Biotechnol Bioeng* 93 (2006), pp. 332–343.
26. N. Bursac, M. Papadaki, R.J. Cohen, F.J. Schoen, S.R. Eisenberg and R. Carrier et al., Cardiac muscle tissue engineering: toward an in vitro model for electrophysiological studies, *Am J Physiol* 277 (1999), pp. H433–H444.
27. B. Chehroudi and D.M. Brunette, Subcutaneous microfabricated surfaces inhibit epithelial recession and promote long-term survival of percutaneous implants, *Biomaterials* 23 (2002), pp. 229–237.
28. K. Matsuzaka, M. Yoshinari, M. Shimono and T. Inoue, Effects of multigrooved surfaces on osteoblast-like cells in vitro: scanning electron microscopic observation and mRNA expression of osteopontin and osteocalcin, *J Biomed Mater Res A* 68 (2004), pp. 227–234.
29. W. Wu, W.L. Lee, Y.Y. Wu, D. Chen, T.J. Liu and A. Jang et al., Expression of constitutively active phosphatidylinositol 3-kinase inhibits activation of caspase 3 and apoptosis of cardiac muscle cells, *J Biol Chem* 275 (2000), pp. 40113–40119.
30. K.D. Schluter, Y. Goldberg, G. Taimor, M. Schafer and H.M. Piper, Role of phosphatidylinositol 3-kinase activation in the hypertrophic growth of adult ventricular cardiomyocytes, *Cardiovasc Res* 40 (1998), pp. 174–181.
31. S. Britland, H. Morgan, B. Wojciak-Stodart, M. Riehle, A. Curtis and C. Wilkinson, Synergistic and hierarchical adhesive and topographic guidance of BHK cells, *Exp Cell Res* 228 (1996), pp. 313–325.
32. J.L. Charest, M.T. Eliason, A.J. Garcia and W.P. King, Combined microscale mechanical topography and chemical patterns on polymer cell culture substrates, *Biomaterials* 27 (2006), pp. 2487–2494.
33. D. Pasqui, A. Rossi, R. Barbucci, S. Lamponi, R. Gerli and E. Weber, Hyaluronan and sulphated hyaluronan micropatterns: effect of chemical and topographic cues on lymphatic endothelial cell alignment and proliferation, *Lymphology* 38 (2005), pp. 50–65.
34. S. Britland and C. McCaig, Embryonic *Xenopus* neurites integrate and respond to simultaneous electrical and adhesive guidance cues, *Exp Cell Res* 226 (1996), pp. 31–38.
35. M.A. Sussman, A. McCulloch and T.K. Borg, Dance band on the Titanic: biomechanical signaling in cardiac hypertrophy, *Circ Res* 91 (2002), pp. 888–898.

36. A.C. Nag, Study of non-muscle cells of the adult mammalian heart: a fine structural analysis and distribution, *Cytobios* 28 (1980), pp. 41–61
37. J. Meyle, K. Gultig and W. Nisch, Variation in contact guidance by human cells on a microstructured surface, *J Biomed Mater Res* 29 (1995), pp. 81–88.
38. N. Bursac, F. Aguel and L. Tung, Multiarm spirals in a two-dimensional cardiac substrate, *Proc Natl Acad Sci USA* 101 (2004), pp. 15530–15534.
39. E.T. den Braber, J.E. de Ruijter, H.T. Smits, L.A. Ginsel, A.F. von Recum and J.A. Jansen, Effect of parallel surface microgrooves and surface energy on cell growth, *J Biomed Mater Res* 29 (1995), pp. 511–518.
40. P.T. Ohara and R.C. Buck, Contact guidance in vitro. A light, transmission, and scanning electron microscopic study, *Exp Cell Res* 121 (1979), pp. 235–249.
41. K. Rakusan and B. Korecky, The effect of growth and aging on functional capillary supply of the rat heart, *Growth* 46 (1982), pp. 275–281.
42. P.A. Gomes, K.M. de Galvao and E.F. Mateus, Excitability of isolated hearts from rats during postnatal development, *J Cardiovasc Electrophysiol* 13 (2002), pp. 355–360.
43. R. Nuccitelli, Endogenous ionic currents and DC electric fields in multicellular animal tissues, *Bioelectromagnetics (Suppl 1)* (1992), pp. 147–157.
44. P. Clark, P. Connolly, A.S. Curtis, J.A. Dow and C.D. Wilkinson, Cell guidance by ultrafine topography in vitro, *J Cell Sci* 99 (Part 1) (1991), pp. 73–77.
45. M. Wodnicka, M. Pierzchalska, J. Bereiter-Hahn and J. Kajstura, Comparative study on effects of cytochalasins B and D on F-actin content in different cell lines and different culture conditions, *Folia Histochem Cytobiol* 30 (1992), pp. 107–111.
46. R.N. Leach, J.C. Desai and C.H. Orchard, Effect of cytoskeleton disruptors on L-type Ca channel distribution in rat ventricular myocytes, *Cell Calcium* 38 (2005), pp. 515–526
47. T. Okada, H. Otani, Y. Wu, S. Kyoi, C. Enoki and H. Fujiwara et al., Role of F-actin organization in p38 MAP kinase-mediated apoptosis and necrosis in neonatal rat cardiomyocytes subjected to simulated ischemia and reoxygenation, *Am J Physiol Heart Circ Physiol* 289 (2005), pp. H2310–H2318.
48. N. Ghosh-Choudhury, S.L. Abboud, B. Chandrasekar and G. Ghosh Choudhury, BMP-2 regulates cardiomyocyte contractility in a phosphatidylinositol 3 kinase-dependent manner, *FEBS Lett* 544 (2003), pp. 181–184.
49. C.J. Vlahos, W.F. Matter, K.Y. Hui and R.F. Brown, A specific inhibitor of phosphatidylinositol 3-kinase, 2-(4-morpholinyl)-8-phenyl-4H-1-benzopyran-4-one (LY294002), *J Biol Chem* 269 (1994), pp. 5241–5248.
50. P. Clark, P. Connolly, A.S. Curtis, J.A. Dow and C.D. Wilkinson, Topographical control of cell behaviour: II. Multiple grooved substrata, *Development* 108 (1990), pp. 635–644.
51. E. Eisenbarth, J. Meyle, W. Nachtigall and J. Breme, Influence of the surface structure of titanium materials on the adhesion of fibroblasts, *Biomaterials* 17 (1996), pp. 1399–1403.
52. L. Tung, N. Sliz and M.R. Mulligan, Influence of electrical axis of stimulation on excitation of cardiac muscle cells, *Circ Res* 69 (1991), pp. 722–730.
53. W.W. Sharp, L. Terracio, T.K. Borg and A.M. Samarel, Contractile activity modulates actin synthesis and turnover in cultured neonatal rat heart cells, *Circ Res* 73 (1993), pp. 172–183.
54. P. McDermott, M. Daood and I. Klein, Contraction regulates myosin synthesis and myosin content of cultured heart cells, *Am J Physiol* 249 (1985), pp. H763–H769.
55. L.A. Cameron, P.A. Giardini, F.S. Soo and J.A. Theriot, Secrets of actin-based motility revealed by a bacterial pathogen, *Nat Rev Mol Cell Biol* 1 (2000), pp. 110–119.
56. J.A. Cooper and D.A. Schafer, Control of actin assembly and disassembly at filament ends, *Curr Opin Cell Biol* 12 (2000), pp. 97–103.
57. A. Toker and L.C. Cantley, Signalling through the lipid products of phosphoinositide-3-OH kinase, *Nature* 387 (1997), pp. 673–676.

58. J.R. McMullen, T. Shioi, W.Y. Huang, L. Zhang, O. Tarnavski and E. Bisping et al., The insulin-like growth factor 1 receptor induces physiological heart growth via the phosphoinositide 3-kinase(p110alpha) pathway, *J Biol Chem* 279 (2004), pp. 4782–4793.
59. J.R. McMullen, T. Shioi, L. Zhang, O. Tarnavski, M.C. Sherwood and P.M. Kang et al., Phosphoinositide 3-kinase(p110alpha) plays a critical role for the induction of physiological, but not pathological, cardiac hypertrophy, *Proc Natl Acad Sci USA* 100 (2003), pp. 12355–12360
60. M. Zhao, H. Bai, E. Wang, J.V. Forrester and C.D. McCaig, Electrical stimulation directly induces pre-angiogenic responses in vascular endothelial cells by signaling through VEGF receptors, *J Cell Sci* 117 (2004), pp. 397–405.
61. M. Zhao, B. Song, J. Pu, T. Wada, B. Reid and G. Tai et al., Electrical signals control wound healing through phosphatidylinositol-3-OH kinase-gamma and PTEN, *Nature* 442 (2006), pp. 457–460
62. P.A. Janmey, The cytoskeleton and cell signaling: component localization and mechanical coupling, *Physiol Rev* 78 (1998), pp. 763–781.
63. T. Courtney, M.S. Sacks, J. Stankus, J. Guan and W.R. Wagner, Design and analysis of tissue engineering scaffolds that mimic soft tissue mechanical anisotropy, *Biomaterials* 27 (2006), pp. 3631–3638.
64. J.J. Stankus, J. Guan and W.R. Wagner, Fabrication of biodegradable elastomeric scaffolds with sub-micron morphologies, *J Biomed Mater Res A* 70 (2004), pp. 603–614.
65. T. Shimizu, M. Yamato, Y. Isoi, T. Akutsu, T. Setomaru and K. Abe et al., Fabrication of pulsatile cardiac tissue grafts using a novel 3-dimensional cell sheet manipulation technique and temperature- responsive cell culture surfaces, *Circ Res* 90 (2002), pp. e8–e40.

### **3. Microgrooved surfaces with integrated electrodes for simultaneous application of topographical and electrical cues in cell culture<sup>2</sup>**

#### **3.1 Introduction**

In vivo, cells are exposed to multiple biochemical and physical cues including topographical and electrical cues. The cell phenotype, including its orientation and elongation, is ultimately determined by the interaction amongst these multiple cues and may change with time as the type and magnitude of the cues changes. In contractile tissues such as myocardium, functional properties can directly be correlated to the orientation and elongation of cardiomyocytes [1] that occupy 90% of the volume of native myocardium. Thus, our ability to create high-fidelity cultures of cardiomyocytes in vitro critically depends on the availability of advanced cell culture systems that combine multiple physical and biochemical cues. These efforts are focused on both two-dimensional systems (2D) where cultures of cardiomyocytes may serve as platforms for drug development and three-dimensional systems (3D) where cultivation of functional cardiac patches is the ultimate goal.

Fully differentiated adult cardiomyocytes are elongated and rod-shaped, containing well developed contractile apparatus, identified as a characteristic cross-striation pattern in cells stained for contractile proteins, with intercalated discs as electro-mechanical cell end-to-end coupling. Gap junctions, located in intercalated discs at the ends of cells in adult myocardium [2], are responsible for rapid propagation of electrical signals between the cells. When cultivated on simple two-dimensional substrates (2D) as monolayers or single cells, cardiomyocytes are known to de-differentiate due to the lack of appropriate micro-environmental cues [3, 4]. In this process the defined contractile apparatus disappears and the cells slowly assume irregular oval or star shape. Mechanical stimulation [5-8], pharmacological [9] or electrical [10-15] induction of contractions as well as cultivation on patterned substrates [16, 17] were utilized previously in order to

---

<sup>2</sup> This chapter contains text identical to that of a manuscript submitted in 2008 under the same title, with the following authors: Hoi Ting Heidi Au, Bo Cui, Zane Chu, Teodor Veres and Milica Radisic

provide one of the micro-environmental cues required for maintenance of cardiomyocyte phenotype and contractile function in vitro.

The mechanically activated signaling pathways were implicated in the response of cardiomyocytes to the electrical field stimulation [18], as the presence of contraction following electrical stimulation was required for the observed beneficial effect on cell elongation, contractile properties and hypertrophy. Cardiomyocytes were also reported to have a preferred orientation in response to field stimulation [19], so that they were more excitable when the long axis of the cell was oriented parallel to the electrical field.

Most currently available cell culture systems provide only isolated microenvironmental cues such as independent application of either topographical [16], electrical [10], adhesive [20, 21] or biochemical cues [22]. Thus development of advanced cell cultivation systems incorporating multiple cues is urgently needed. In our previous study [23] we used abraded polyvinyl surfaces that were placed between two parallel carbon electrodes to combine electrical and topographical cues into a single system. Although this approach allowed us to gain valuable insight in the response of fibroblasts and cardiomyocytes to combined electrical and topographical cues, the system contained several shortcomings: a) since topographical cues were created by abrading the surface using a fine lapping paper, there was variability in abrasion shape, width and depth on the same surface as well as between the surfaces; b) polyvinyl is not a preferred material for cell culture; and c) multiple surfaces had to be placed between two parallel carbon electrodes, thus forcing us to apply identical electrical stimuli and soluble factors (biochemical cues) to different surfaces.

We report here the development of a microfabricated system, incorporating topographical and electrical cues on a single chip, which overcomes all of the above shortcomings and enables cultivation of highly differentiated cardiomyocytes. The cell culture chips were created by hot embossing of polystyrene, which is a standard tissue culture plastic material, in order to create microgrooves and microridges of precisely defined depth, width and periodicity. The gold electrodes were electrodeposited such that the microgrooves oriented either parallel or perpendicular to the electrodes, enabling studies of interaction between topographical and electrical cues. Most importantly, the electrical stimulation parameters and biochemical cues can be independently controlled

on each chip. These features will ultimately make the described system a useful and unique platform for studies of stem cell differentiation or drug testing.

## **3.2 Methods**

### 3.2.1 Hot embossing mold fabrication

The mold for hot embossing was fabricated by standard photolithography for the surfaces with 4 mm period grating and deep-UV lithography for the 1 mm period grating. The trench was etched by RIE (PlasmaLab 80 Plus, Oxford Instruments, UK) using a mixture of gas of 20sccm CF<sub>4</sub> and 2sccm O<sub>2</sub> at 10mTorr and 100W, leading to an etching rate ~20 nm/min. The depth of the trench was 0.4mm.

### 3.2.2 Hot embossing for preparation of microstructured polystyrene surfaces

We used hot embossing (EVG, Austria) to create a polystyrene replica of the silicon mold. We dispersed the polystyrene pellets (120 kg/mol) evenly over an area of 30 cm<sup>2</sup> on top of the mold and covered it with another flat wafer. Both the mold and the flat wafer were treated with an anti-adhesion silane layer (1H, 1H, 2H, 2H-perfluorooctyl-trichlorosilane) to facilitate the separation. We heated up the stack to 160°C, applied a force of 1500N, waited for 2 minutes and then evacuated the system to below 1 Torr, followed by applying the final force of 10000N for 5 minutes. The system was then vented and cooled down to 90°C before removing the force. The thickness of the polystyrene sheet was 300-400 nm.

### 3.3.3 Electrode fabrication

The grating at the electrode area (the area between electrodes covered with Si pieces to protect it from etching) was first etched by O<sub>2</sub> plasma with a power of 100W, 20sccm O<sub>2</sub> and 100mTorr (etching rate 100nm/min) for 10 minutes, so that the sidewall of the grating ridges became inclined which was essential to ensure a continuous metal film (otherwise, metal film would break at the vertical ridge-edges). Next, the electrode area was coated with 30 nm Cr adhesion layer and 70 nm Au conducting layer. Electroplating using Au electrolyte from Technic Inc was subsequently carried out to

deposit ~800nm Au film on the electrode area. The chips were fabricated such that the microgrooves were oriented either perpendicular or parallel to the electrodes. As a control, smooth polystyrene surfaces were used between the electrodes.

#### 3.3.4 O<sub>2</sub> Plasma Treatment

For improved cell adhesion, all substrates were treated with oxygen plasma with a power of 100W, 20sccm O<sub>2</sub> and 10mTorr for 20 seconds.

#### 3.3.5 Scanning electron microscopy

The microgrooved surfaces were examined using Hitachi S4800 field-emission scanning electron microscope (SEM).

#### 3.3.6 Cell Source

We obtained cardiomyocytes from 2-day old neonatal Sprague-Dawley rats as described in previous studies[23] and according to a protocol approved by the University of Toronto Committee on Animal Care. Briefly, the hearts were quartered and subjected to an overnight digest at 4°C in 0.06% (w/v) solution of trypsin (Sigma) in Ca<sup>2+</sup> and Mg<sup>2+</sup> free Hank's balanced salt solution (HBSS) (Gibco). A series of five 4-8min digestions in collagenase II (Worthington, 220 units/mL) in HBSS followed. The resulting cell suspension was pre-plated for 1 hr in T75 flasks to enrich for cardiomyocytes.

#### 3.3.7 Cell Culture

The cells were cultured in Dulbecco's Modified Eagle Medium (DMEM) containing 4.5 g/L glucose, with 10% (v/v) fetal bovine serum (FBS), 1% HEPES and penicillin-streptomycin (100 units/mL and 100 µg/mL). Sheets of microgrooved polystyrene were cut into pieces of 1 cm<sup>2</sup> area, and were each placed in one well of a 12-well tissue culture dish with the side of the microgrooves facing up. The pieces were then soaked in 70% ethanol overnight and exposed to UV light in a biosafety cabinet for 2 hours. Each piece of polystyrene was coated with 60 µL of fibronectin (25 ng/µL, Sigma) in phosphate buffer saline (PBS) for 90 min.

For experiments without electrical stimulation, 500 000 cardiomyocytes in 60  $\mu$ L of culture medium were seeded onto the fibronectin coated surfaces for 1 hr to allow the cells to attach, then 2 mL of culture medium were added into each well. The cells were cultivated for 7 days, at which point they were fixed in 4% paraformaldehyde (PFA) solution in PBS (made from powder, Sigma).

For experiments with electrical stimulation, chips with built-in electrodes were used. A platinum wire was wrapped around each electrode in a secure manner to ensure consistent contact with the electrode. The chip was then placed in a well of a 12-well dish, with the wires extending to the outside of the well. The chips were secured such that they did not touch the bottom of the well. This an arrangement was made to prevent the cells from attaching to the tissue culture wells instead of microgrooved substrate itself. The surfaces were treated with 70% ethanol and UV irradiation followed by fibronectin coating as described above. Cells were seeded and cultivated for 24 hrs in the same manner as in the experiments without electrical stimulation. After 24 hrs, the platinum wires were connected to a programmable electrical stimulator (Grass s88x) [23-25]. Electrical field stimulation was applied in a form of symmetric biphasic pulses at the frequency of 1Hz, amplitude of 1.15V/cm per phase and duration of 1ms per phase. The desired stimulation regime was verified with an oscilloscope with this particular setup in place. With respect to the electric field direction, there were at least N=3 samples within each group (parallel, perpendicular, smooth). Electrical field stimulation was stopped at day 7 and cells were fixed with 4% PFA as described above.

### 3.3.8 Cell Staining and Assessment

To visualize morphology and phenotype of cardiomyocytes cultured under the different conditions, immunofluorescent staining using the following primary antibodies was performed as previously described [23]: monoclonal anti-sarcomeric  $\alpha$ -actinin made in mouse at dilution factor of 1:50 (Sigma) and polyclonal anti-connexin-43 antibody made in rabbit at 1:100 (Chemicon). Live-dead staining was performed as described previously using CFDA and PI according to the manufacturer's protocol (CFDA = carboxyfluorescein diacetate, succinimidyl ester, 10 $\mu$ M; PI = propidium iodide, 75  $\mu$ g/mL Molecular Probes)[23]. Images were taken using a fluorescence microscope

(Olympus IX2-UCB) or a confocal microscope (Olympus FV5-PSU confocal with IX70 microscope).

### 3.3.9 Image Analysis

ImageJ software was used to determinate cell alignment and elongation as described previously [23]. Briefly, cell elongation was defined as the ratio of the long axis of the cell compared to its short axis. Cell alignment was determined by measuring the angle of deviation of the long axis of the cell from the microgroove line. For cells cultured on the control surfaces without microgrooves, the angle was taken to be the angle between the long axis of the cell and the electric field lines or a fixed horizontal line in non-stimulated samples.

### 3.3.10 Excitation threshold and maximum capture rate

Functional properties of cardiomyocytes were determined by measuring excitation threshold (ET) and maximum capture rate (MCR). For non-stimulated samples, the ET and MCR were measured on day 7, in an electrical stimulation chamber consisting of two parallel carbon electrodes spaced 1cm apart and connected to an electric stimulator (Grass s88x)[23]. Measurements were taken with the sample placed both parallel and perpendicular, respectively one after the other, to the carbon electrodes. For experiments with electrical stimulation, ET and MCR were determined using the electrodes on the substrate itself, at day 1 and on day 7 just prior to fixing the cells. ET was defined as the minimum voltage required to induce synchronous contractions of at least 75% of the cells in the field of view, by monophasic pulses of duration of 2 ms and frequency of 1Hz. MCR was the maximum beating frequency that could be induced at 200% of the ET.

### 3.3.11 Statistical Analysis

SigmaStat 3.0 software was used for statistical analysis. Tests for normality and equal variance were performed on all quantitative data sets. If the data sets satisfied the assumptions of normal distribution and equal variance, one-way ANOVA in conjunction with the Student-Newman-Keuls test was used to compare multiple groups and t-test was used to compare two groups. Otherwise, we performed the Kruskal-Wallis one-way

ANOVA on ranks in conjunction with Dunn's method for pairwise comparisons. The groups were considered significantly different if  $p < 0.05$ .

### 3.3 Results and Discussion

#### 3.3.1 Hot embossing of polystyrene for fabrication of microgrooved surfaces with built-in electrodes

The main objective of this study was to create a microfabricated cell culture substrate that will enable integration of precise topographical and electrical cues into a single system and their independent control. For this purpose, we chose to utilize hot embossing as a high throughput molding process of low cost and high pattern transfer fidelity. Unlike photolithography which can pattern polymers by lithography followed by pattern transfer via etching, hot embossing creates a pattern inside a polymer within a single step. It is suitable for patterning a broad range of thermoplastic polymers including those that are biodegradable, biocompatible or semiconducting. Hot embossing has been used previously to create micron scale features in polymethyl methacrylate [26-28], polyimide [26], polyethylene [29] and polycarbonate [29]. In addition, hot embossing is a "dry" process, which is essential for patterning polymers susceptible to degradation by solvents, water or other chemicals. Auger, Veres and colleagues were the first to use polystyrene surfaces with micron-scale features created by hot-embossing for cell culture [30]. Polystyrene is a standard plastic material used in tissue culture, thus motivating its use in this study as well.

The microgrooves fabricated in polystyrene via hot embossing technique were used to introduce topographical cues to the cell culture, while the electrodes made via gold electroplating were used to introduce electrical cues. The distance between electrodes was chosen as 1cm, consistent with our previous work [23, 24], as well as to enable easy control of the electric field strength, which is measured in units of V/cm. (Figure 3.1A). Two different geometries were assessed independently of electrical field stimulation: 1) substrates consisting of 0.5 $\mu\text{m}$ -wide grooves and 0.5 $\mu\text{m}$ -wide ridges (1 $\mu\text{m}$  period) (Figure 3.1B), and 2) substrates consisting of 3 $\mu\text{m}$ -wide grooves and 1 $\mu\text{m}$ -wide ridges (4 $\mu\text{m}$  period) (Figure 3.1C). The depth of the microgrooves was 400nm and

identical in both cases. Scanning electron microscopy images indicated that the microgrooves were of uniform size and spacing and mostly defect-free (Figure 3.1B,C). While the groove width was significantly smaller than the width of V-shaped abrasions used in our previous studies (1  $\mu\text{m}$  compared to 12  $\mu\text{m}$ ) [23], the depth was on the same order of magnitude. The oxygen-plasma treatment, as well as the additional coating of fibronectin prior to cell culture, facilitated cell adhesion to the surfaces during seeding and culture. High cell seeding density and efficient cell adhesion is important for achieving confluent monolayers, as cardiomyocytes do not proliferate.

This approach enabled key advances over the set-up used previously for simultaneous application of electrical and topographical cues [23]. In our previous studies, the V-shaped micro-channels were fabricated on polyvynil surfaces via manual abrasion, resulting in an uneven surface of varying abrasion dimensions. Previously, in order to subject the samples to an electric field stimulus, all substrates had to be placed inside an electrical stimulation chamber, between two parallel carbon electrodes. These carbon electrodes were in turn connected to the programmable electrical stimulator [23]. In this new setup, each chip was directly connected to the stimulator, eliminating difficulties involved in securing samples at the correct position between the electrodes and enabling independent application of the electrical cues to each substrate. In addition, each substrate was placed in its own culture medium well, ensuring that no cross-talk via soluble factors occurs between the substrates.

### 3.3.2 Cardiomyocyte phenotype and function on microgrooved polystyrene surfaces

Cells subjected to topographical cues without electrical field stimulation were significantly more elongated than those on non-abraded surfaces (Figure 3.2A, C) with the aspect ratio in the range of 4-6, in comparison to the aspect ratio of 3 for non-abraded surfaces. In addition, the 1  $\mu\text{m}$  grating resulted in a significantly higher elongation than the 4  $\mu\text{m}$  grating.

Cardiomyocytes were significantly more aligned on surfaces with topographical cues as compared to those on non-abraded surfaces (Figure 3.2B, C). Cells on surfaces with grating period of both 4  $\mu\text{m}$  and 1  $\mu\text{m}$  had an average angle of deviation of 4°, whereas those on non-abraded surfaces had an angle of deviation of approximately 42°.

An angle of deviation of zero indicates perfect alignment, whereas an angle of 45° indicates maximal misalignment. Moreover, narrow distribution in orientation for cells on surfaces with microgrooves indicated the consistency of the applied topographical cues, relative to a wide distribution on the non-abraded surfaces, indicating lack of guidance for alignment (Figure 3.2B). In our previous studies[23], the uneven surfaces made via manual abrasion resulted in a wider distribution of cell orientation angles, where the average angle was in the range of 10-12°, in comparison to the current narrower distribution and smaller average angle of 4°. Thus, the uniform channels obtained by hot embossing provided topographical cues in a more reliable manner.

The fact that similar responses in cellular alignment and elongation were observed, in this study and in our previous studies [23], is consistent with a previously reported finding that the depth of the channels [31], rather than the width, governs these cellular processes. Cellular orientation may be determined by confining focal adhesion molecules within the ridges of the microgrooves since the adhesion clusters and the ridges are on the same order of magnitude (~1-2  $\mu\text{m}$ ) [32, 33]. The adhesion molecules are coupled to the cell's cytoskeleton, thus resulting in the overall orientation of the cell along the direction of the ridges.

Live/dead staining indicated that the great majority of cells were alive in all of the experimental groups (Figure 3.2C). Immunofluorescence staining was used to validate the phenotype of the cardiomyocytes. Staining was performed for cardiac gap junction protein Connexin-43 (Figure 3.2D) and contractile protein sarcomeric  $\alpha$ -actinin (Figure 3.3). Connexin43 (Cx43) is required for electrical communication between the cells and as such it is essential for contraction of both engineered and native cardiac tissue. Immunostaining for Cx43 revealed that cells in the non-stimulated groups developed gap junctions necessary for intercellular communication (Figure 3.2D). However, the distribution of gap junctions was punctate, characteristic of the neonatal myocardium where gap junctions are distributed over the entire surface of ventricular cardiomyocytes [2]. In addition, there were no significant differences between the cells cultivated on microgrooved and smooth surfaces.

Sarcomeric  $\alpha$ -actinin it is responsible for attaching actin filaments to Z-lines thereby cross-linking thin filaments in adjacent sarcomeres. It is found in both neonatal

and mature cardiomyocytes. Contractile proteins such as  $\alpha$ -actinin become increasingly more organized in the heart as development progresses [34]. Staining for sarcomeric  $\alpha$ -actinin, revealed that more than 90% of the cells at day 7 time were indeed cardiomyocytes and not other cell types (Figure 3.3 and 3.5). Confocal microscopy revealed the large extent to which the cell monolayers were ordered by topographical cues and cross-striations (perpendicular to the long axis of the cells), indicative of extremely well-developed contractile apparatus (Figure 3.3).

Spontaneous contractions of the monolayers were apparent as early as day 4 in culture. Next, we assessed the monolayer's electrical excitability on the substrate by measuring excitation threshold (ET) and maximum capture rate (MCR). The excitation threshold is defined as the minimum voltage required to induce synchronous beating of 75% of the cells in the field of view. It is indicative of the stimulus amplitude required to achieve contraction of a cell or a cell monolayer. Generally, healthy and easily excitable cardiomyocytes have low ETs. MCR, another measure of electrical excitability, is defined here as the maximum beating frequency of the cells measured at 200% of the ET. MCR values indicate the contractile versatility of the cells and ability to beat at high frequencies. Low ET and high MCR values are desirable for the purposes of devising in vitro models for drug testing as well as the tissue engineering of cardiac patches.

ET was measured at the end of the culture period (day 7) by placing the microgrooved samples first parallel then perpendicular to the direction of the electric field. At day 7, the average ET was higher if the measurement was taken with the aligned cells placed perpendicular to the electric field (Table 3.1). When placed parallel to the electric field, however, the same sample would exhibit a lower ET value consistent with the previous studies of Tung and colleagues [35]. Previously, the average ET value for cardiomyocytes in vitro was documented to be about 2.3V/cm [23, 25]. Average ET values measured in the parallel direction and those on smooth surfaces were approximately equal to or slightly lower than this value, whereas cells placed perpendicular to the electric field had values higher than 3.0V/cm. This implies that the orientation of the cell monolayer (or a tissue-engineered construct) with respect to the electric field is an important factor in determining and enhancing electrical excitability of the cells. For the non-stimulated samples, there was no significant difference in MCR

when the measurements were taken with the cells oriented parallel or perpendicular to the field lines (Table 1). In addition, the values for 4 $\mu$ m, 1 $\mu$ m period grating and non-abraded surfaces were comparable.

### 3.3.3 Electrical stimulation during culture of cardiomyocytes

We hypothesized that electric field stimulation applied via electrodes integrated within the tissue culture substrate will yield cells with a differentiated phenotype. By placing the cells on the same surface on which the electrodes reside, the electrical stimuli may be applied more directly with less resistance, while the electric field strength remains the same. This setup may also eliminate resistances to electrical current that is inherent to the bioreactor consisting of carbon electrodes placed in a glass chamber [23, 24]. The chosen field amplitude of 1.15V/cm, delivered in biphasic pulses, was equivalent to the 2.3V/cm, monophasic pulses, used in the previous studies [23]. During the culture period, pH in the medium was maintained and no gas formation was observed indicating an absence of electrolysis.

Effects of electric field stimulation, in addition to simultaneous topographical cues, on cardiomyocytes alignment and elongation are illustrated in Figure 4. Cardiomyocytes cultured on microgrooves parallel to the electric field were significantly more aligned than those cultured perpendicular to the electric field as well as those cultured on smooth surfaces (Figure 3.4A). This is consistent with previous findings that cardiomyocytes prefer to align in the direction of the electric field [23, 24], and hence may also have developed a phenotype closer to that found in the native environment.

Comparison between stimulated samples (Figure 3.4A) and non-stimulated samples (Figure 2A) indicated that electrical field stimulation significantly improved cellular elongation on smooth surfaces (aspect ratio of  $2.5 \pm 1.1$  for non-stimulated vs.  $5.2 \pm 2.2$  for stimulated cells,  $p < 0.05$ ), and on surfaces where the gratings of 1 $\mu$ m period were oriented parallel to the electric field (aspect ratio of  $5.6 \pm 5.6$  for non-stimulated vs.  $8.9 \pm 3.8$  for stimulated,  $p < 0.05$ ). Hence, this suggests that electric field stimulation may further improve cellular elongation when topographical cues are also used to guide cellular alignment in the preferred direction (parallel) with respect to the electric field.

For the stimulated samples, the average angle of deviation was significantly smaller in the cases where topographical cues were present, compared to the random cellular orientation on the smooth surfaces (Figure 3.4B). Comparison of stimulated samples (Figure 3.4B) to the corresponding non-stimulated samples (1 $\mu$ m period and smooth surface, Figure 3.2B) indicated that electrical stimulation has no significant effect of cell orientation, although the average orientation angle was slightly smaller on the stimulated smooth surfaces ( $37 \pm 25^\circ$ ) compared to the non-stimulated smooth surfaces ( $42 \pm 22^\circ$ ). Taken together, these findings indicate that topographical cues are a stronger determinant of cellular orientation than the electric field stimulation, consistent with previous findings [23].

Live/dead staining indicated that the great majority of cells were alive in all of our experimental groups (Figure 3.2C and Figure 3.4C) with no significant differences in cell viability between respective stimulated and non-stimulated samples (Figure 3.2C: a,b, and Figure 3.4C: a,b). An exception was the group cultivated on non-abraded surfaces in the presence of electrical field stimulation (Figure 3.4C: c) where a larger number of red nuclei (dead cells) were observed in comparison to the cells cultivated on microstructured surfaces (Figure 3.4C:a,b).

Electrical field stimulation clearly resulted in the abundance of gap junctional protein Cx43 (Figure 3.4D) indicating that electrical stimulation may facilitate cell-cell communication. Interestingly, cardiomyocytes cultured on microgrooves and subjected to electric field stimulation demonstrated a higher abundance of gap junctional proteins at the ends of the elongated cells (arrows in Figure 3.4D: a,b) consistent with the appearance of Cx43 in adult cardiomyocytes. This effect was not noted in any other sample groups. Although electrical field stimulation clearly induced the presence of Cx43 to change from punctate (Figure 3.2D) characteristic of the neonatal heart to the one confined to cell periphery, some Cx43 was observed at the lateral sides of the cells, especially on smooth surfaces (Figure 3.4D: c), indicating that further maturation was required.

Cross-striations characteristic of healthy cardiomyocytes were observed in the stimulated groups (sarcomeric  $\alpha$ -actinin staining, Figure 3.5). On microgrooved surfaces, the cross-striations were perpendicular to the cell's long axis as well as the microgroove

direction; while on the smooth surfaces, there was no preferred directionality as multiple overlapping cross-striations were observed (Figure 3.5).

Upon application of electrical field stimulation, ET of the cells cultured on smooth surfaces increased, but remained the same for cells cultivated on the grooves oriented parallel to the electrical field and decreased significantly for cells cultivated on the grooves orientated perpendicular to the electric field (Table 3.2). ET values for the parallel group and smooth controls were comparable to that reported in our previous studies [23], whereas those for the perpendicular group were significantly lower than what we reported previously and comparable to the ET found in the neonatal rat heart [23, 25]. No significant differences in MCR were observed for the stimulated samples, although at Day 7 a trend towards a higher MCR in the parallel group was observed (Table 3.2).

#### 3.3.4 Advantages over previous cell culture set-ups

Large number of previous studies was focused on independently providing either electrical cues or contact guidance cues to cardiomyocytes during culture. For example, chronic supra-threshold electrical field stimulation of cardiomyocytes provided by parallel electrodes placed around standard 2D cell culture substrates was shown to preserve contractility of cardiomyocytes [10], maintain calcium transients [11], promote hypertrophy [12], increase protein synthesis [13, 14] and maintain action potential duration and maximum capture rate [15]. Topographical cues or micro-contact printing of extracellular matrix components were previously used to introduce contact guidance cues. Entcheva and colleagues [36] used electrospinning to fabricate oriented biodegradable non-woven polylactide (PLA) scaffolds for cultivation of neonatal rat cardiomyocytes which oriented along the fiber direction and acquired a remarkably well developed contractile apparatus. Attachment and alignment of cardiomyocytes has been modulated using grooved and pegged silicone membranes[17]. Abraded polyvynil coverslips were used to create oriented cardiomyocyte monolayers for studies of electrical impulse propagation and arrhythmia[37]. Spatially organized cardiomyocyte cultures were created on biodegradable polyurethane films with micropatterned laminin lanes[20]. Elongated

cardiomyocyte phenotype was achieved by patterning non-adhesive photoresist lanes on a glass substrate [38, 39].

In our previous study, we used abraded polyvinyl surfaces placed between two parallel electrodes to simultaneously apply topographical and electrical cues to the monolayers of 3T3 fibroblasts and neonatal rat cardiomyocytes. The main finding of that study was that surface topography more strongly determined orientation of fibroblasts and cardiomyocyte, yet pulsatile electrical field stimulation had appreciable effects on cellular elongation. This response was completely abolished by inhibition of actin polymerization and only partially by inhibition of PI3K pathway. However, the system described in our previous study had several shortcomings including the non-uniform nature of abrasions as topographical cues as well as the inability to independently control the electrical stimulation modes on different surfaces.

We described here a microfabricated cell culture chip with integrated topographical and electrical cues. The precise topographical cues were enabled by hot embossing of polystyrene while electrical stimulation was provided by electrodeposited gold electrodes. Our results here demonstrate that the phenotype of cardiomyocytes and their contractile properties can be modulated in a facile manner using these microfabricated chips. The general findings regarding the interactive effects of electrical field stimulation and topographical cues are in agreement with those in our previous studies [23]. The current results also demonstrated that topography was a stronger determinant of cellular orientation, while cell elongation could be enhanced using electrical field stimulation provided that the topography acted in concert with electrical field. In the case of cardiomyocytes, for enhanced elongation the topographical cues had to be orientated parallel to the electric field lines.

We also demonstrated that the microfabricated cell culture chips maintained and enhanced the differentiated phenotype of cardiomyocytes. As such the system is superior to the standard tissue culture wells that yield de-differentiated cardiomyocytes with time in culture. In addition, no pharmacological agents were required to maintain the contractility and differentiated phenotype of cardiomyocytes.

Due to the stated advantages, we anticipate that the described chips will become a useful tool in drug testing and studies in maturation of stem cell derived cardiomyocytes.

The base material for these chips, the tissue culture polystyrene, was selected due to its compatibility with culture of cells derived from many different sources. The chips can easily be integrated into an array with independent wells for drug testing, where electrical stimulation parameters to each chip are independently controlled. Furthermore, non-invasive imaging of the electrophysiological properties in response to a pharmacological agent is possible on-line using optical mapping. The transparent nature of the base material also ensures compatibility with fluorescence and optical microscopy enabling real-time monitoring of gene expression (in conjunction with fluorescent reporters), cell morphology and impulse propagation during drug testing.

We demonstrated here that the described system enables maturation of cardiomyocytes derived from neonatal rat cardiomyocytes. These findings have significant implications in the maturation of cardiomyocytes derived from stem cells. Embryonic stem (ES) cells are capable of generating bona fide cardiomyocytes in large numbers [40-42], [43, 44]. However, most studies agree that the developmental level of these cardiomyocytes corresponds to those found in the neonatal heart, and the maturation of ES cell derived cardiomyocytes to an adult phenotype has not been achieved yet [45]. The described cell culture chips may become a useful tool in these maturation studies, due to the integrated application of electrical and topographical cues and ability to independently apply biochemical cues (e.g. growth factors) to different substrates.

### **3.4 Conclusions**

Hot embossing enabled fabrication of polystyrene cell culture chips with precise topographical cues consisting of microgrooves and microridges with periodicity of 1 and 4  $\mu\text{m}$ . Electroplating of Au enabled integration of the electrodes for electric field stimulation into the microgrooved cell culture chips. Simultaneous application of biphasic electrical pulses and topographical cues enhanced the phenotype and maturation level of neonatal rat cardiomyocytes as evidenced by a well developed contractile apparatus (sarcomeric  $\alpha$ -actinin staining) and gap junctions confined to the cell-cell end junctions rather than the punctate distribution found in neonatal cells. Biphasic electric

field stimulation of cardiomyocytes cultivated on microgrooves oriented parallel to the field lines, significantly enhanced the levels of cellular elongation beyond those found on smooth surfaces as well as non-stimulated microgrooved surfaces. Cellular orientation was strongly determined by the topographical cues.

### 3.5 Figures and Tables

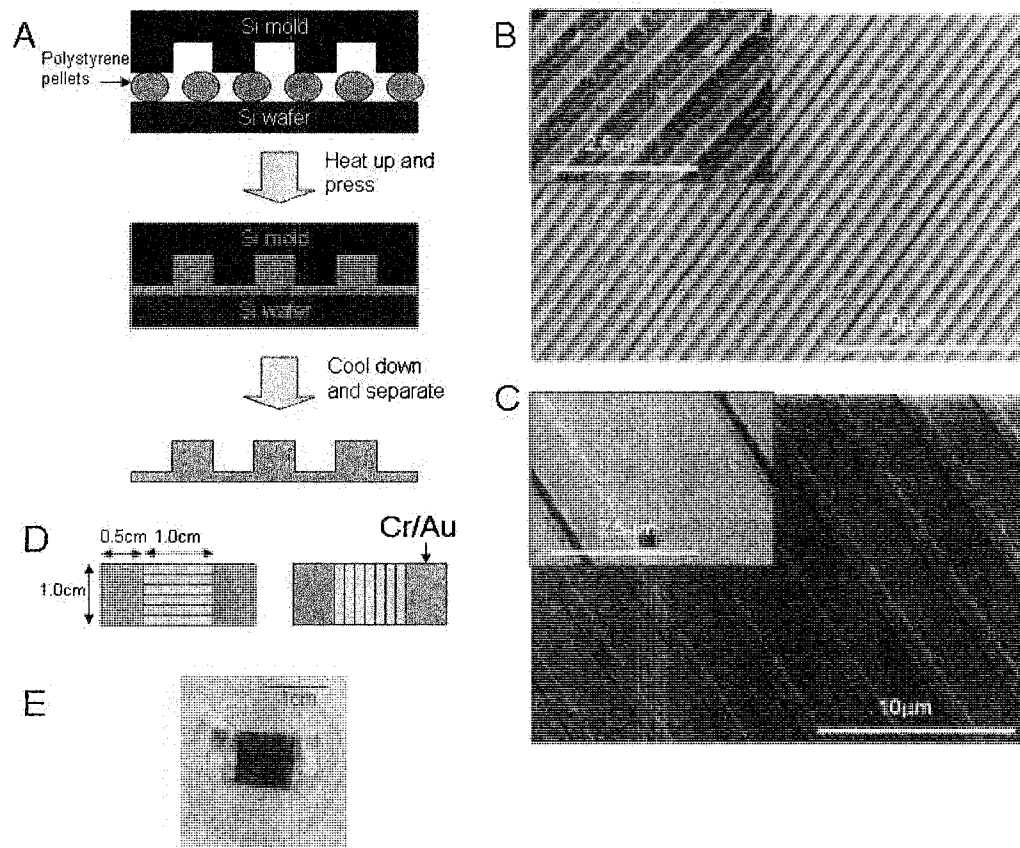


**Figure 3.1. Microgrooved surfaces prepared by hot embossing of polystyrene.** A) Schematics of hot-embossing process. Scanning electron micrograph of the microgrooved surface with B)  $1\mu\text{m}$  period,  $0.5\mu\text{m}$  groove width,  $400\text{nm}$  groove height and C)  $4\mu\text{m}$  period,  $3\mu\text{m}$  groove width,  $400\text{nm}$  groove height. D) Schematics of the orientation of grooves with respect to the electrodes. E) Photomicrograph of a cell culture chip with cardiomyocytes between electrodes (blue) visualized by Giemsa staining.

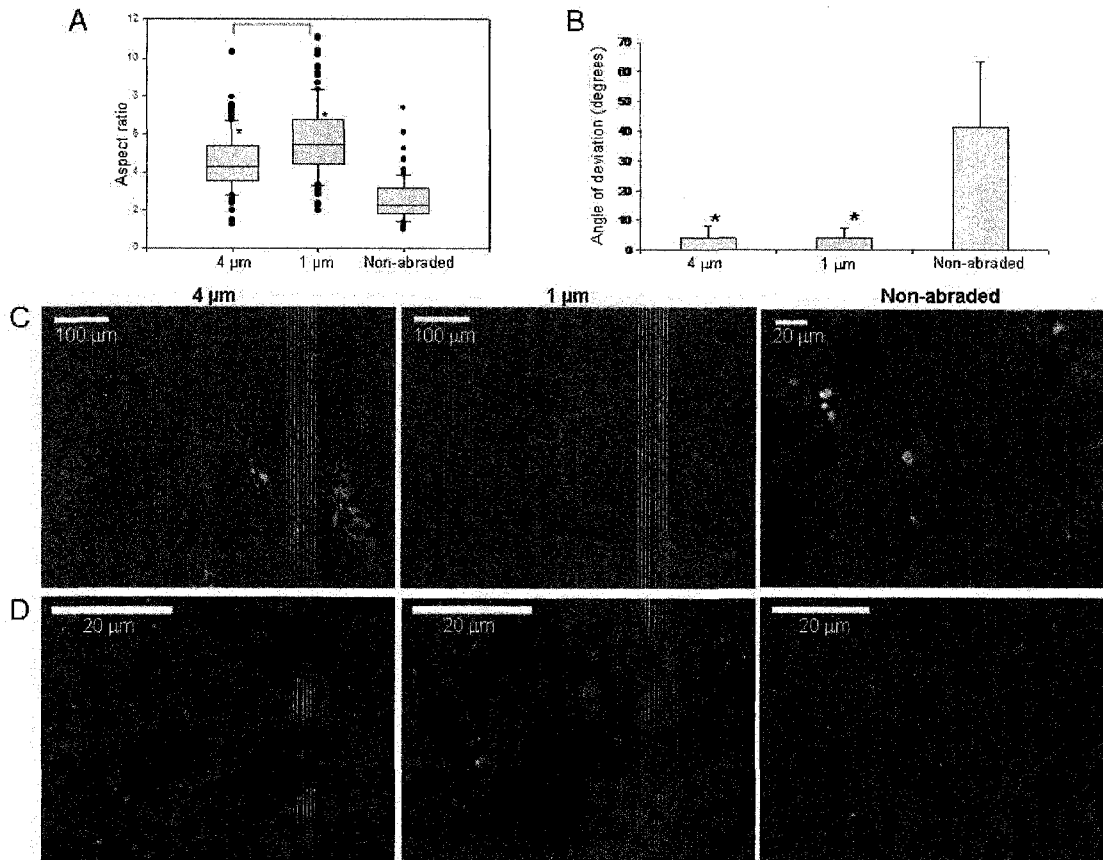


**Figure 3.2. Cardiomyocytes cultivated on microgrooved polystyrene surfaces without electrical field stimulation. A) Aspect ratio B) Orientation angle C) Live/dead staining and D) Fluorescent micrographs of cells immunostained for Connexin-43 (green dots). Nuclei were counterstained blue with DAPI**

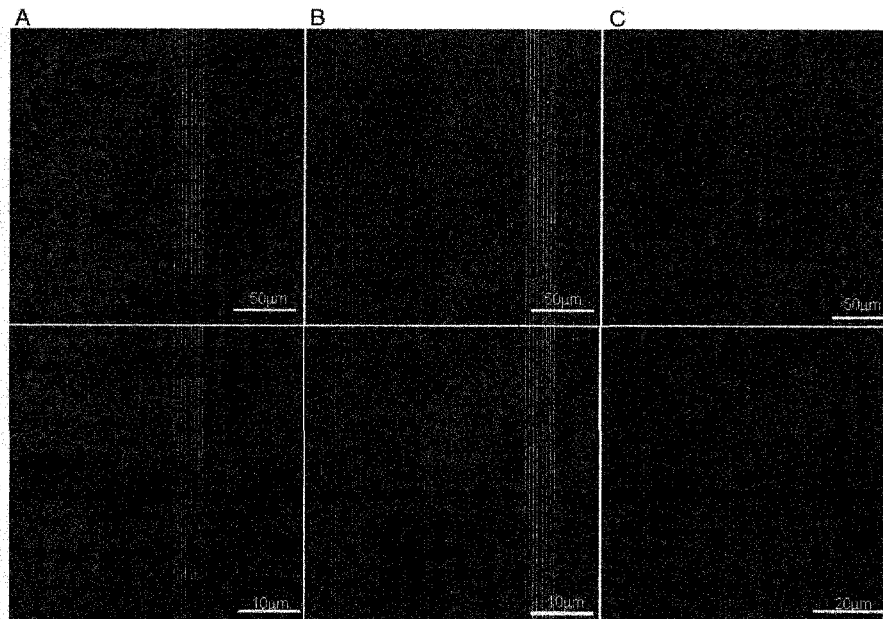


**Figure 3.3. Sarcomeric- $\alpha$ -actinin staining of cardiomyocytes cultivated on the microgrooved polystyrene surfaces with A) 4  $\mu\text{m}$  period, B) 1  $\mu\text{m}$  period, and C) Smooth controls. Images were obtained by confocal microscopy.**

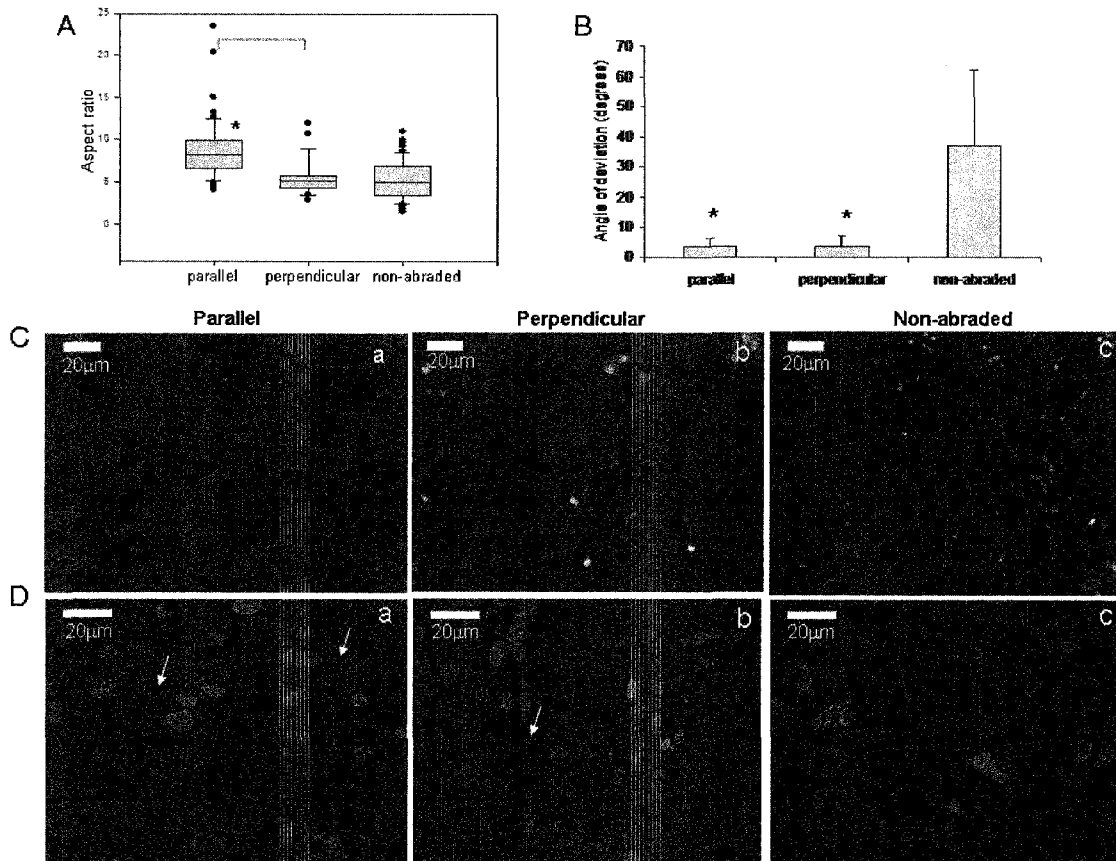


**Figure 3.4. Cardiomyocytes cultivated on microgrooved surfaces (1 $\mu$ m period) in the presence of electric field stimulation.** Electrical stimulation was achieved via symmetric biphasic square pulses at the frequency of 1 Hz, pulse duration of 1ms per phase and amplitude of 1.15V/cm per phase. A) Aspect ratio, B) Orientation angle, C) Live/dead staining, and D) Fluorescent micrographs of cells immunostained for Connexin-43 (green dots). Nuclei were counterstained blue with DAPI. Arrows indicate the localization of Connexin-43 at cell-cell junctions.



**Figure 3.5. Sarcomeric- $\alpha$ -actinin staining of cardiomyocytes cultivated on microgrooved surfaces (1 $\mu$ m period) in the presence of electric field stimulation.** Electrical stimulation was achieved via symmetric biphasic square pulses at the frequency of 1 Hz, pulse duration of 1ms per phase and amplitude of 1.15V/cm per phase. A) Microgrooves oriented parallel to the field lines, B) Microgrooves oriented perpendicular to the field lines, and C) Smooth surface. Nuclei were counterstained blue with DAPI. Images were obtained by fluorescence microscopy.

**Table 3.1. Functional properties of cardiomyocytes cultivated on microgrooved surfaces without electric field stimulation.** At the end of cultivation (day 7) samples were field-paced using monophasic pulses of 2ms duration to assess their electrical excitability parameters. Brackets indicate the number of samples that could be induced to contract by stimulation, over the total number of samples tested in that group. \* Significantly different than the non-abraded control.

Periodicity	4 $\mu$ m		1 $\mu$ m		Smooth
	Parallel	Perpendicular	Parallel	Perpendicular	
Direction with respect to electric field during test					
ET (V/cm)	2.8 $\pm$ 1.8 (3/3)	3.4 $\pm$ 1.4 (3/5)	1.9 $\pm$ 0.5 (3/3)	3.9 $\pm$ 1.0* (4/5)	2.1 $\pm$ 1.0 (3/3)
MCR (Hz)	2.5 $\pm$ 0.3 (3/3)	2.2 $\pm$ 0.2 (3/5)	2.5 $\pm$ 0.3 (3/3)	2.4 $\pm$ 0.3 (4/5)	2.5 $\pm$ 0.9 (3/3)

**Table 3.2: Electrical excitability of cardiomyocytes cultivated on microgrooved surfaces of 1 $\mu$ m period in the presence of electric field stimulation.** Electrical field stimulation during culture was achieved via symmetric biphasic square pulses at the frequency of 1 Hz, pulse duration of 1ms per phase and amplitude of 1.15V/cm per phase. At the end of cultivation (day 7) samples were field-paced using monophasic pulses of 2ms duration to assess their electrical excitability parameters. Brackets indicate the number of samples that could be induced to contract by stimulation, over the total number of samples tested in that group. & Significantly differently than the same group at day 1.

Time point	Day 1			Day 7		
	Parallel	Perpendicular	Smooth	Parallel	Perpendicular	Smooth
Direction with respect to the electric field during culture and test						
ET (V/cm)	2.4 $\pm$ 1.3 (3/4)	3.7 $\pm$ 0.3 (2/3)	2.1 $\pm$ 1.5 (3/3)	2.4 $\pm$ 1.2 (4/4)	1.2 $\pm$ 0.5& (3/3)	3.8 $\pm$ 1.9 (2/3)
MCR (Hz)	4.2 $\pm$ 0.6 (3/4)	3.9 $\pm$ 0.6 (2/3)	3.9 $\pm$ 1.0 (3/3)	3.6 $\pm$ 1.4 (4/4)	2.6 $\pm$ 0.4 (3/3)	2.6 $\pm$ 0.8 (2/3)

### 3.6 References

1. Severs, N.J., The cardiac muscle cell. *Bioessays*, 2000. 22(2): p. 188-199.
2. Peters, N.S., et al., Spatiotemporal relation between gap junctions and fascia adherens junctions during postnatal development of human ventricular myocardium. *Circulation*, 1994. 90(2): p. 713-25.
3. Matsuura, K., et al., Adult cardiac Sca-1-positive cells differentiate into beating cardiomyocytes. *J Biol Chem*, 2004. 279(12): p. 11384-91.
4. Bird, S.D., et al., The human adult cardiomyocyte phenotype. *Cardiovasc Res*, 2003. 58(2): p. 423-34.
5. Zimmermann, W.H., et al., Tissue engineering of a differentiated cardiac muscle construct. *Circulation Research*, 2002. 90(2): p. 223-230.
6. Simpson, D.G., et al., Regulation of cardiac myocyte protein turnover and myofibrillar structure in vitro by specific directions of stretch. *Circ Res*, 1999. 85(10): p. e59-69.
7. Zhuang, J., et al., Pulsatile stretch remodels cell-to-cell communication in cultured myocytes. *Circ Res*, 2000. 87(4): p. 316-22.
8. Gopalan, S.M., et al., Anisotropic stretch-induced hypertrophy in neonatal ventricular myocytes micropatterned on deformable elastomers. *Biotechnol Bioeng*, 2003. 81(5): p. 578-87.
9. Fast, V.G. and E.R. Cheek, Optical mapping of arrhythmias induced by strong electrical shocks in myocyte cultures. *Circ Res*, 2002. 90(6): p. 664-70.
10. Berger, H.J., et al., Continual electric field stimulation preserves contractile function of adult ventricular myocytes in primary culture. *Am J Physiol*, 1994. 266(1 Pt 2): p. H341-9.
11. Holt, E., et al., Electrical stimulation of adult rat cardiomyocytes in culture improves contractile properties and is associated with altered calcium handling. *Basic Res Cardiol*, 1997. 92(5): p. 289-98.
12. Johnson, T.B., et al., Electrical stimulation of contractile activity accelerates growth of cultured neonatal cardiocytes. *Circ Res*, 1994. 74(3): p. 448-59.
13. Ivester, C.T., et al., Contraction accelerates myosin heavy chain synthesis rates in adult cardiocytes by an increase in the rate of translational initiation. *J Biol Chem*, 1995. 270(37): p. 21950-7.
14. Kato, S., et al., Growth effects of electrically stimulated contraction on adult feline cardiocytes in primary culture. *Am J Physiol*, 1995. 268(6 Pt 2): p. H2495-504.
15. Sathaye, A., et al., Electrical pacing counteracts intrinsic shortening of action potential duration of neonatal rat ventricular cells in culture. *J Mol Cell Cardiol*, 2006. 41(4): p. 633-41.
16. Bursac, N., et al., Cardiomyocyte cultures with controlled macroscopic anisotropy: a model for functional electrophysiological studies of cardiac muscle. *Circ Res*, 2002. 91(12): p. e45-54.
17. Deutsch, J., et al., Fabrication of microtextured membranes for cardiac myocyte attachment and orientation. *J Biomed Mater Res*, 2000. 53(3): p. 267-75.
18. Strait, J.B. and A.M. Samarel, Isoenzyme-specific protein kinase C and c-Jun N-terminal kinase activation by electrically stimulated contraction of neonatal rat ventricular myocytes. *J Mol Cell Cardiol*, 2000. 32(8): p. 1553-66.
19. Tung, L., N. Sliz, and M.R. Mulligan, Influence of electrical axis of stimulation on excitation of cardiac muscle cells. *Circ Res*, 1991. 69(3): p. 722-30.
20. McDevitt, T.C., et al., In vitro generation of differentiated cardiac myofibers on micropatterned laminin surfaces. *J Biomed Mater Res*, 2002. 60(3): p. 472-9.

21. Gaudesius, G., et al., Coupling of cardiac electrical activity over extended distances by fibroblasts of cardiac origin. *Circulation Research*, 2003. 93(5): p. 421-428.
22. Darrow, B.J., et al., Functional and structural assessment of intercellular communication. Increased conduction velocity and enhanced connexin expression in dibutyryl cAMP-treated cultured cardiac myocytes. *Circ Res*, 1996. 79(2): p. 174-83.
23. Au, H.T., et al., Interactive effects of surface topography and pulsatile electrical field stimulation on orientation and elongation of fibroblasts and cardiomyocytes. *Biomaterials*, 2007. 28(29): p. 4277-93.
24. Radisic, M., et al., Functional assembly of engineered myocardium by electrical stimulation of cardiac myocytes cultured on scaffolds. *Proc Natl Acad Sci U S A*, 2004. 101(52): p. 18129-34.
25. Radisic, M., et al., Medium perfusion enables engineering of compact and contractile cardiac tissue. *Am J Physiol Heart Circ Physiol*, 2004. 286(2): p. H507-16.
26. Charest, J.L., et al., Hot embossing for micropatterned cell substrates. *Biomaterials*, 2004. 25(19): p. 4767-75.
27. Kricka, L.J., et al., Fabrication of plastic microchips by hot embossing. *Lab Chip*, 2002. 2(1): p. 1-4.
28. Abgrall, P., L.N. Low, and N.T. Nguyen, Fabrication of planar nanofluidic channels in a thermoplastic by hot-embossing and thermal bonding. *Lab Chip*, 2007. 7(4): p. 520-2.
29. Han, A., et al., Multi-layer plastic/glass microfluidic systems containing electrical and mechanical functionality. *Lab Chip*, 2003. 3(3): p. 150-7.
30. Guillemette, M., et al., submitted.
31. Qyang, Y., et al., The renewal and differentiation of Isl1+ cardiovascular progenitors are controlled by a Wnt/beta-catenin pathway. *Cell Stem Cell*, 2007. 1(2): p. 165-79.
32. den Braber, E.T., et al., Orientation of ECM protein deposition, fibroblast cytoskeleton, and attachment complex components on silicone microgrooved surfaces. *J Biomed Mater Res*, 1998. 40(2): p. 291-300.
33. den Braber, E.T., et al., Quantitative analysis of fibroblast morphology on microgrooved surfaces with various groove and ridge dimensions. *Biomaterials*, 1996. 17(21): p. 2037-44.
34. Lemanski, S.F., C.P. Kovacs, and L.F. Lemanski, Analysis of the three-dimensional distributions of alpha-actinin, ankyrin, and filamin in developing hearts of normal and cardiac mutant axolotls (*Ambystoma mexicanum*). *Anat Embryol (Berl)*, 1997. 195(2): p. 155-63.
35. Tung, L., N. Sliz, and M.R. Mulligan, Influence of Electrical Axis of Stimulation on Excitation of Cardiac-Muscle-Cells. *Circulation Research*, 1991. 69(3): p. 722-730.
36. Zong, X., et al., Electrospun fine-textured scaffolds for heart tissue constructs. *Biomaterials*, 2005. 26(26): p. 5330-8.
37. Bursac, N., et al., Cardiac muscle tissue engineering: toward an in vitro model for electrophysiological studies. *Am J Physiol*, 1999. 277(2 Pt 2): p. H433-44.
38. Rohr, S., D.M. Scholly, and A.G. Kleber, Patterned growth of neonatal rat heart cells in culture. Morphological and electrophysiological characterization. *Circ Res*, 1991. 68(1): p. 114-30.
39. Thomas, S.P., et al., Synthetic strands of neonatal mouse cardiac myocytes: structural and electrophysiological properties. *Circ Res*, 2000. 87(6): p. 467-73.
40. Laflamme, M.A., et al., Cardiomyocytes derived from human embryonic stem cells in pro-survival factors enhance function of infarcted rat hearts. *Nat Biotechnol*, 2007. 25(9): p. 1015-24.
41. Amit, M. and J. Itskovitz-Eldor, Derivation and spontaneous differentiation of human embryonic stem cells. *J Anat*, 2002. 200(Pt 3): p. 225-32.

42. Boheler, K.R., et al., Differentiation of pluripotent embryonic stem cells into cardiomyocytes. *Circ Res*, 2002. 91(3): p. 189-201.
43. Sachinidis, A., et al., Cardiac specific differentiation of mouse embryonic stem cells. *Cardiovasc Res*, 2003. 58(2): p. 278-91.
44. Kattman, S.J., T.L. Huber, and G.M. Keller, Multipotent flk-1+ cardiovascular progenitor cells give rise to the cardiomyocyte, endothelial, and vascular smooth muscle lineages. *Dev Cell*, 2006. 11(5): p. 723-32.
45. Kehat, I., et al., Human embryonic stem cells can differentiate into myocytes with structural and functional properties of cardiomyocytes. *J Clin Invest*, 2001. 108(3): p. 407-14.

## 4. The differentiation of human embryonic stem cells derived cardiomyocytes

### 4.1 Introduction

Recently, embryonic stem cells (ESC) have surfaced as an exciting cells source which may provide opportunities for tissue regeneration in various biomedical applications. *In vitro*, ESCs have been shown to differentiate spontaneously into contractile cardiomyocytes both in rodents and in human [1], a property that is of great interest to cardiac tissue engineering and regenerative medicine. Several years ago, cardiac progenitors were derived from a  $Bry^+$  population from the mouse ESC's endoderm [2, 3]. These cells were also demonstrated to have mesoderm potential, and can give rise to cells of cardiovascular lineage including endothelial cells and cardiomyocytes [2]. However, the protocols for the process to specifically drive ESCs to differentiate into CMs are far from being optimized.

Despite the great opportunities that hESC-CM may provide, further characterization is needed before they can be utilized in any tissue engineering strategy. Among the many problems (as with other potential cell sources) associated with hESC-CMs, including the need to create proper engraftment and the need to scale up cell production, the first and foremost apparent obstacle is the need to understand the mechanisms by which hESCs differentiate into CMs. These hESC-CMs can subsequently be matured via other methods to a phenotype comparable to that of native cardiomyocytes. Currently, work is being done by several groups [4-6] to characterize hESC-CMs in their structural and functional properties, as well as their and transcriptional profile (i.e. gene expression). Laflamme et al and van Laake et al. both recently reported that the injection of hESC-CMs into rats and mice (done respectively by the two groups) improved cardiac function induced for up to a 4-week time period in animals in which MI was induced [7, 8]. Moreover, they also discovered that these hESC-CMs are similar in its molecular signature (i.e. gene expression profile) as compared to native human heart cells. These findings suggest that hESC-CM maybe be a promising cell source to use for cardiac tissue engineering or cell transplantation therapies. Despite the ethical issues that surround the use of ESC and ESC-derived cells,

these cells may still prove to be an invaluable model for studying the differentiation of pluripotent cells into specific cells types, especially in the light of cardiac development. The findings may eventually be applicable to iPS cells, which have yet to be defined.

The proper understanding of the cellular mechanisms for cell differentiation will be critical in creating selection protocols for differentiating ESCs into CMs at high, frequencies that can manipulated according to the desired application. Once the cells have committed to the cardiac lineage, these cells can be subjected to a maturation protocol such that an adult phenotype can be derived. Recently, Yang et al. have reported a method to derive cardiac progenitors from a  $KDR^+$  ( $flk1^+$ ) hESC population [9], consistent with previous findings that  $flk1$  marks a population that give rise to endothelial cells in the heart [10]. This  $KDR^+$  population, which is also interestingly negative for  $c-kit$  (contrary to other findings [11]), was demonstrated to give rise to beating CMs at a frequency of greater than 50% when cultured in monolayers [9]. The protocol involves a three-stage induction method. In stage one, a primitive population is formed with the addition of activin A, bone morphogenetic protein 4 (BMP4), and basic fibroblast growth factor (bFGF) [9]. In stage 2, at day 4 of differentiation, activin A, BMP4 and bFGF are replaced by Dickkopf homolog 1 (DKK1), an inhibitor of the WNT pathway, which was added to induce the specification of the cardiac mesoderm [9]. DDK1 is a critical agent because the Wnt/ $\beta$ -Catenin pathway plays an important role in controlling the renewal and expansion of  $isl1^+$  progenitors [12]. Vascular endothelial growth factor (VEGF), also added in stage 2, plays a critical role in promoting the proliferation of  $KDR^+$  cells at this stage [9]. In stage 3, which commences at day 8 of differentiation, bFGF is again added to support the development of cells committed to the cardiac lineage [9].

In the process of differentiation, these cells would have at one point expressed the progenitor marker *isl1* as reported by Laugwitz et al. [13], and would eventually express cardiac troponin T, a cardiac marker, beyond day 10 of the differentiation protocol [9]. However, this population is far from being pure ventricular cardiomyocytes; instead it contains a mixture of atrial CMs, ventricular CMs, pacemaker cells, and undifferentiated or partially differentiated cardiac progenitors. These contractile cells appear very globular and tend to form round clusters in culture, similar to that of undifferentiated ESC. To date, a method for fully maturing these cells in order to achieve the adult ventricular

CM phenotype—highly elongated with contractions that can be paced upon electrical stimulation—has yet to be developed.

Mature adult human cardiomyocytes are elongated, contractile cells with developed transverse tubular structures as well as z-line structures (revealed by sarcomeric  $\alpha$ -actinin staining as an indication of the existing contractile apparatus) [14, 15]. They typically express an abundance of sarcomeric  $\alpha$ -actinin, myosin light chain-2 (MLC-2), tropomyosin, troponin and cadherin, an adhesion molecule [14]. Atrial CMs were shown to transcribe MLC-2a, while ventricular CMs expressed both MLC-2a and MLC-2v (isoforms of MLC-2) [14]. Both atrial and ventricular CMs from human adult myocardial tissue express atrial natriuretic factor (ANF) [14]. Neonatal cardiomyocytes, by contrast, are smaller in size. They are also much easier to culture, grow more rapidly and are thus more widely used as a model in cell culture studies [15]. In hypertrophic response to electrical stimuli,  $\beta$ -myosin heavy chain ( $\beta$ -MHC) is upregulated in neonatal rat CMs [16]. Sacromeric  $\alpha$ -actinin is also expressed in neonatal CMs, despite less developed tubular structures. Furthermore, genes such as  $\alpha$ -smooth muscle actin are more highly expressed in immature rat CMs [15, 17]. Cells derived from an embryonic source may also have a tendency to cluster and form round colonies, reminiscent of that exhibited by ESCs, in addition to displaying various degrees of myofibrillar structure organization [18]. Interestingly, it was reported that electrical stimulation enhances the organization of myofibrillar proteins in neonatal rat ventricular cardiomyocytes, promotes mitochondrial activity and cellular hypertrophy in addition to upregulating the expression of cardiac MLC and ANF [16]. These may be signs of CM maturation. Therefore, we anticipated that electrical stimulation may play a role in driving the maturation of hESC-CM.

Thus, it is our goal to develop a way by which we can manipulate the hESC-CM to consistently yield the desired, adult CM phenotype for the purpose of tissue engineering. Because ESC-CMs are similar to neonatal CMs on the development level, especially in their myofibrillar organization [18], we propose to utilize the same culture system as we previously applied to neonatal CMs, in hope of achieving similar effects. We report here the preliminary studies of a system that may assist in the maturation of hESC-CMs via the application of surface topography and electrical field stimulation.

## 4.2 Methods

### 4.2.1 Cells

The hESC-CMs were obtained from the laboratory of Dr. Gordon Keller at the McEwen Centre for Regenerative Medicine, part of the University Health Network based in Toronto, Canada. The cells were cultured by the Keller Lab following a three-stage induction protocol which they had previously developed [9]. Briefly, hESCs were initially propagated on mouse embryonic fibroblast feeder layers. The feeder layer was then depleted, and the hESC were cultivated in suspension to yield embryoid bodies (EBs). While cultured in suspension, various growth factors, agents and inhibitors were added at specific time points (or “stages”) to induce mesoderm specification to the cardiac lineages [9]. At day 19, the EBs were dissociated into single cells with trypsin and applied in our experiments as described below. Here, we refer to this population of cells as the hESC-CMs, although it contains other non-myocyte cell types.

### 4.2.2 Cell culture

Cells were cultured on abraded and non-abraded polyvinyl coverslips as described previously in section 2.2.1. The abrasions were made in the same manner as previously described. Initially, surfaces made with lapping paper of grain sizes from 1  $\mu\text{m}$  to 80  $\mu\text{m}$  were tested, in two independent experiments with two samples per group. Later on, we focused on using only the surface made by the 12  $\mu\text{m}$  lapping paper as the “abraded” surface. The seeding density was varied between 85000 to 200000 cells per coverslip initially; later experiments utilized 200000 cells per coverslip. In addition to the coverslips, some samples were also created using the microstructured tissue culture polystyrene described in Chapter 3.

For experiments without electrical field stimulation, the tables were placed individually in a 24-well tissue plate with 1 table per well. The hESC-CMs were seeded in 60  $\mu\text{L}$  of culture medium (2mM glutamine, 50  $\mu\text{g}/\text{mL}$  ascorbic acid, 150  $\mu\text{g}/\text{mL}$  transferrin,  $4 \times 10^{-4}$  MTG, 10  $\text{ng}/\text{mL}$  VEGF, 0.5  $\text{ng}/\text{mL}$  bFGF), as provided by the Keller Lab. The constructs were incubated at 37°C, 5%  $\text{CO}_2$  for at least 1 hour prior to feeding (i.e. filling each well with 1 mL of culture medium). The samples were then returned to

the incubator for a period of 4 days of culture. Upon ending the experiment, the samples were fixed in 10% formalin and stored at 4°C in PBS.

For experiments with electrical field stimulation, the coverslips were placed in a glass electrical stimulation chamber between a pair of carbon electrodes, as previously described in section 2.2.3. Unlike previous experiments, however, each coverslip had only one type of surface on it—either abraded or non-abraded. Tables were placed in the stimulation chamber prior to cell seeding. Cells were seeded and fed in the same manner as for the non-stimulated experiments. Stimulation commenced at day 2 with biphasic pulses the frequency of 1 Hz, amplitude of 3V/cm per phase and duration of 6 ms per phase.

#### 4.2.3 Cell staining and assessment

Immunofluorescent staining for  $\alpha$ -sarcomeric actinin was performed using monoclonal anti-sarcomeric  $\alpha$ -actinin made in mouse at dilution factor of 1:50 (Sigma). Images were taken using a fluorescence microscope (Olympus IX2-UCB).

#### 4.2.4 Image Analysis

ImageJ software was used to determine cell alignment and elongation as previously described in section 2.2.5.4. Both alignment and elongation were determined from sarcomeric  $\alpha$ -actinin immunostain images. Only cells in which the outline could be clearly seen were assessed.

#### 4.2.5 Excitation Threshold and Maximum Capture Rate

Excitation threshold (ET) and Maximum Capture Rate (MCR) were assessed before stimulation began on day 2 as well as after the stimulation has been terminated on day 4, for stimulated experiments. For non-stimulated experiments, ET and MCR were measured just prior to the termination of the experiment on day 5. The MCR was measured at 200% ET or to a maximum of 8V, whichever was higher, with monophasic pulses of 2 to 6 ms.

#### 4.2.6 Statistical Analysis

SigmaStat 3.0 software was used for statistical analysis. Tests for normality and equal variance were performed on all quantitative data sets. If the data sets satisfied the assumptions of normal distribution and equal variance, one-way ANOVA in conjunction with the Student-Newman-Keuls test was used to compare multiple groups and t-test was used to compare two groups. Otherwise, we performed the Kruskal-Wallis one-way ANOVA on ranks in conjunction with Dunn's method for pairwise comparisons. The groups were considered significantly different if  $p < 0.05$ .

### **4.3 Results**

#### 4.3.1 Morphology of cell cultures seeded on various surfaces

All non-stimulated samples were fixed after the cultivation period of 5 days and immunostained for sarcomeric  $\alpha$ -actinin. Qualitatively, 1 to 5 % of the cells stained positive for sarcomeric  $\alpha$ -actinin, which indicates that these cells were CMs. Samples of actinin<sup>+</sup> cells are shown in Figures 4.1 and 4.2. Actinin<sup>+</sup> cells were found in cultures seeded on all surfaces, abraded or non-abraded, although their morphology of these cells appeared different depending on the features of the surface on which they were seeded (Figure 4.1). Actinin<sup>+</sup> cells were also found in cultures grown on microstructured TCPS (Figure 4.2). These results indicate that mature CMs were present and viable within these cultures.

Figure 4.1 shows the effects of contact guidance resulting from the various sizes of abrasions on which hESC-CMs were seeded. Cell clusters can be seen on the surface made by lapping paper of grain sizes 80  $\mu\text{m}$  and 3  $\mu\text{m}$ , as well as on the non-abraded control (Figure 4.1). However, on surfaces made by lapping paper of grain sizes between 9  $\mu\text{m}$  and 60  $\mu\text{m}$ , there appeared to be a greater number of elongated cells which proliferated in the direction of the abrasions; some of these cells were actinin<sup>+</sup> CMs (Figure 4.1). In addition, cell elongation and alignment were also observed on microstructured TCPS surface (Figure 4.2A). Contractile apparatus, as indicated by the cross-striations made apparent by the actinin staining, was present in most of the elongated, actinin<sup>+</sup> cells (Figure 4.1 and Figure 4.2); in contrast, this is not seen in round

cell clusters despite that they were also positive for actinin (Figure 4.1). These elongated hESC-CMs were observed to form a beating monolayer on the TCPS surface with abrasions at a 1  $\mu\text{m}$  grating period (Figure 4.2B).

The actinin<sup>+</sup> cells were then quantitatively assessed in terms of cellular elongation and alignment via image analysis. Cells cultured on the “40  $\mu\text{m}$ ” surface (i.e. the coverslip abraded with lapping paper of grain size of 40  $\mu\text{m}$ ), as well as those on the microstructured TCPS surface with abrasions at a 4  $\mu\text{m}$  grating period, were significantly more elongated than cells cultured on the smooth, non-abraded control; the aspect ratios were above 6 in both cases (Figure 4.3A). Moreover, significant alignment was promoted by surfaces made by lapping paper with grain sizes of 9  $\mu\text{m}$ , 40  $\mu\text{m}$ , 60  $\mu\text{m}$  and the TCPS with abrasions at a 4  $\mu\text{m}$  grating period, as compared to random orientation exhibited by the non-abraded control with an average angle of deviation of close to 45 degrees (the maximum degree of deviation). These results indicate that contact guidance may be helpful in promoting cellular alignment and elongation of hESC-CMs, a phenomenon that is favourable in the process of achieving a mature CM phenotype.

#### 4.3.2 Functional properties

Preliminary ET and MCR values were obtained for non-stimulated samples after 5 days in culture. On various abraded surfaces, ET ranged from 3.1 to 5.6 V/cm, and MCR ranged from 1.9 to 6.3 Hz (Table 4.1). On the non-abraded control, ET and MCR were measured to be 5.5 V/cm and 3.3 Hz, respectively. Only data from samples which can be induced to beat and to respond were included. Samples cultivated on the abraded surface made of the lapping paper of grain size 3  $\mu\text{m}$  could not be paced properly. Preliminary results show that most samples cultivated on abraded surfaces exhibited lower ET and higher MCR values than the non-abraded control (Table 4.1).

#### **4.4 Discussion**

*In vivo*, cardiomyocytes are elongated and organized in the native heart. Here, we strived to achieve the same effects with the hESC-CM as we did with the neonatal rat CMs in chapter 2. Due to the tendency of hESC-CM to form aggregates and clusters,

cellular elongation, especially those of contractile cells, was much less apparent as compared to neonatal CMs. In this study, only cells stained positive for sarcomeric  $\alpha$ -actinin (i.e. the cardiomyocytes) were assessed for alignment and elongation. However, it is interesting to note that the non-myocytes portion of the population (the cells that did not stain positive for actinin, possibly a mixture of endothelial or smooth muscle cells) were overall very responsive to surface topography and appeared very aligned to the abrasions, qualitatively (data not shown).

#### 4.3.1 Variability of cell cultures

One of the greatest challenges associated with the hESC-CM cultures is the variability intrinsic within each batch of cells obtained. The variability renders the effects of various independent variables, such as seeding density and size of the abrasions, difficult to establish. For example, it has been previously determined that after dissociation from EBs into single cells, only cultures initially plated at 60000 to 75000 per 96 well will yield beating monolayers [19]. This is the equivalent of at least 185000 cells per coverslip in our study; thus we chose 200000 cells to be the seeding density. However, the final confluency reached and the rate at which the monolayer became confluent varied greatly between different experiments; hence, it was extremely difficult to identify an optimal seeding density. We observed qualitatively in our preliminary tests that beating monolayers were most frequently achieved if the cell seeding density approached 200000 cells per coverslip (data not shown), thus we employed this seeding density for most of our experiments.

In cases where culture conditions were kept constant, with consistent topography features (abrasions of consistent size) and length of cultivation period, the cells may respond differently depending on the origin of that batch of cells. Figure 1 represents the best-case scenario obtained from repeated experiments. Clustering to a large extent was present in all cases, despite the appearance of elongated cells in certain areas. Multiple experiments revealed that it was difficult to achieve the same level of cellular elongation and alignment consistently, even if all independent variables were kept constant.

In addition, the cells were also known to be highly sensitive to the composition of the culture medium [19]. Since the hESC-CMs are very sensitive to the culture medium

composition (effects can be detected even between different lots of the same ingredients) according to the Keller Lab [19], it is possible that the contaminants may be secreting substances beneficial to the cell culture.

#### 4.3.2 Presence of cardiac marker and contractile apparatus

All samples were at least partially positive for sarcomeric  $\alpha$ -actinin, confirming the presence of cardiomyocytes within the hESC-derived population despite the variable proportions thereof between each batch of cells. Cross-striations, as previously mentioned, are characteristic of healthy cardiomyocytes. They were mostly observed in contractile cells that were elongated, and absent or less apparent in contractile clusters. On microstructured surfaces, the cross-striations were perpendicular to the cell's long, while on the smooth surfaces, there was no preferential directionality. Cross-striations, if present, were observed to have multiple overlappings, consistent with what was previously observed with the neonatal CMs (Figure 4.1 and 4.2). Amongst the various sample groups cultivated on abraded surfaces, monolayers of CMs with cross-striations were most apparent on the surface made by lapping paper of 12  $\mu\text{m}$  grain size (Figure 4.1), as well as on the hot-embossed TCPS surface with a grating period of 1  $\mu\text{m}$  (Figure 4.2). The presence of contractile apparatus is an indication of that CMs have achieved or are approaching maturity.

#### 4.3.3 Cellular alignment and elongation for non-stimulated constructs

The polyvinyl coverslips with various sizes of abrasions, in addition to the microfabricated surfaces described in Chapter 3, were tested with an initial seeding density of 200000 cells per coverslip. It appeared that surfaces made by lapping paper with grain size between 12  $\mu\text{m}$  and 60  $\mu\text{m}$  (Figure 1) would yield CMs which are more elongated as compared to the cell clusters seen on monolayers cultivated on the other surfaces, including the non-abraded control. This suggests that abrasions of certain sizes may be more favourable in promoting cellular elongation and in driving maturation of hESC-CMs. However, the resulting confluence from each experiment, despite constant initial seeding density, was variable. Often, the contractile cells like to remain in aggregates on top of other cells, regardless of the underlying surface topography, in lieu

of the cellular elongation that one would usually expect. It is unclear whether the clustering was an artefact resulting from the variability between cell batches, or whether it was a result of the different sizes of the abrasions.

Among the cells which could be properly assessed (i.e. cells of which the outline was clear and apparent), the aspect ratio of cells ranges approximately from 3 to 6 (Figure 3A). These elongated cells were also mostly aligned parallel (with angles of deviation of approximately  $10^\circ$ ) to the abrasions or microfabricated channels on which they were cultivated (Figure 3B). Contact guidance was effective in improving cellular alignment, as demonstrated by a significantly lower angle of deviation in all abraded and microfabricated groups, relative to the non-abraded control (which has an angle of deviation of approximately  $45^\circ$ , corresponding to the maximal degree of random orientation). Contact guidance also appears to improve cellular elongation to a mildly visible extent in some cases, although the effect may not be statistically significant, as in the case of the “12  $\mu\text{m}$ ” surface (Figure 1). Cellular elongation, and the appearance of contractile apparatus, as discussed in the previous section (Figure 1 and 2), are indication that mature cardiomyocytes were present. The maturation of hESC-CM is thus demonstrated to be hopeful via this system.

#### 4.3.4 Contractile Properties for non-stimulated constructs

Prior to dissociation, the EBs from which the hESC-CM were obtained exhibited rhythmic contractions, consistent with previous observations [20]. Due again to the heterogeneity of the hESC-CM population and the variability between each batch of cells acquired, reliable data for excitation threshold and maximum capture rate could not be accurately obtained. On occasions, if the constructs had a very high proportion of non-myocytes, the monolayer would not beat at all, whether spontaneously or induced with the stimulator. Most frequently, however, we observed round aggregates that are rapidly and spontaneously contracting at a frequency between 1 to 2 Hz. For cultures in which an adequate number of cardiomyocytes survived, contractions usually commenced within 2 to 3 days of the initial seeding. Contractile clusters are often observed to beat in waves, one after another, instead of synchronously as an entire monolayer. These cultures were difficult to pace with external stimulation. We suspect that a mixture of other contractile

cell types, such as pacemaker cells which have a strong mechanism for firing their own action potentials, rendered pacing by external electrical field difficult.

Despite the obstacles, preliminary measurements were obtained from samples which could successfully be induced to beat (Table 4.1). The duration of the pulse delivered must be at least 2 ms (twice as long as the 1 ms usually employed [21]), and pacing was more often successful with a pulse length of 4 to 6 ms. In addition, since many of the samples already exhibited rapid spontaneous contractions at the day 4 time point, the pacing pulse was delivered at 2 Hz to ensure that the contractions observed during the measurement process were a result of the external stimulus. In comparison to data from the neonatal rat CMs presented in chapter 2 and 3, the hESC-CMs appear to exhibit higher ETs and lower MCRs (Tables 2.1, 2.2 3.1, 4.1). However, more repetitions are necessary to confirm the validity of the results.

On abraded surfaces, cells tended to exhibit lower ETs and higher MCRs as compared to the non-abraded control. As described in chapters 2 and 3, low ETs and high MCR values reflect the greater versatility of the CMs in response to stimulation, a property that is desired in tissue engineering constructs.

#### 4.3.5 Selection of an abraded surface

We sought to select one, out of the different coverslips with various sizes of abrasions, to use as the abraded surface against the non-abraded control in further experiments. The manually abraded coverslips serve as a more convenient and cost effective alternative to the microfabricated system, and are thus preferable over the hot-embossed TCPS, if the effects of both surfaces on cell culture were comparable (Figure 4.3). Upon initial inspection under the light microscope, it appeared that the surface made with lapping paper of 12  $\mu\text{m}$  (the “12  $\mu\text{m}$  surface”) had achieved the best cellular elongation and alignment, qualitatively. In addition, the initial ET and MCR measurement seemed to be superior to that achieved by the other surfaces (initial data not shown). Consequently, we performed more experiments with the “12  $\mu\text{m}$  surface” in order to obtain more data. Upon repetition, the 12  $\mu\text{m}$  surface continued to achieve better cellular elongation and alignment as compared to the non-abraded control (Figure 4.3), although the differences were not statistically significant. In addition, average ET and

MCR values from the “12  $\mu\text{m}$ ” samples were comparable to the initial measurement of ET and MCR of the single “30  $\mu\text{m}$ ” or “40  $\mu\text{m}$ ” sample that could be induced to beat, even though the values may not seem as ideal (Table 4.1). However, the effects achieved by the “30  $\mu\text{m}$ ” or “40  $\mu\text{m}$ ” abraded coverslips have yet to be tested for reproducibility.

#### 4.3.6 Application of electrical field stimulation

After examining the initial effects of contact guidance on the maturation of hESC-CMs, we proceeded to study the additional effects that electrical field stimulation may provide. We anticipated that electrical field stimulation may enhance the maturation of hESC-CMs. The appropriate stimulation regime must be established for the design of these experiments. As with previous experiments with the neonatal CMs, it is important to ensure that the electrical field potential applied is at or beyond the ET. Therefore, prior to the initiation of the applied electrical field on day 2, the samples were individually assessed for ET in order to ensure that the applied stimulus would be over the threshold. Overall, the average field strength required to induce contractions in most of the cardiomyocytes (mostly globular, distinct from the thinner appearance of the non-myocytes) within the field of view of the microscope was approximately 4.5 to 6.0V/cm. At the lower field strength, approximately half of the cells could be induced to beat, and most of what appeared to be a CM could usually be observed to be beating if 6.0V/cm was applied. The duration of the pulse was also found to be important. Increasing the field strength alone (even to as high as 8 to 10 V/cm) was ineffective in inducing contractions, unless the duration of the pulse was at least 4 ms to 6 ms. This may be in part due to the fact that immature cells need a stronger signal to elicit a response. Hence, the stimulation regime set consisted of biphasic pulses at 6 V/cm and duration of 6 ms at a frequency of 1 Hz. It was determined in an initial experiment that a more ambitious regime at a frequency higher than 1 Hz for a prolonged period of time (i.e. more than a few hours) resulted in significant cell death.

Thus far, this section of the project is still in progress. Experiments performed, to date, have not been successful due to cell viability and low numbers of contractile cell count. This may be in part, again, due to the variability between the cell batches. More work is necessary to produce reliable data.

#### **4.4 Conclusions**

Most hESC-CMs are not fully differentiated, and they do not exhibit the same phenotype as mature ventricular CMs. Our preliminary studies here demonstrated that the described system may enable the maturation of hESC-CM into an adult phenotype, applicable for the purpose of cardiac tissue engineering. Part of the complexity in establishing a system to consistently drive maturation this population lies within the fact that there exists a large amount of uncontrollable variability between each batch of cells, resulting in much difficulty in confidently establishing the effects of the external stimuli on the cellular development of the hESC-CMs, as well as their contractility. Although the fully matured phenotype of hESC-CM has not been completely achieved, this system showed some promising effects on a small number of cells, as demonstrated by their cellular alignment and elongation. Work is currently in progress to optimize the system. Future work will involve assessing the hESC-derived population for other cell types as well, including endothelial and smooth muscle cells. In addition, we could attempt isolation strategies to separate the CMs from ESCs and other non-myocytes, including the depletion of these cells using cell surface markers such as CD31 for endothelial cells. Enriching for CMs may eventually allow us to study the CM population more precisely in their behaviour and to control their proportion within the cell culture.

## 4.5 Figures and Tables

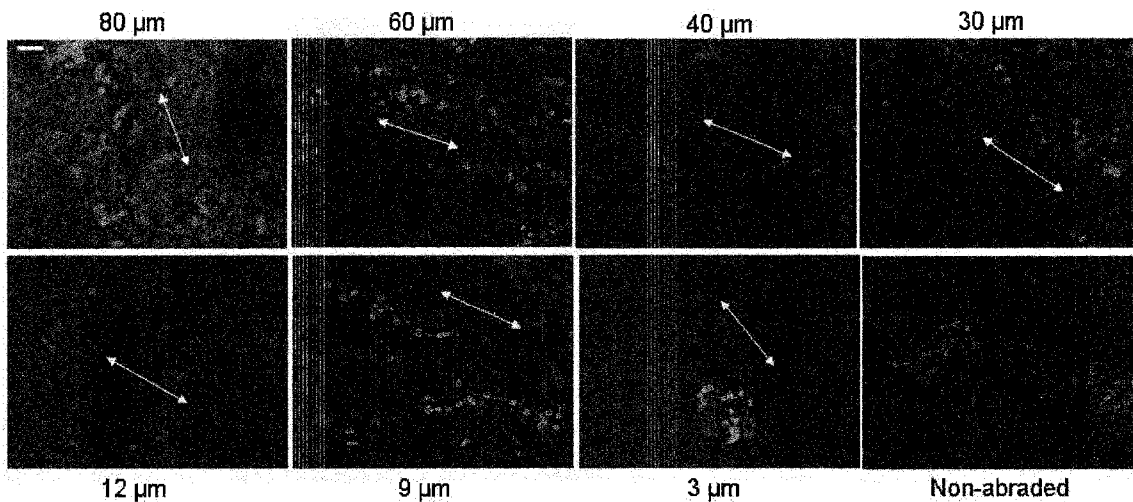


**Figure 4.1. Immunostaining for sarcomeric  $\alpha$ -actinin in hESC-CMs cultivated on manually abraded coverslips.** Labels refer to the grain size of the lapping paper used to create the microabrasions. Samples were cultured with an initial seeding density of 200000 cells per coverslip. Arrows indicate the direction of the abrasion. Scale bar = 40 $\mu$ m

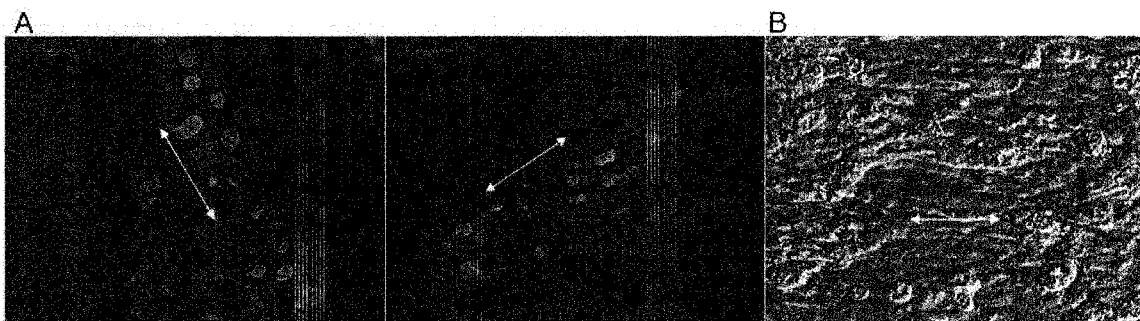


**Figure 4.2. Immunostaining for sarcomeric  $\alpha$ -actinin on hESC-CMs cultivated on microstructured surfaces made by hot embossing.** Arrows indicate the direction of the microstructured channels. A) Orientation and morphology of the cells expressing  $\alpha$ -actinin on microfabricated grooves of 1  $\mu$ m period (left) and of 4  $\mu$ m period (right) Scale bar = 20 $\mu$ m. B) Brightfield image of contracting monolayer of differentiated hESC-CMs. Scale bar = 80 $\mu$ m

**Table 4.1. Approximate ET and MCR values of non-stimulated hESC-CMs after 5 days of cultivation.** The “NRC” surfaces refer to the microstructured surfaces made by hot embossing, and the number refers to the period of grating. For all others, the number in the sample name refers to the grain size of the lapping paper used to manually make the abrasions. N indicates the number of samples within that groups of which successful measurements of ET and MCR could be obtained

Samples	ET (V/cm)	MCR (Hz)	# of samples (N)
NRC 1 $\mu\text{m}$	5.6	3.9	2
NRC 4 $\mu\text{m}$	4.3	1.9	1
80 $\mu\text{m}$	4.8	4.4	1
60 $\mu\text{m}$	4.2	5	1
40 $\mu\text{m}$	3.1	4.6	1
30 $\mu\text{m}$	4.2	6.3	1
12 $\mu\text{m}$	3.5	4.5	4
9 $\mu\text{m}$	4.8	5	1
3 $\mu\text{m}$	Could not pace	Could not pace	0
Non-abraded	5.5	3.4	2

#### 4.6 References

1. Murry, C.E. and G. Keller, *Differentiation of embryonic stem cells to clinically relevant populations: lessons from embryonic development*. Cell, 2008. **132**(4): p. 661-80.
2. Kubo, A., et al., *Development of definitive endoderm from embryonic stem cells in culture*. Development, 2004. **131**(7): p. 1651-62.
3. Moretti, A., et al., *Multipotent embryonic *is11+* progenitor cells lead to cardiac, smooth muscle, and endothelial cell diversification*. Cell, 2006. **127**(6): p. 1151-65.
4. Kattman, S.J., E.D. Adler, and G.M. Keller, *Specification of multipotential cardiovascular progenitor cells during embryonic stem cell differentiation and embryonic development*. Trends Cardiovasc Med, 2007. **17**(7): p. 240-6.
5. Laugwitz, K.L., et al., *Islet1 cardiovascular progenitors: a single source for heart lineages?* Development, 2008. **135**(2): p. 193-205.
6. Synnergren, J., et al., *Molecular signature of cardiomyocyte clusters derived from human embryonic stem cells*. Stem Cells, 2008.
7. Laflamme, M.A., et al., *Cardiomyocytes derived from human embryonic stem cells in pro-survival factors enhance function of infarcted rat hearts*. Nat Biotechnol, 2007. **25**(9): p. 1015-24.
8. van Laake, L.W., et al., *Human embryonic stem cell-derived cardiomyocytes and cardiac repair in rodents*. Circ Res, 2008. **102**(9): p. 1008-10.
9. Yang, L., et al., *Human cardiovascular progenitor cells develop from a *KDR+* embryonic-stem-cell-derived population*. Nature, 2008. **453**(7194): p. 524-8.

10. Kattman, S.J., T.L. Huber, and G.M. Keller, *Multipotent flk-1+ cardiovascular progenitor cells give rise to the cardiomyocyte, endothelial, and vascular smooth muscle lineages*. Dev Cell, 2006. **11**(5): p. 723-32.
11. Bearzi, C., et al., *Human cardiac stem cells*. Proc Natl Acad Sci U S A, 2007. **104**(35): p. 14068-73.
12. Qyang, Y., et al., *The renewal and differentiation of Isl1+ cardiovascular progenitors are controlled by a Wnt/beta-catenin pathway*. Cell Stem Cell, 2007. **1**(2): p. 165-79.
13. Laugwitz, K.L., et al., *Postnatal isl1+ cardioblasts enter fully differentiated cardiomyocyte lineages*. Nature, 2005. **433**(7026): p. 647-53.
14. Bird, S.D., et al., *The human adult cardiomyocyte phenotype*. Cardiovasc Res, 2003. **58**(2): p. 423-34.
15. Schaub, M.C., et al., *Various hypertrophic stimuli induce distinct phenotypes in cardiomyocytes*. J Mol Med, 1997. **75**(11-12): p. 901-20.
16. Xia, Y., et al., *Electrical stimulation of neonatal cardiomyocytes results in the sequential activation of nuclear genes governing mitochondrial proliferation and differentiation*. Proc Natl Acad Sci U S A, 1997. **94**(21): p. 11399-404.
17. LaFramboise, W.A., et al., *Cardiac fibroblasts influence cardiomyocyte phenotype in vitro*. Am J Physiol Cell Physiol, 2007. **292**(5): p. C1799-808.
18. Kehat, I., et al., *Human embryonic stem cells can differentiate into myocytes with structural and functional properties of cardiomyocytes*. J Clin Invest, 2001. **108**(3): p. 407-14.
19. Gagliardi, M. 2008, McEwen Centre for Regenerative Medicine. p. Culture of hESC-CM.
20. Capi, O. and L. Gepstein, *Myocardial regeneration strategies using human embryonic stem cell-derived cardiomyocytes*. J Control Release, 2006. **116**(2): p. 211-8.
21. Au, H.T., et al., *Interactive effects of surface topography and pulsatile electrical field stimulation on orientation and elongation of fibroblasts and cardiomyocytes*. Biomaterials, 2007. **28**(29): p. 4277-93.

## 5. The identification and isolation of $isl1^+$ cardiac progenitors in the neonatal rat heart

### 5.1 Introduction

In the course of the last half a decade, the debate over whether there exist mammalian cardiac stem cells, and whether mammalian cardiomyocytes are indeed terminally differentiated with the inability to self-renew, have gained much prominence in the field of regenerative medicine. There is a growing body of evidence that the heart may indeed possess a population of immature cells, though committed to the cardiac lineage, that are capable of differentiating into functional cardiomyocytes and vascular cells [1-6]. Several groups have reported cardiac “stem” cells in both the rodent and human hearts [1, 7, 8] under different stem cell markers such as c-kit [1, 9, 10], sca-1 [1, 11, 12], MDR1 [13] and SSEA-1 [1]. However, due to the various different findings and the inconsistency in characterizing these cells, much controversy remains about the origin, existence and regenerative capacity of these so-called “stem cell” populations.

Moreover, even if a cardiac stem or progenitor can be identified, they are far from being able to minimize the risk for myocardial infarction or other cardiovascular diseases. In fact, it was reported that such stem or progenitors suffer cell death to a similar extent as cardiomyocytes in the event of serious injury, such as MI [14]. However, it would be invaluable and convenient if these stem cells can be harvested, expanded *in vitro*, and reinjected or delivered to the site of injury; the function in the heart may hence be improved [7, 8]. The cell source for therapy in this case is autologous, thus greatly decreasing the risk for immune rejection. Several groups have already reported that these cells can “refresh cardiomyocytes” or regenerate the myocardium. [9, 14, 15] under conditions of stress, as stem cell or progenitor derived CMs were found within the infarct zone. In addition, Ott et al. demonstrated that the adult human heart contains a multipotent SSEA-1<sup>+</sup> population that is capable of giving rise to a flk1<sup>+</sup> or isl1<sup>+</sup> cardiac progenitors [1]. Isl1<sup>+</sup> progenitors were also found by Laugwitz et al. in neonatal mouse, rat and human hearts [16].

Since its first report by Cai et al in 2003, *Isl1* has become known as a marker for cardiac progenitor cells [4]. *Isl1* is a homeobox transcription factor that is expressed in the mesoderm and pharyngeal endoderm, but not in the developed heart [16, 17]. During mammalian cardiogenesis, *Isl1*<sup>+</sup> progenitors are essential for the development of the secondary heart field, and are responsible for a large number of the cells comprising the outflow tract and right atrium and ventricle [17]. It was found that mice with a homozygous knockout of *Isl1*, i.e. *Isl1*<sup>-/-</sup>, lack the outflow tract and the right ventricle [17]. The expression of *Isl1* thus appears to be essential for the survival and proliferation of cells in the secondary heart field (anterior portion of the heart). However, *Isl1*<sup>+</sup> cells are not confined solely to those areas, as they were also found in both atria as well as the left ventricle [17]. *Isl1* expression is suppressed as the cells differentiate, suggesting that *Isl1* is essential in the maintenance of precursor cells which continue to proliferate and migrate as the heart is generated within the embryo [17]. After birth, a small population of *Isl1*<sup>+</sup> progenitors (approximately 500 to 600) remains resident in the neonatal heart [3, 16].

In this project, we are primarily interested in this group of resident *Isl1*<sup>+</sup> progenitors, as reported to exist in the neonatal mouse by Laugwitz et al [16]. Laugwitz et al. isolated *Isl1*<sup>+</sup> cardiac progenitors from a genetically modified murine system. In order to elucidate the contribution of *Isl1*<sup>+</sup> precursors to the various cell types in the developing and matured hearts, *Isl1*-mER-CRE-mER/R26R double heterozygous mice were generated [16]. Cells within these animals that express or had expressed *Isl1* at one point would have a stop sequence cleaved out, as mediated by the CRE protein; this process consequently results in the expression of the lacZ (which codes for the β-gal protein) under the Rosa26 promoter endogenous in the mice [16]. Treatment with 4-hydroxytamoxifen allows the CRE protein to translocate to the nucleus such that the Cre-mediated recombination can proceed. It was found that *Isl1*<sup>+</sup> contributes to the development of the proximal aorta, part of the pulmonary artery and coronary arteries, in addition to a large part of the cardiac conduction system including nodal and pacemaker cells [2, 16]. Cells were also found to co-express lacZ with markers of the endothelial and smooth muscle cells [2], revealing the *Isl1*<sup>+</sup> progenitors contribute to the vascular cells of the heart [2, 16]. In addition, these cells were reported to have the capacity to self-

renew when cultured on a cardiac mesenchymal cell (CMC) feeder layer, and to differentiate into functional cardiomyocytes at high frequencies (approximately 25%) [16]. Analysis of action potentials showed that cells derived from  $isl1^+$  progenitors resemble native ventricular and atrial CMs, which supports the proposition that  $isl1^+$  progenitors are versatile in their ability to differentiate into various functional cardiomyocytes [17].

In the protocol developed by Laugwitz et al.,  $isl1^+$  progenitors were driven to differentiate to cardiomyocytes via co-culture with neonatal CMs [16]. Wildtype neonatal mouse CMs were co-cultured with  $isl1^+/\beta\text{-gal}^+$  cells which had been FACS sorted using a fluorescent marker named  $C_{12}\text{FDG}$ , which binds the  $\beta\text{-gal}$  protein. Expression of CM markers such as troponin T and sarcomeric  $\alpha\text{-actinin}$  were assessed and found in CMs derived from the progenitors [16]. Similarly, co-culture experiments with human coronary artery smooth muscle cells were performed as an attempt to differentiate the  $isl1^+$  into smooth muscle cells (SMCs) [16]. SMCs derived from  $isl1^+$  progenitors were also found to be functional, and achieved their differentiated phenotype without cell fusion [16]. These results show that  $isl1^+$  progenitors were able to differentiate into CMs and SMCs according to cues from the surrounding microenvironment, and not via cell fusion with existing CMs. The capacity to differentiate *in vitro*, without cell fusion, may be important for fabricating a tissue engineering construct.

In addition to the neonatal animal,  $isl1^+$  progenitors may also be derived from an embryonic cell source. Moretti et al. have transfected a mouse ES cell line to create a nuclear lacZ knock-in in  $isl1$  locus of the genomic DNA [3]. In this manner, cells which express  $isl1$  will also express  $\beta\text{-gal}$ , and can be detected via molecules that bind to  $\beta\text{-gal}$ . The ES cells were induced to form EBs, and  $isl1$  expression was detected in EBs after 4-6 days of culture [3].  $Isl1^+$  progenitors may also co-express  $Nkx2.5$  or  $flk1$ , which then differentiate into CMs and smooth muscle cells, or endothelial and smooth muscle cells, respectively [3]. Both  $isl1^+$  cells derived from EBs and  $isl1^+$  progenitors from the neonatal mouse (as mentioned above), can be expanded on a CMC feeder layer, which allows for the maintenance of the progenitor phenotype without differentiation amongst these cells [3, 16].

The extent to which CMC modulates the renewal and specification of  $isl1^+$  progenitors was studied by Qyang et al [18], who suggested that the Wnt/ $\beta$ -catenin pathway is a critical component of the CMC environment. 6-bromoindirubin-3'-oxime (BIO), an inhibitor of glycogen synthase kinase-3 (GSK-3), was previously identified to promote both mouse and human ES cells self-renewal by activating the Wnt/ $\beta$ -catenin pathway [19]. Inhibition of GSK-3 activity results in the accumulation of  $\beta$ -catenin, which subsequently activates transcription of its target genes [20]. Qyang et al found that BIO was effective in promoting the expansion of  $isl1^+$  progenitors in a dose-dependent manner; the most effective dose was 2.5  $\mu$ M which resulted in a 7-fold increase of  $isl1^+$  progenitors compared to the control group [18]. Moreover, they also examined the effects of a Wnt3a-producing feeder layer on  $isl1^+$  cell proliferation and Wnt3a-conditioned medium, and found that Wnt3a (a ligand in the Wnt/ $\beta$ -catenin pathway) increased  $isl1^+$  cell number by 2 and 6-fold respectively [18]. In contrast, inhibiting the Wnt pathway with Dickkopf-1 (DKK1) resulted in a 40% decrease in  $isl1^+$  cells compared to the control [18]. These findings strongly suggest that activation of Wnt/ $\beta$ -catenin pathway plays a critical role in determining self-renewal of  $isl1^+$  progenitors derived from ESCs [18], and that BIO or Wnt3a may be an important agent to consider in attempting to expand  $isl1^+$  progenitors.

Due to their multipotent potential to differentiate into various cardiac lineages and their autologous origin,  $isl1^+$  progenitors are of great interest for cardiac tissue engineering. To this date, however, the ability to efficiently isolate and propagate the  $isl1^+$  progenitor population, while conserving their multipotency, remains extremely challenging [17]. The goal of this study is to identify and characterize the equivalent  $isl1^+$  population in the wildtype neonatal rat heart. However, due to the lack of a genetically modified system, we do not have the option of identifying cells which are  $isl1^+$  (or were once  $isl1^+$ ) via the  $\beta$ -gal protein. Instead, an alternative method must be sought. Once the population is identified, it is our hope to establish a procedure for the separation and expansion of these progenitors in order to further assess their feasibility for the purpose of cardiac tissue engineering.

## 5.2 Methods

### 5.2.1 Cells

Primary cardiac cells were obtained from a series of collagenase digests of neonatal rat hearts, as described in section 2.2.2. The non-myocytes from the preplating step were kept in culture for 4 days following the isolation procedure in CM culture medium, also as previously described in chapters 2 and 3. Briefly, a cell suspension of cardiac cells were obtained from 13 neonatal rat hearts. This cell suspension was then subjected to a pre-plating procedure (in which the cell suspension was deposited on tissue culture polystyrene for one hour) to separate the cardiomyocytes from the non-myocytes. After 1 hour, the liquid was removed from the tissue culture surface, and the cells which remained adhered, the non-myocyte fraction, was fed with culture medium. From here on, this non-myocyte fraction is referred to as PP1 (preplate 1) cells.

Pre-plating was achieved in 96-well plate (50  $\mu$ L of cell suspension as described above, per well), 24-well plate (270  $\mu$ L of cell suspension per well), T25 (3.3 mL per flask) or T75 (10 mL per flask), depending on the purpose. From here on, this non-myocyte fraction will be referred to as PP1 (preplate 1) cells. Cultures in well-plates were typically used for immunochemical assessment, whereas cultures in flasks were used for cell separation experiments (described in the appendix).

### 5.2.2 Cell Culture

All PP1 cultures were maintained on the tissue culture surface onto which they originally adhered; no passaging of cells was performed. Three different media were used, but cultures were subjected to only one of the following during the course of the experiment:

- 1) Regular CM medium, which was used also for the culture of neonatal rat cells
- 2) “Laugwitz medium” for stimulating  $isl1^+$  progenitor proliferation (DMEM/F12 1:1, containing 2% FBS, 10 ng/mL epidermal growth factor (EGF), 1X B27 supplement) [16]
- 3) BIO medium (DMEM containing 2.5  $\mu$ M BIO, 10% NCS, 1% penicillin-streptomycin). This concentration of BIO was chosen based on previously published data [18].

After the cultivation period (at 37°C and 5% CO<sub>2</sub>), the cultures were either fixed with 4% paraformaldehyde (for immunocytochemistry), with 100% methanol (for flow cytometry, more details to follow in section 5.2.2), or subsequently subjected to a cell separation procedure. The cultivation period for immunocytochemistry was 4 days, whereas flow cytometry was performed on PP1 cultures of 4 days, 9 days and 10 days of age.

RIN-m rat pancreatic beta islet cells (ATCC # CRL-2056) were cultivated and propagated according to the protocol from ATCC [21]. This cell line served as a positive control for the expression of *isl1*.

### 5.2.3 Identification of the *isl1*<sup>+</sup> progenitors

To identify the cells in which *isl1* was expressed, immunofluorescent staining was performed using the anti-*isl1* monoclonal antibody (39.4D5 from the Developmental Studies Hybridoma Bank, University of Iowa) at a concentration of at least 2 µg/mL [16]. The cells were first fixed with 4% and permeabilized with 0.1% Triton X-100. Either a FITC anti-mouse (Sigma F9006 , 1:64) or an AMCA anti-mouse (Vector Labs CI-2000, 1:100) secondary antibody was used for detection. RIN-m cells served as a positive control. Immunostaining for Vimentin and TnI were also performed, as previously described in chapter 2, for identifying other non-myocyte cell types.

Immunohistochemistry was performed using the same dilution of the primary antibody according to the protocol from the laboratory of Dr. W.L. Stanford [22]. The NovaRed Substrate Kit (Vector Labs SK-4800) or the SG Substrate Kit for Peroxidase (SK-4700) was used for detection.

Flow cytometry for the *isl1* marker was performed on PP1 at day 4, day 9 and day 10. The culture was trypsinized in the same manner as in a standard cell passage procedure, and single cells were centrifuged at 1000 rpm for 5 minutes into aliquots of 2 x 10<sup>6</sup> cells. The cells were then subjected to treatment with lysing buffer (0.5% Triton X-100, 1% BSA in PBS) for 15 minutes at 4°C, followed by fixation in 100% cold methanol for at least 10 minutes. After washing with PBS, the aliquots were incubated at room temperature with the primary antibody (1:20 in solution) for 30 minutes, at which point they were washed once and subsequently incubated with the FITC secondary (same as for immunostaining, but at a dilution factor of 1:1000) for 30 minutes at room temperature.

The cells were then resuspended in PBS and strained into FACS tubes. Analysis was performed at the flow cytometry facility at the Princess Margaret Hospital, University Health Network, in Toronto.

### 5.3 Results

#### 5.3.1 Autofluorescence and immunostaining for *isl1*

Figure 5.1 demonstrates the extent to which autofluorescence interferes with the assessment via immunostaining of *isl1*. RIN-m, a rat pancreatic beta islet cell line, stained positive for *isl1* as expected (Figure 5.1A). This served as the positive control for the *isl1* immunostain, and demonstrated that the antibody reacts properly with the rat species. If the immunostain was performed on RIN-m without the anti-*isl1* primary antibody, no staining was visible; this indicates that the secondary antibody was specific to the labelling of *isl1* (Figure 5.1A) and served as a negative control. To confirm the specificity to which the anti-*isl1* binds the *isl1* protein, we also attempted to stain the D4T endothelial cell line for *isl1*. As anticipated, no staining was found in D4T cells since endothelial cells are expected to be *isl1*<sup>-</sup> (Figure 5.1A).

However, it was discovered that the PP1 cells exhibited fluorescence without prior labelling by a fluorescent agent. PP1 cells which were fixed at the end of the cultivation period at day 4 exhibited a level of fluorescence comparable to that of the positive control (Figure 5.1 A and B). Furthermore, the level of autofluorescence was highly variable between different experiments or batches of cells (Figure 5.1B). Figure 5.1B compares two images demonstrating autofluorescence from two separate experiments, both ended at day 4 in cultivation. We noticed that autofluorescence can be detected under the different channels of the microscope (red, green and blue), but was most visible under the green channel.

Another obstacle in immunostaining of *isl1* is the presence of non-specific staining in primary cells isolated from the animal. Figure 5.1C reveals the result of non-specific binding of the green FITC secondary antibody, in the absence of labelling with a primary antibody, to a large portion of the cells in the sample. It can be concluded the apparent fluorescence originated from the antibody, as opposed to endogenous

au fluorescence, because it was largely visible only under the green channel of the microscope (Figure 5.1C). Neither autofluorescence nor non-specific staining was observed in the cell lines used as the positive and negative controls (data not shown).

### 5.3.2 Flow cytometry

PP1 cells were subjected to flow cytometry analysis in order to determine the fraction of *isl1*<sup>+</sup> cells at day 4, day 9 and day 10 of cultivation. The antibody was proven to be able to adequately label rat cells for flow cytometry, as demonstrated by the RIN-m cell line (Figure 5.2A), where a shift in peak to the right was apparent when the primary anti-*isl1* antibody was added. At day 4, a small number of *isl1*<sup>+</sup> cells appeared to be present in cells cultured with the Laugwitz and BIO media (Figure 5.2 C and D). Figure 5.2C and D reveals data from a single experiment, but are representative of the overall trend (Figure 5.3). Figure 5.3 shows the average number of *isl1*<sup>+</sup> cells obtained over all independent experiments (N=3). However, it should be noted that N=1 in the “Laugwitz” group (Figure 5.3).

At day 9 and 10, no *isl1*<sup>+</sup> cells were found in cultures in all media (data not shown). The level of noise in the negative controls for these experiments was overwhelmingly high for any *isl1*<sup>+</sup> fraction to be accurately detected; in fact, the percentage approached a negative number when the noise from the negative control was taken into account.

### 5.3.3 Cell morphology during the cultivation period

PP1 cultures were observed for morphology changes during their cultivation period. Typically, spontaneous contractions in PP1 cells grown in the regular CM medium became visible at day 4 of culture (data not shown). Beating clusters consist of mostly elongated CMs; beating was usually maintained until at least day 10 of culture, at which point experiments were ended. Figure 5.4 shows a typical beating monolayer of PP1 cells at day 7, cultured in regular CM medium. However, it is interesting to note that PP1 cells cultured in the “BIO medium” for the same period of time exhibited a generally flat morphology in its monolayer. No globular cells were seen (Figure 5.4). In contrast to that culture in the regular medium, no contractions were noted.

#### 5.3.4 Immunostaining for DDR2

DDR2 staining was performed on both NIH3T3 fibroblasts (cell line) as well as primary cardiac fibroblasts which comprises of the majority of the PP1 cells. DDR2 is a cell surface receptor that is specific to fibroblasts [23]. Successful labelling was achieved with the 3T3 fibroblasts, as shown in Figure 5.5.

### **5.4 Discussion**

#### 5.4.1 Issues with identification

Previously, we have demonstrated with reverse transcriptase-polymerase chain reaction (RT-PCR) that the level of mRNA transcripts increased in neonatal rat PP1 cells over the course of approximately 2 weeks, with the most significant increase taking place between day 6 and day 15 of culture [24]. *Isl1*<sup>+</sup> transcription was significantly higher at day 15 compared to that at day 6 [24]. This is consistent with previously reported data demonstrating that *isl1* expression increases between day 5 and 14 in the mouse mesenchymal fraction [16]. In addition, we found that *isl1* transcription continued to persist at least to a period of 6 weeks from the initial seeding [24]. These results suggest that *isl1* transcription is present in the primary rat cells that we isolated. Therefore, we proceeded with immunostaining and flow cytometry as an attempt to confirm the results obtained by RT-PCR.

Autofluorescence in primary cardiac cells represented the greatest obstacle in the identification of *isl1*<sup>+</sup> progenitor cells via immunofluorescent staining. Initially, because we made the erroneous belief that there was a significant number of *isl1*<sup>+</sup> progenitors within the PP1 which appeared to have peaked at day 4 or 5 (Figure S5.1, in appendix). Although the trend could be possible, the numbers of *isl1*<sup>+</sup> positive cells were surprisingly inconsistent with what was previously reported in cardiac mesenchymal layers (the equivalent of PP1 in this case) [16]. Upon more cautious examination, however, we discovered that the green fluorescence which appeared to indicate positive *isl1* staining was actually endogenous (Figure 5.1B). Even live cells exhibited a strong level of autofluorescence, suggesting that the mysterious autofluorescence was neither a

result of the immunostaining procedure nor the usage of any of the reagents in the staining process (data not shown). The matter that is autofluorescing within the cells remains unknown.

There are several reasons for which we were initially misled to believe that the *isl1* protein was properly labelled. Firstly, the positive staining exhibited by beta pancreatic RIN-m cells was faint, albeit definite; the level of fluorescence exhibited by positively stained RIN-m cells was comparable to the level of autofluorescence of the PP1 cells, which led to even greater difficulty in determining whether the cells of interest in the PP1 cultures were positive for *isl1*<sup>+</sup> (Figure 5.1 A and B). Secondly, it was only discovered at a later stage of experimentation that primary cells derived from the animal (PP1 cells) and immortal cell line (i.e. RIN-m pancreatic cells) are not equally sensitive to the same immunostaining protocol. The conditions for *isl1* detection were initially optimized using the RIN-m cell line as a positive control; thus when the same protocol yielded what appeared to be positive results in the PP1 samples, supported by simultaneous positive and negative controls, we mistakenly assumed that the result was significant. Finally, there were on occasion high levels of non-specific staining, preventing the cells which might have in fact been positive, if any, to be identified clearly (Figure 5.1C).

For this reason, we resorted next to using a blue AMCA secondary antibody instead of the FITC antibody that we previously employed. Since autofluorescence of PP1 cells was most strongly detected under the green and red channels of the fluorescent microscope, but significantly less visible under the blue channel, labelling with a blue antibody would ensure that any fluorescence seen under the blue channel was a result of the labelling. Staining with the blue antibody revealed that none of the cells in the PP1 cultures was *isl1*<sup>+</sup> (data not shown), suggesting that *isl1*<sup>+</sup> cells may indeed be absent or were in numbers too low to be detected. We also attempted to perform immunohistochemistry, since it does not rely on fluorescence for detection, to label and identify *isl1*<sup>+</sup> cells. However, the detection system was not sensitive to give a confident positive control, and the idea was thus abandoned.

Next, we also performed flow cytometry in hope the higher sensitivity in detection would help distinguish the cells which autofluoresced from those that were in

fact labelled with the anti-is11 antibody. Flow cytometry analysis was done for PP1 cells cultured in the various media for various lengths of culture period (day 4, 9, 10). The results show that there may be a small number of is11<sup>+</sup> cells in cultures with the “Laugwitz” or BIO medium at the day 4 time point, after the deduction of noise present in the negative control (Figure 5.3). However, further work will be needed to confirm this data. The negative controls for the various conditions fluctuated between yielding 0 to 0.1% of false positive cells upon repetition, and this may be large enough for any small yield in the samples to be disregarded as negative. The fact there appeared to be no is11<sup>+</sup> progenitors at day 9 and 10 in culture was suspicious. It remains still entirely possible that the is11<sup>+</sup> progenitors exist and were not detected because of their scarcity, but the level of background noise must first be further reduced for this result to become more apparent.

#### 5.4.2 Improving the culture medium

Given that the regular CM culture medium may lack components that promotes or sustain is11<sup>+</sup> progenitor growth, we strived to identify the ingredients which may be the most essential for this purpose. We followed the recipe, invented by Laugwitz et al, for the medium reported to stimulate is11<sup>+</sup> cell growth as a general guideline. However, there remain some undisclosed details with regards to its exact composition which we had to assume. The “Laugwitz” medium contains epidermal growth factor (EGF) as well as the B27 supplement, which when added in DMEM/F12 (as in this case), was found to support the growth and survival of EGF-responsive precursor cells in the central nervous system. Because is11 is expressed in many of these EGF-responsive neural stem cells [25], it is reasonable to anticipate that EGF and B27 supplement may assist in the proliferation of is11<sup>+</sup> cells in the heart as well.

In another separate recipe, we added BIO (6-bromoindirubin-3'-oxime), a molecule demonstrated to promote both human and mouse ESC renewal by activating the Wnt/ $\beta$ -catenin pathway [18]. BIO acts to inhibit GSK-3 activity (GSK-3 phosphorylates  $\beta$ -catenin and marks it for degradation, preventing it from activating genes that may be involved in self-renewal), thereby promoting the expansion of is11<sup>+</sup> progenitor cells. Adding BIO was reported to increase the number of is11<sup>+</sup> cells by 7-fold [18]. Our flow

cytometry results were inconsistent with this data, but BIO was shown to improve  $isl1^+$  numbers within the PP1 (Figure 5.2 and 5.3). Interestingly, we observed that the morphology of the PP1 cells were significantly altered with the “BIO medium”, in which the number of beating clusters were significantly lower and the cells tend to possess a flat morphology (Figure 5.4). This suggests that the “BIO medium” may be promoting the proliferation of different cell types within the PP1 cells, as compared to the regular CM medium. Furthermore, based on our preliminary results from flow cytometry, both the Laugwitz and BIO media seemed to have an effect on increasing  $isl1^+$  numbers, relative to the cultures grown in the regular CM medium which did not yield any significant fraction of  $isl1^+$  cells (Figure 5.2 B,C,D). However, these results should be confirmed with repetition in further experiments. Other factors that may have contributed to the inconsistency between our results and those previously reported include different methods for cell isolation from the neonatal heart, different culturing protocols, and the species of animals employed in the experiment (mouse versus rat) [16].

#### 5.4.3 Prospects of isolating and enriching for the $isl1^+$ population

Before the discovery of the autofluorescence issue, we attempted to establish several techniques for separating what appeared to be the  $isl1^+$  cells for the purpose of enriching and expanding the population. Since the issue of autofluorescence was uncovered, the results showing the existence of  $isl1^+$  cells in PP1 cultures were considered to be invalid. The pursuit to establish methods for separating the  $isl1^+$  cells have been temporarily delayed until a method to confidently assess the presence of the  $isl1$  protein is found. The methods that were tried are discussed in the appendix of chapter 5 (Appendix S5), along with the related results obtained thus far. Qualitatively, it was that that the 2% EDTA solution in PBS supplemented with 5% FBS was the most effective non-enzymatic method for dissociating cells from the tissue culture flasks; however, we could not determine the viability of  $isl1^+$  cells following this process (Appendix S5.2). To date, the isolation of any  $isl1^+$  progenitors have proven to be extremely challenging, due to the scarcity of the population and the difficulty in labelling the  $isl1$  protein.

In addition, immunostaining for DDR2 was performed to explore the possibility of using magnetic activated cell sorting (MACS) technique to deplete the fibroblasts from

the PP1 population as an attempt to enrich for cardiac progenitors. Since *isl1* is a transcription factor found within the nucleus, it is not feasible to label the *isl1* protein with an antibody in live cells since they cannot be kept viable upon permeabilization, which is necessary for the staining of intracellular markers. As an alternative, we propose to deplete the cardiac fibroblasts, which comprise of most of the remainder of the PP1 fraction. This strategy involves labelling cardiac fibroblasts for DDR2, a cell-surface receptor that is not expressed on endothelial cells, smooth muscle cells, or CMs [23]. The primary anti-DDR2 antibody will then be attached to a magnetic secondary antibody; once the cell mixture is passed through a magnetic column, the eluted fraction should theoretically be almost free of fibroblasts. Since fibroblasts are highly proliferative, decreasing their proportion among the non-myocytes may yield more opportunity for the progenitor cells to visibly increase in their numbers. Preliminary studies show that DDR2 labelling is very strong in the NIH3T3 fibroblast cell line (Figure 5.5), but success is, thus far still, limited with cardiac fibroblasts.

## 5.5 Conclusions

Out of the four aims of this thesis, the one that raised the most difficult challenges was the identification and isolation of *isl1*<sup>+</sup> cells. Part of the difficulty lies within the fact that relatively few studies have been reported in this area, and that groups investigating cardiac progenitor sources do not necessarily agree on a hallmark that defines a cardiac progenitor cell. Several attempts have been made to identify the *isl1*<sup>+</sup> progenitor population within the neonatal rat heart, both in terms of its existence and its size. Apart from previous work indicating that *isl1* transcription does indeed take place in the PP1 cells, we have been unsuccessful at confirming the expression of the *isl1* protein due to the scarcity of the *isl1*<sup>+</sup> population as well as issues of autofluorescence. Assessment techniques for the detection of the *isl1* protein, such as immunostaining and flow cytometry, need to be optimized before attempts at enriching for *isl1*<sup>+</sup> cells can proceed. Thus far, the most promising method for dissociating PP1 cell monolayers is the 2% EDTA solution with 5% FBS. This method may be used for enrichment and passaging procedures, if it can be determined that the *isl1*<sup>+</sup> progenitors will survive.

## 5.6 Figures

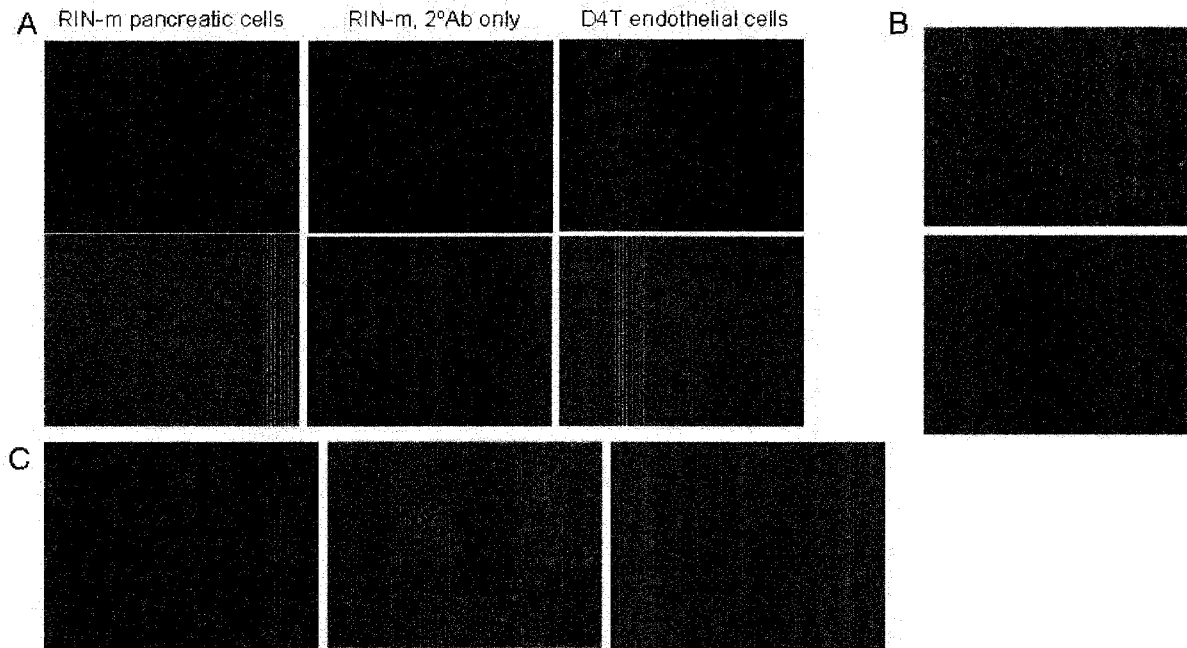


**Figure 5.1. Autofluorescence and non-specific staining in primary cells.** A) Immunostaining for isl1 in RIN-m and D4T cell lines. RIN-m serves as a positive control and D4T serves as a negative control. Both controls are clear. In addition, no non-specific staining was observed in RIN-m cells when only the secondary antibody was used. Green = isl1, Blue = nuclei. B) Unstained PP1 cells exhibit different levels of autofluorescence, depending on the batch of cells. C) Non-specific staining can occur in primary cells to a much greater extent compared to cell lines (compare to middle column in A). Blue = nuclei, Green = FITC secondary antibody attached non-specifically to cells. A small degree of autofluorescence can be seen in the red channel

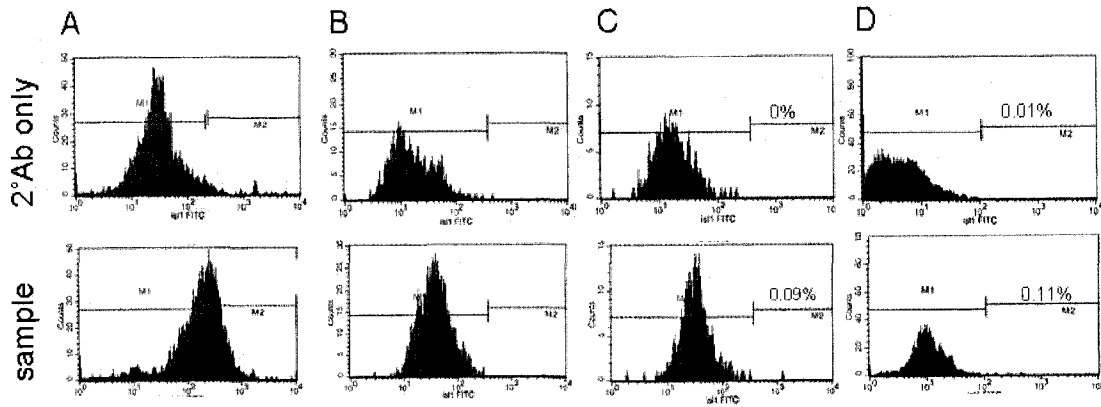


**Figure 5.2. Flow cytometry analysis on PP1 cells cultured in various media at day 4.** A) RIN-m pancreatic cells serve as a positive control. A shift in peak is clearly revealed. B) PP1 cells cultured in regular CM medium. C) PP1 cells cultured in the “Laugwitz” medium. D) PP1 cells cultured in medium supplemented with BIO. In cases C and D, there may be a small number of  $is11^+$  cells.

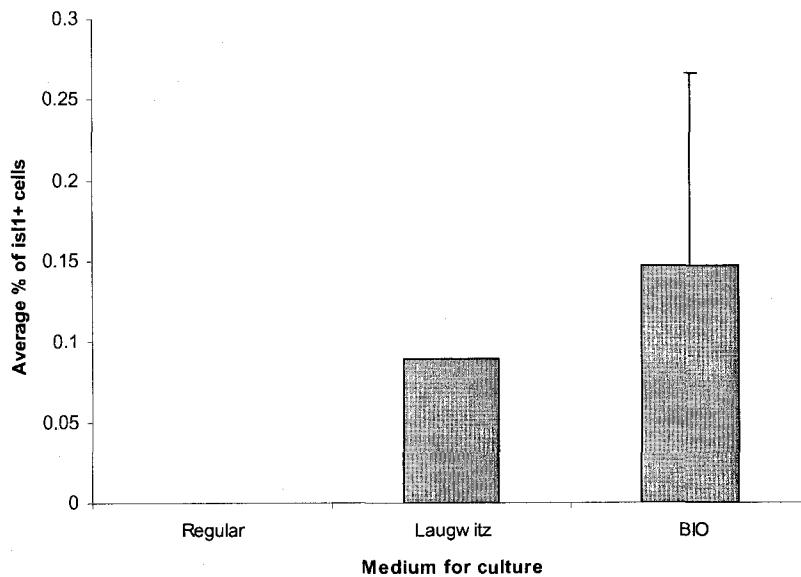


**Figure 5.3. Average percentage of  $is11^+$  progenitors as indicated by flow cytometry analysis on PP1 cells cultured in various medium at day 4.** N =3 for cultures in “Regular” and “BIO” media, and N=1 for culture in the “Laugwitz” medium. The Laugwitz and BIO media may be contributing to the proliferation of the scarce  $is11^+$  population for a short period of time.

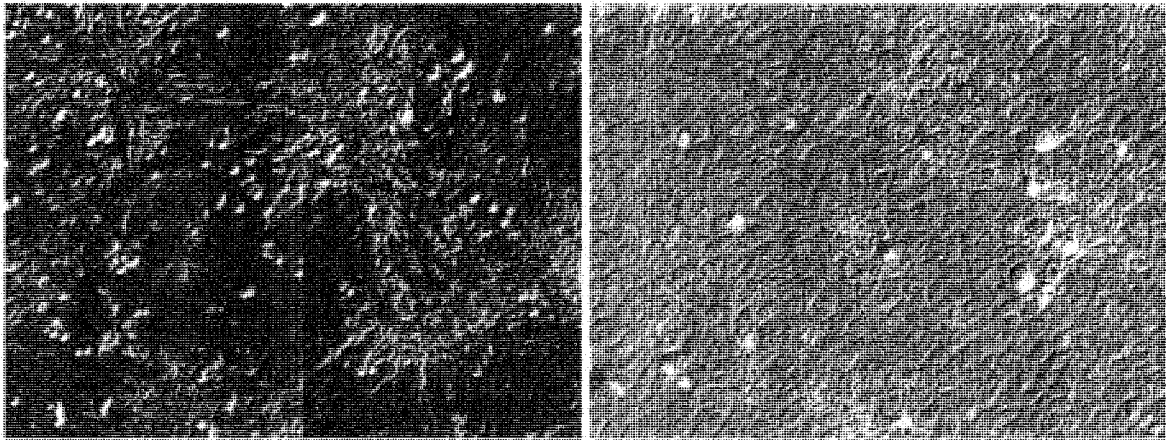


**Figure 5.4. Effects of BIO on cell morphology.** Left) PP1 cultured in regular CM medium at day 7. Beating clusters are comprised of elongated cells. Right) PP1 cultured in BIO medium at day 7. Cells appeared to be flat; no contractions were observed. Scale bar = 20 $\mu$ m

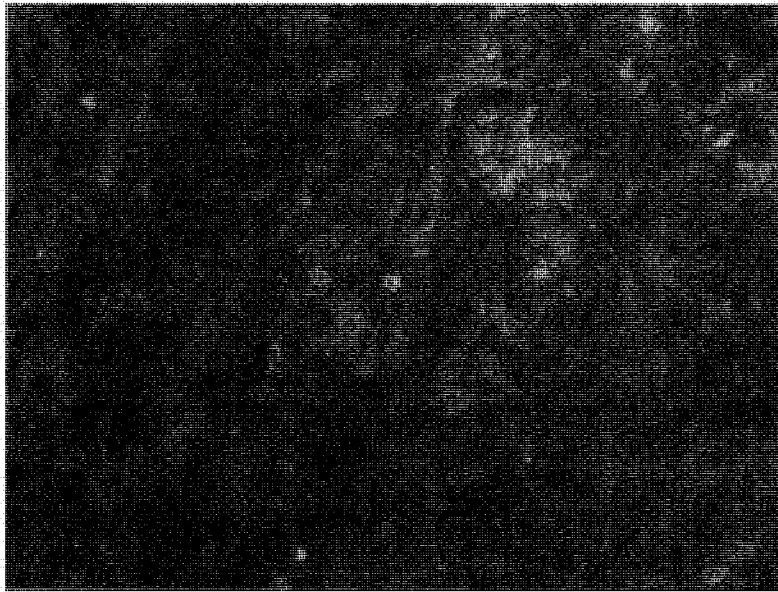


**Figure 5.5. Immunostaining of cell surface receptor DDR2 in NIH3T3 fibroblasts.** Red = DDR2; Blue = nuclei.

## 5.7 References

1. Ott, H.C., et al., *The adult human heart as a source for stem cells: repair strategies with embryonic-like progenitor cells*. Nat Clin Pract Cardiovasc Med, 2007. **4 Suppl 1**: p. S27-39.
2. Laugwitz, K.L., et al., *Isl1 cardiovascular progenitors: a single source for heart lineages?* Development, 2008. **135**(2): p. 193-205.
3. Moretti, A., et al., *Multipotent embryonic isl1+ progenitor cells lead to cardiac, smooth muscle, and endothelial cell diversification*. Cell, 2006. **127**(6): p. 1151-65.
4. Cai, C.L., et al., *Isl1 identifies a cardiac progenitor population that proliferates prior to differentiation and contributes a majority of cells to the heart*. Dev Cell, 2003. **5**(6): p. 877-89.
5. Beltrami, A.P., et al., *Evidence that human cardiac myocytes divide after myocardial infarction*. N Engl J Med, 2001. **344**(23): p. 1750-7.
6. Beltrami, A.P., et al., *Adult cardiac stem cells are multipotent and support myocardial regeneration*. Cell, 2003. **114**(6): p. 763-76.
7. van Laake, L.W., et al., *Human embryonic stem cell-derived cardiomyocytes and cardiac repair in rodents*. Circ Res, 2008. **102**(9): p. 1008-10.
8. Laflamme, M.A., et al., *Cardiomyocytes derived from human embryonic stem cells in pro-survival factors enhance function of infarcted rat hearts*. Nat Biotechnol, 2007. **25**(9): p. 1015-24.
9. Bearzi, C., et al., *Human cardiac stem cells*. Proc Natl Acad Sci U S A, 2007. **104**(35): p. 14068-73.
10. Bellafiore, M., et al., *Research of cardiomyocyte precursors in adult rat heart*. Tissue Cell, 2006. **38**(6): p. 345-51.
11. Nelson, T.J., et al., *CXCR4+/FLK-1+ biomarkers select a cardiopoietic lineage from embryonic stem cells*. Stem Cells, 2008. **26**(6): p. 1464-73.
12. Matsuura, K., et al., *Adult cardiac Sca-1-positive cells differentiate into beating cardiomyocytes*. J Biol Chem, 2004. **279**(12): p. 11384-91.
13. Barile, L., et al., *Endogenous cardiac stem cells*. Prog Cardiovasc Dis, 2007. **50**(1): p. 31-48.
14. Hsieh, P.C., et al., *Evidence from a genetic fate-mapping study that stem cells refresh adult mammalian cardiomyocytes after injury*. Nat Med, 2007. **13**(8): p. 970-4.
15. Gonzalez, A., et al., *Activation of cardiac progenitor cells reverses the failing heart senescent phenotype and prolongs lifespan*. Circ Res, 2008. **102**(5): p. 597-606.
16. Laugwitz, K.L., et al., *Postnatal isl1+ cardioblasts enter fully differentiated cardiomyocyte lineages*. Nature, 2005. **433**(7026): p. 647-53.
17. Moretti, A., et al., *Biology of Isl1+ cardiac progenitor cells in development and disease*. Cell Mol Life Sci, 2007. **64**(6): p. 674-82.
18. Qyang, Y., et al., *The renewal and differentiation of Isl1+ cardiovascular progenitors are controlled by a Wnt/beta-catenin pathway*. Cell Stem Cell, 2007. **1**(2): p. 165-79.

19. Meijer, L., et al., *GSK-3-selective inhibitors derived from Tyrian purple indirubins*. *Chem Biol*, 2003. **10**(12): p. 1255-66.
20. Reya, T. and H. Clevers, *Wnt signalling in stem cells and cancer*. *Nature*, 2005. **434**(7035): p. 843-50.
21. ATCC, *Product Information Sheet for CRL-2057*.
22. Reid, T., *Double Immunohistochemistry of Culture Cells*.
23. Goldsmith, E.C., et al., *Organization of fibroblasts in the heart*. *Dev Dyn*, 2004. **230**(4): p. 787-94.
24. Chu, Z., *The Transcriptional Profile of Neonatal Rat Islet-1+ Cardiac Progenitor Cells*, in *Division of Engineering Science, Faculty of Applied Science and Engineering*. 2008, University of Toronto: Toronto. p. 76.
25. Svendsen, C.N., et al., *Increased survival of rat EGF-generated CNS precursor cells using B27 supplemented medium*. *Exp Brain Res*, 1995. **102**(3): p. 407-14.

## 6. Summary

This thesis consists of four aims. The first three underline methods which differentiate various immature cardiac cells into the contractile adult cardiac phenotype, desired for the purpose of cardiac tissue engineering. The final sub-project is an exploration of the  $isl1^+$  progenitors found within the neonatal rat heart.

Firstly, we observed an interactive effect of surface topography and electrical field stimulation on elongation and orientation of fibroblasts and CMs, cultured on polyvinyl carbonate substrates with abrasions made manually by lapping paper of various sizes and subjected to stimulation in an electrical stimulation chamber. From the non-stimulated experiments, we observed that the V-shaped abrasions which were 13  $\mu\text{m}$  wide and 700 nm deep exhibited the strongest effect on neonatal rat CM elongation and orientation as well as a statistically significant effect on the orientation of neonatal rat fibroblasts. Hence, these abrasions were employed in the electrical stimulation experiment. The stimulation regime consisted of square pulses of 1 ms duration at a frequency of 1 Hz and an electric field strength of either 2.3 V/cm or 4.6 V/cm. The samples were positioned between carbon electrodes such that the abrasions were either parallel or perpendicular to the electric field lines, with non-abraded surfaces serving as controls. The field stimulation did not affect cell viability. In addition, field stimulation assisted in the development of contractile apparatus, as revealed by the presence of striated cardiac Troponin I and actin filaments, in cardiomyocytes cultured on the abraded surfaces. Furthermore, the orientation and elongation response of CMs was abrogated by the inhibition of actin polymerization (by the drug Cytochalasin D) and partially inhibited by the blockage of the PI3K pathway (via the drug LY294002). Overall, we observed the following:

- i. Fibroblast and cardiomyocyte elongation on non-abraded surfaces was significantly enhanced by electrical field stimulation.
- ii. Electrical field stimulation promoted orientation of fibroblasts in the direction perpendicular to the field lines (if the sample was cultured with the abrasions also placed perpendicular to the field lines).

- iii. Topographical cues were a significantly stronger determinant of CM orientation than electrical field stimulation
- iv. Electrical field stimulation, at a field strength of 4.6V/cm, had a slight effect in modulating the orientation of CM in the absence of contact guidance.

Secondly, we developed a microfabricated system incorporating topographical and electrical cues on a single TCPS chip, which enabled cultivation of differentiated cardiomyocytes. The cell culture chips were created by hot embossing of polystyrene, to create microgrooves and microridges of precisely defined depth, width and periodicity. Substrates consisting of 0.5 $\mu$ m-wide grooves and 0.5 $\mu$ m-wide ridges (1 $\mu$ m period) and those consisting of 3 $\mu$ m-wide grooves and 1 $\mu$ m-wide ridges (4 $\mu$ m period) were investigated with smooth surfaces used as controls. The depth of the microgrooves was 400nm. The two gold electrodes were electrodeposited 1cm apart such that the microgrooves in-between were oriented either parallel or perpendicular to the electrodes, enabling studies of interaction between topographical and electrical cues. Neonatal rat cardiomyocytes cultivated on microgrooved substrates for 7 days were elongated and aligned along the microgrooves forming a well developed contractile apparatus, as evidenced by sarcomeric  $\alpha$ -actinin staining, with a more pronounced effect on substrates with 1 $\mu$ m periodicity compared to 4 $\mu$ m periodicity. Notably, simultaneous application of biphasic electrical pulses and topographical cues resulted in gap junctions confined to the cell-cell end junctions, rather than the punctate distribution found in neonatal cells. Electrical field stimulation further enhanced cardiomyocyte elongation when microgrooves were oriented parallel to the electric field. The culture chips were compatible with fluorescence and optical microscopy, and also provided the ability to independently control field stimulation parameters, biochemical and topographical cues on each chip, as opposed to cultivation within one electrical stimulation chamber in which multiple samples must be subjected to the same conditions. This system may therefore become a useful tool in drug development and maturation of cardiomyocytes derived from ESCs.

Next, we proceeded to test the effect of contact guidance and electrical field stimulation, as applied by the previously described systems, on the culture of hESC-CMs. We observed that cellular alignment of hESC-CM could be achieved with both the manually abraded polyvinyl carbonate coverslips, as well as with the hot-embossed TCPS with microfabricated structures. Cellular elongation appeared to be improved by microstructures of certain sizes. Moreover, the presence of a developed contractile apparatus was revealed by staining for sarcomeric  $\alpha$ -actinin, a cardiac marker. We then sought to investigate the effects of electrical field stimulation, in addition to topographical cues, on the hESC-CM cultures. The abraded polyvinyl carbonate surfaces made by lapping paper of grain size 12  $\mu\text{m}$  was employed in preliminary electrical stimulation experiments as a more conveniently available alternative to the microfabricated TCPS system with deposited electrodes. This surface was chosen because it appeared to promote good cellular alignment and elongation based on initial qualitative assessments. Further work is needed to elucidate the effects of electrical field stimulation, in interaction with contact guidance, on the maturation of hESC-CMs.

Finally, we attempted to isolate and characterize the  $isl1^+$  progenitor population within the neonatal rat heart, with the objective of maturing them to the adult phenotype. Previously obtained RT-PCR data revealed that the transcription of  $isl1$  increases within the PP1 population over time; however, we were unable to confirm these results with immunostaining and flow cytometry. The scarcity of the  $isl1^+$  population, in addition to autofluorescence of cells within the PP1 fraction, rendered the identification of these cells via immunoassaying of the  $isl1$  protein extremely challenging. We also explored different methods for separation the  $isl1^+$  population, such as differential preplating, from the PP1 cells, such that they could be expanded; however success in this area was largely limited since we did not have a confident method for identifying  $isl1^+$  cells.

In summary, we confirmed our hypothesis that the application of surface topography and electrical stimulation is helpful in achieving the maturation of CMs. The application of such stimuli was most effective in maturing neonatal rat CMs on a 2-dimensional construct, but also demonstrates some promise in hESC-CM for the same purpose. Both of these populations may contain undifferentiated cardiac progenitors, whose multipotent potential we may want to explore. Finally, we also investigated

methods for isolating and characterizing the  $isl1^+$  progenitors in the neonatal rat heart. Despite limited success, certain key milestones, such as improvement in cell dissociation methods were achieved.

## 6.1 Future Work

Since the application of surface topography and electrical field stimulation was highly successful in creating organized, 2-dimensional constructs exhibiting a mature cardiac phenotype, the idea can theoretically be extended to a three-dimensional model. One strategy, as previously mentioned, is to manufacture scaffolds with the microstructures in order to guide cellular organization to match the desired outcome. This strategy could be used to direct cellular elongation and orientation as well as cellular maturation. For added convenience, it is also possible to integrate electrodes into the scaffold (as our studies in Chapter 3 also demonstrated) to facilitate the application of electrical stimulation within the construct, without the necessity and complexity of using existing electrical stimulation chamber designs, which would be bulky and may not be amenable or appropriate for our specific studies. If cellular maturation can be achieved to an adequate degree in a 3D model, it may have significant implications for engineering 3D constructs.

Additional work on the maturation of hESC-CMs can be pursued. Currently, the effects of electrical stimulation are under study. Once the optimal conditions for maturing and differentiating hESC-CM have been established, the same culture conditions and external stimuli may be applied to differentiate cardiac precursors derived from iPS cells. To date, there have been no extensive studies of the effect of electrical stimulation of the maturation of CMs derived from iPS cells.

Finally, it may be instructive to establish a method to properly label  $isl1^+$  progenitors within the neonatal rat heart that, contrary to that used by Laugwitz et al, has not been genetically modified. This will enable us to identify existing  $isl1^+$  cells and to assess the feasibility of different protocols to isolate this population. Discoidin domain receptor 2 (DDR2), a fibroblast surface marker, could be used to deplete cardiac fibroblasts from the heterogeneous mixture of cells comprising the native heart cell

isolate by fluorescence activated cell sorting (FACS) or magnetic activated cell sorting (MACS), and thus should be further explored for this purpose. If the  $isl1^+$  progenitors can be efficiently harvested from the neonatal rat heart in reasonable and sufficient numbers, they can also be subjected to the optimal contact guidance and stimulation parameters explored in this thesis in order to optimize a procedure for inducing their expansion, maturation and differentiation. Since resident progenitors are autologous, they would not be prone to issues surrounding immune mismatch in clinical applications and would be most desirable as a cell source in cardiac tissue repair.

## 6.2 Recommendations

Specific recommendations to be considered are as follows:

- 1) The cultivation of hESC-CM on microstructures created via hot embossing should be explored in greater detail, once we have the availability to fabricate these surfaces in sufficient quantities.
- 2) In our initial assessment of hESC-CM cultivation on the family of manually abraded surfaces, the surfaces made by lapping paper of grain sizes of 40  $\mu\text{m}$  and 30  $\mu\text{m}$  demonstrated the ability to significantly improve cellular elongation and alignment. Contractile properties of cells grown on these surfaces also appeared desirable, thus the effects of the “40  $\mu\text{m}$ ” and “30  $\mu\text{m}$ ” surfaces should be further explored in future experiments.
- 3) The hESC-derived cells, obtained from the Keller lab, contain cells that are committed to the cardiac lineage, but are not cardiomyocytes. The ability of these hESC-derived cells to differentiate into endothelial cells and smooth muscle cells should be assessed via immunostaining of respectively CD31 and smooth muscle actin, respectively, while their capacity to form gap junctions with neighbouring cells could be assessed by immunoassaying for connexin-43.

- 4) Currently,  $isl1^+$  progenitors are obtained as the “unwanted fraction” from separation of non-adherent neonatal rat cardiomyocytes from adherent non-myocytes by pre-plating of the native heart cell isolate on TCPS. The protocol should be modified, with the aim to isolate the  $isl1^+$  progenitors instead of CMs. Prior to attempting isolation of  $isl1^+$  cells from the neonatal rat heart, we should try to reproduce the results as published by Laugwitz et al., utilizing mice that have not been genetically modified.
- 5) DDR2 labelling in cardiac fibroblasts should be better examined as a marker for use in FACS- or MACS-based removal of fibroblasts from the non-myocyte population to improve the yield of  $isl1^+$  progenitors.
- 6) Autofluorescence issues should be conclusively verified and eliminated before attempting any assays or assessments involving fluorescence-based identification of cells.

## 7. Appendices

### S2. Supplementary Figures for Chapter 2

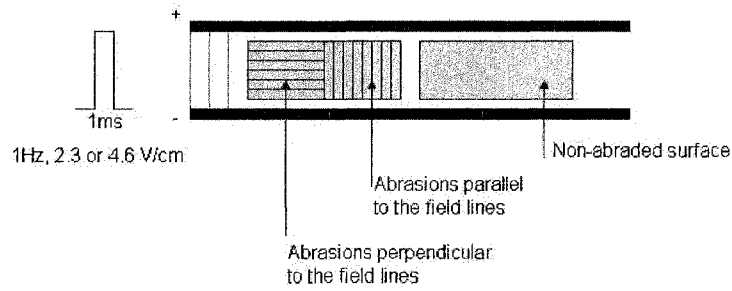


**Figure S1. Schematics of experimental set-up used to study the interaction of topographical cues and electrical field stimulation.**

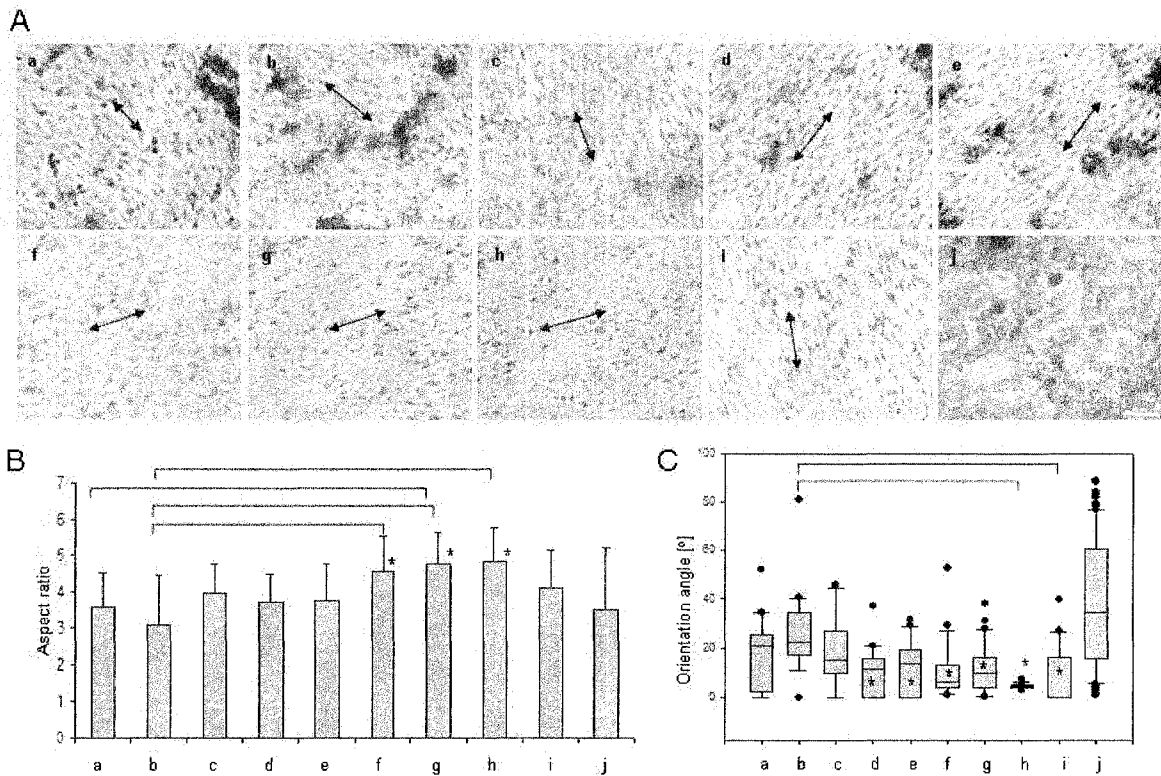


**Figure S2. Fibroblasts cultivated on surfaces with abrasions of various sizes. A)** Giemsa stains of fibroblasts cultured for 1 week on abraded surfaces made by lapping

paper of different grain size. The letters a to i represent respective lapping grain sizes of 1, 3, 5, 9, 12, 30, 40, 60, 80  $\mu\text{m}$ . j represents a non-abraded surface. Arrows indicate the direction of abrasion. B) Aspect ratio, defined as the ratio between the length and width of the cell. \* indicates a statistically significant difference in comparison to non-abraded surface. C) Alignment of non-stimulated fibroblasts. Alignment is assessed by the angle at which cells deviate from the abrasions they grow on. Box plots indicate the spread of alignment angles on various abrasions. (Scale bar: 100  $\mu\text{m}$  for a to i and 50  $\mu\text{m}$  for non-abraded).

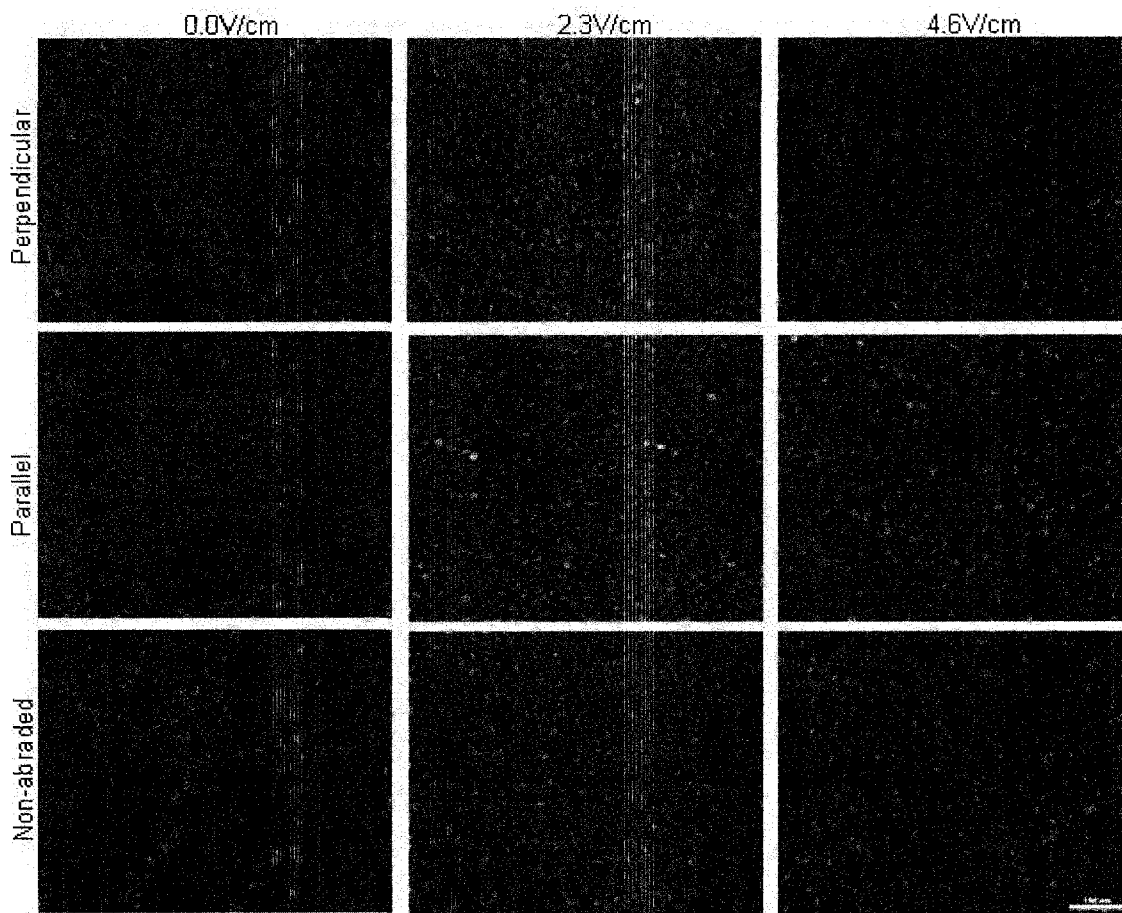


**Figure S3. Live/dead staining of fibroblasts cultivated in the presence of electrical field stimulation on non-abraded and abraded surfaces.** Live cells were stained with CFDA (green) and dead cells with PI (red). Abraded surfaces were placed either perpendicular or parallel to the field line. Field stimulation, square pulses, 1ms duration, 1Hz and voltage as indicated, was applied 24 hr after seeding and maintained for additional 72 hr. Scale bar 100 $\mu\text{m}$ .

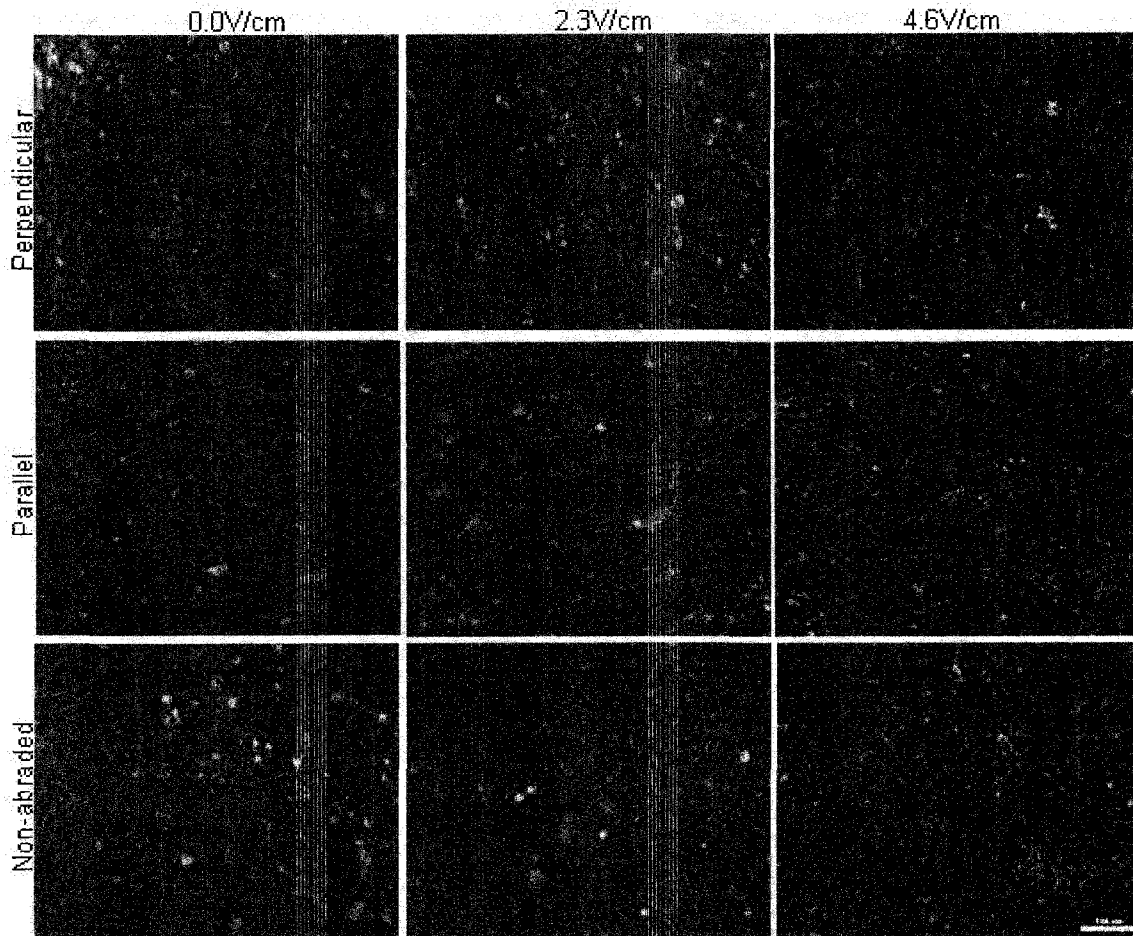


**Figure S4. Live/dead staining of cardiomyocytes cultivated in the presence of electrical field stimulation on non-abraded and abraded surfaces.** Live cells were stained with CFDA (green) and dead cells with PI (red). Abraded surfaces were placed either perpendicular or parallel to the field line. Field stimulation, square pulses, 1ms duration, 1Hz and voltage as indicated, was applied 24 hr after seeding and maintained for additional 72 hr. Scale bar 100 $\mu$ m.

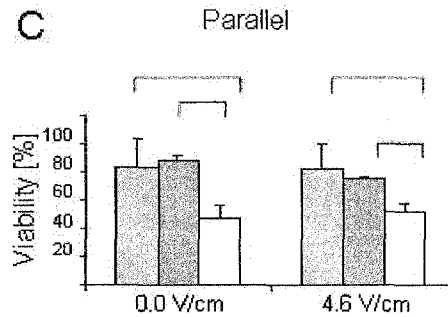
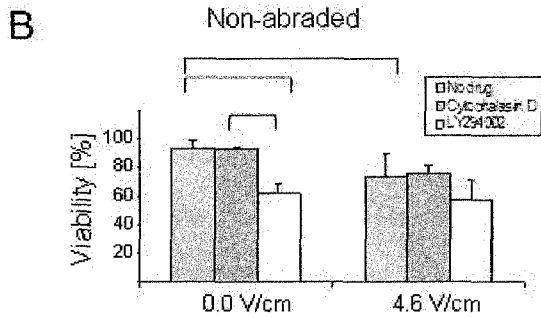
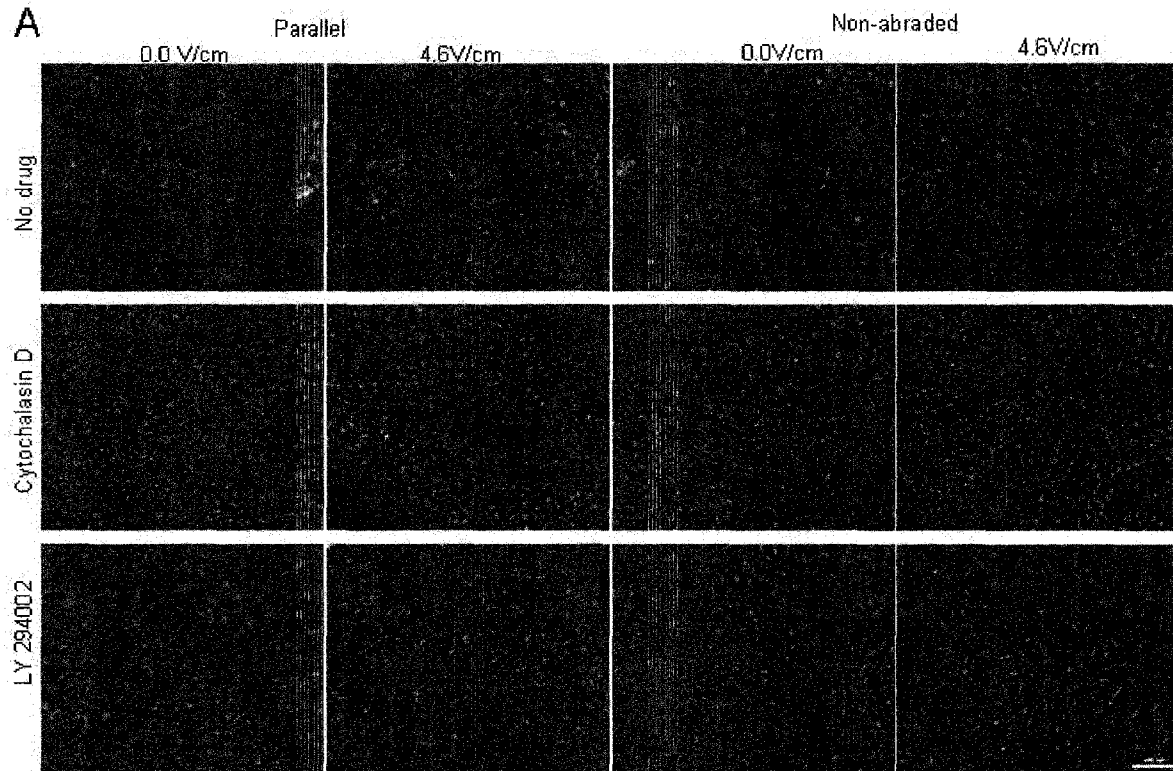


**Figure S5. Effect of pharmacologic agents on viability of cardiomyocytes cultivated in the presence of electrical field stimulation (0.0V/cm or 4.6V/cm) on non-abraded and abraded surfaces placed parallel to the field lines.** Viability was determined by manual counts. A) Live/dead staining was performed using CFDA which stains live cells green and PI which stains live cells dead B) Percentage of live cells on non-abraded surfaces C) Percentage of live cells on abraded surfaces. Scale bar 100 $\mu$ m. N=5 -6 images analyzed per treatment. ( $p < 0.05$  was considered significant).

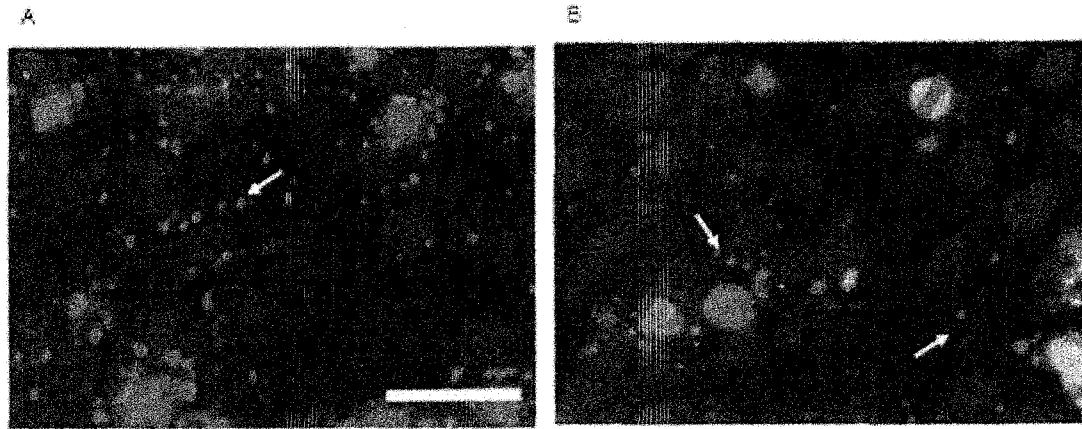


**Figure S6. Connexin-43 staining of cardiomyocytes cultivated on (A) non-abraded surfaces and (B) surfaces abraded using lapping paper with grain size 80  $\mu\text{m}$ . Scale bar 20  $\mu\text{m}$ . White arrows illustrate examples of positive staining in the images.**

## **S5. Appendices for Chapter 5**

### **S5.1 Methods to isolate and expand $\text{isl1}^+$ progenitors**

The following methods were used as an attempt to increase the number of  $\text{isl1}^+$  cells obtained.

#### ***S5.1.1 Co-culture technique***

PP1 cells were incubated with 100  $\mu\text{L}$  of red cell tracker dye solution (cat number here) for 15 minutes before they were washed with DMEM and plated into 96-well with culture medium. The cells were fixed in 4% PFA upon 7 days in culture, and thoroughly washed with PBS. A fresh layer of dissociated PP1 (from one of the separation procedures described in the next section) was subsequently seeded on top of the fixed cells and cultured for an additional 2 days before fixing and immunostaining.

#### ***S5.1.2 Separation and cell dissociation techniques***

The following techniques represent different attempts to dissociate PP1 cells from the original substrate on which they were cultured, to separate the PP1 into subpopulations, and to retain survival of these cells.

1) Centrifugal separation method 1: PP1 cells were trypsinized as in a standard passaging procedure. The cell suspension (~5 mL) was then centrifuged subsequently at 500 rpm, 750 rpm and 1000 rpm. After each centrifugation, the supernatant was plated at 200  $\mu$ L per well, careful not to disturb the pellet. The remaining supernatant and the pellet were returned to the centrifuge for the next spin. The pellet resulting from the final spin was resuspended and plated at about 200000 cells per 96-well.

2) Centrifugal separation method 2: Similar to the above procedure, but the supernatant resulting from the first spin was transferred to another tube, while the cell pellet was resuspended in 1 mL of culture medium and plated at 150  $\mu$ L per 96-well well. The supernatant retained was again centrifuged, and the procedure was repeated. Centrifugal speeds for this procedure were 200 rpm, 400 rpm, 600 rpm, 800 rpm and 1000 rpm respectively for 2 minutes each. The supernatant remaining from the final centrifugation was also plated.

3) Collagenase digest: PP1 cells were cultured on collagen-coated TCPS. A type IV collagenase solution was made with at a concentration of 0.1% in PBS. PP1 cells were incubated for 30 minutes in this solution at 37C, 5% CO<sub>2</sub>. The liquid containing the dissociated cells was removed, centrifuged and washed once in PBS. The cells were then resuspended in 5 mL of culture medium and plated at densities of 60  $\mu$ L, 70  $\mu$ L and 100  $\mu$ L per 96-well.

4) Mechanical dissociation: Upon adding PBS or other cell dissociation solutions described in this section, a 5 mL serological pipette was inserted into either a T25 or T75 tissue culture flask to apply scrapping action to the tissue culture surface. The cells were then resuspended to break up large clumps. This technique was applied when the initial dissociation did not appear to have a visible effect.

5) Cold Trypsin-EDTA: Cells were incubated in ice-cold solution of 0.25% trypsin-EDTA on ice for 30 mins.

6) EDTA solution: Solution of 1% and 2 % EDTA were made by diluting a stock 0.5M solution (BioShop EDT111, 18% EDTA) in Hank's Balance Salt Solution (HBSS). In some cases, 5% of FBS was added. Cells were incubated in this solution for 5 minutes at 37C, 5% CO<sub>2</sub>.

7) Cell dissociation buffer: Cells were incubated in a commercial buffer (Sigma C5914) for 5 minutes at 37C, 5% CO<sub>2</sub>. As with the EDTA solution, 5% FBS was added in some cases.

8) Differential pre-plating: During the one hour pre-plating procedure, which is part of the isolation process for CMs from neonatal rat hearts, the liquid (with the suspended cells) was sequentially transferred to a new well (in a 24-well plate) every 10 minutes. Cells which had adhered to the plate surface was fed with culture medium. The culture was maintained for 2 days before the cells were fixed.

Upon dissociation, the cells were centrifuged, resuspended and plated at a density of approximately 100 000 cells per 96-well, unless otherwise specified. The dissociated cells were then cultivated for a period of up to 8 days; any beating, if present, was noted. Samples of PP1 dissociation with collagenase and EDTA, in conjunction with mechanical scrapping, were also cytopun on one occasion as an attempt to determine the initial number of isl1 progenitors in the culture after the dissociation process, before further culture began.

## **S5.2 Discussion: Problems with the separation techniques**

Tissue engineering requires a large, sustainable cell culture which can be maintained and expanded at convenience. If isl1<sup>+</sup> cells do indeed exist in the heart, it would be essential to establish a method their passage and expansion. Primary cardiomyocytes and cardiac progenitor cells did not typically survive the trypsinization process. Once trypsinized, the progenitor cells could not be passaged. Hence, a non-enzymatic dissociation method was sought. Separation via differences in density gradient,

with the assumption that progenitor cells are smaller in size compared to differentiated cells, was not achieved to a satisfactory extent.

No differences were observed between the two centrifugal separation methods, nor in the various cell fractions resulting from the differential preplating procedure (Figure 8), in the total level of *isl1* expression.

Next, the collagenase dissociation method did not work. After 30 minutes of incubation, cells were still very much attached to their culture surface with no signs of reluctance. It is possible that the collagenase did not properly digest the collagen coating underneath the monolayer, or that the solution was not concentrated enough. EDTA, on the other hand, is a metal-chelating agent that removes ions, needed by the cells to maintain attachment, from the cells' milieu. It does not perform any enzymatic action. Higher EDTA concentration (2% vs. 1%) was much more effective in dissociating cells, resulting in shorter incubation time, since it is capable of chelating more ions. On the occasion where the dissociation liquid appeared to be of no avail, cells were much more easily removed by mechanical stress if they were treated with EDTA instead of collagenase. This suggests that EDTA was at least partially effective at promoting cellular detachment. A cold solution of trypsin-EDTA was initially tried because it was assumed that the trypsin enzyme was inactivated at low temperatures, and thus the effect should be equivalent to that of a regular EDTA solution. However, it was decided that the complete absence of trypsin was more desirable, and thus this route was abandoned. Finally, the yield from the commercial cell dissociation buffer was high, but since its effectiveness was comparable to that of the plain 2% EDTA solution, which is a more economical alternative, its use was also discontinued.

Because the incubation period required for the dissociation procedures were often long (15 to 30 minutes), 5% FBS was added to the dissociation solution as an attempt to maintain cell survival during the dissociation process. Cultures that were dissociated with the FBS additive were likely to detach more rapidly, even though it was not obvious if FBS itself had any effect on cell survival. Regardless, the shorter incubation time (~15 minutes) may be enough to minimize cell death.

Importantly, no beating cells were observed in cultured kept following any of the dissociation techniques, which suggests that the CMs may not have survived. It is highly

probable then, that the progenitor cells which tend to follow the same cell fate as CMs under conditions of stress, have also undergone necrosis or apoptosis. Again, it was difficult to assess whether there was any of these dissociation techniques were indeed effective, because of the challenges associated with *isl1* detection.

### S5.3 Supplemental Figures

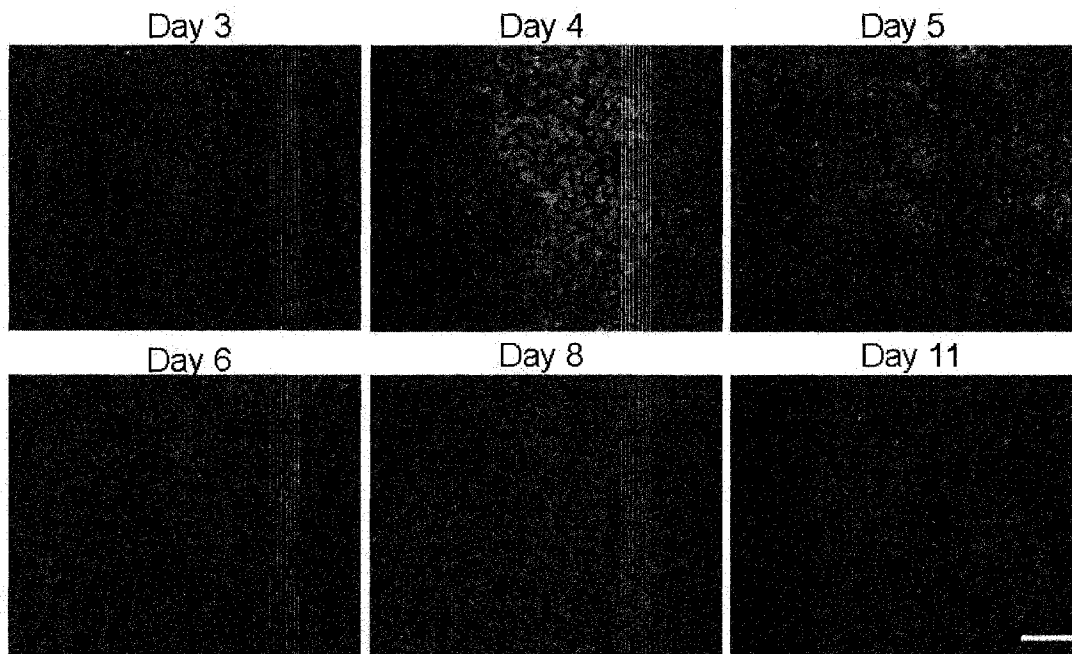


**Figure S5.1. *Isl1* expression and autofluorescence over a period of 11 days of culture.** It was initially believed that *isl1*<sup>+</sup> progenitor population peaks between day 4 and 5. However, it was later discovered that green dots are likely to be a result of autofluorescence. Blue = DAPI; Green = *isl1*/autofluorescence. Scale bar = 50 $\mu$ m